Evaluation of Traditional Hydrogeologic Characterization Approaches in a Highly Heterogeneous Glaciofluvial Aquifer/Aquitard System

by

Matthew Alexander

A thesis
presented to the University of Waterloo
in fulfillment of the
thesis requirement for the degree of
Master of Science
in
Earth Sciences

Waterloo, Ontario, Canada, 2009

AUTHOR'S DECLARATION

I hereby declare that I am the sole author of this thesis. This is a true copy of the thesis, including any required final revisions, as accepted by my examiners.

I understand that my thesis may be made electronically available to the public.

Abstract

Hydraulic conductivity (K) and specific storage (S_s) estimates are two of the most essential parameters when designing transient groundwater flow models that are commonly used in contaminant transport and water resource investigations. The purpose of this study was to evaluate the effectiveness of traditional hydrogeologic characterization approaches in a highly heterogeneous glaciofluvial aquifer at the North Campus Research Site (NCRS), situated on the University of Waterloo campus. The site is instrumented with four Continuous Multichannel Tubing (CMT) wells containing a total of 28 monitoring points and a multi-screen well used for pumping at different elevations. Continuous soil cores to a depth of approximately 18 m were collected during the installation of the CMTs and the multi-screen well. The cores were subsequently characterized using the Unified Soil Classification System and grain size analysis. K estimates were obtained for the core by obtaining 471 samples at approximately 10 cm increments and testing them with a falling head permeameter, as well as by utilizing empirical equations developed to estimate K by Hazen (1911) and Puckett et al. (1985). These estimates showed K to vary from 10^{-3} - 10^{-11} m/s illustrating the highly heterogeneous nature of the geology at the NCRS. A geostatistical analysis performed on the K datasets yielded strongly heterogeneous kriged K fields for the site. K and Ss were also estimated via type curve analysis of slug and pumping test data collected at the site. Seven cross-hole pumping tests were conducted using a straddle packer system in the center multi-screened well and the 4 CMTs installed in a 5-spot pattern. The resulting drawdown responses were recorded in 28 CMT ports and 3 zones in the center well using pressure transducers. The various K and S_s estimates were then evaluated by simulating the transient drawdown data using a 3D forward numerical model constructed using *Hydrogeosphere* (Therrien et al., 2005). Simulation was conducted using 4 separate K and S_s fields: 1) a homogeneous case with K and S_s estimates obtained by averaging equivalent K and S_s values from the cross-hole pumping tests, 2) a layered heterogeneous case with strata determined from site geology, K and S_s estimates from the slug tests, 3) two heterogeneous cases with the kriged K data (permeameter and grain size) and S_s from the slug tests, and 4) a mixed case with kriged K data (permeameter) and a homogeneous S_s value from the pumping tests. Results showed that, while drawdown predictions generally improved as more complexity was introduced into the model, the ability to make accurate drawdown predictions at all of the CMT ports was inconsistent. These results suggest that new techniques may be required to accurately capture subsurface heterogeneity for improved predictions of flow in similar systems.

Acknowledgements

I would like to thank Dr. Walter Illman for providing me the opportunity to embark on this invaluable learning experience. I am extremely appreciative of his guidance and sage advice throughout this process. Thanks also go out to my committee members, Dr. David Rudolph and Dr. Edward Sudicky.

This work would not have been possible without the co-operative efforts of Steve Berg. His hard work at our research site produced an excellent set of field data that was vital to this work. I am also greatly appreciative of his willingness to offer 'lessons from the past' that helped out on many occasions.

Finally, I received superb help with my laboratory work from Juzer Beawerwala and Scott Piggott. Their efforts are greatly appreciated. Technical assistance in the lab was provided by Paul Johnson, Bob Ingleton and Wayne Noble. This work would not have gone so smoothly without their efforts.

Dedication

This work is dedicated to my wonderful wife, Nitika. Your support through this process and tolerance of so many evenings spent without your husband will not be forgotten!

Table of Contents

List of Figures

List of Tables

1. Introduction

The flow of water in the subsurface is controlled by several key properties of the porous media, including hydraulic conductivity (K) and specific storage (S_s). These properties will determine the migration pattern of contaminants through an aquifer and the drawdown pattern in an aquifer hosting a production well. A difficult reality often faced by hydrogeologists is that site geologic conditions are commonly non-ideal, due to the presence of significant heterogeneity in the rock or sediment. When trying to predict the behavior of fluid movement in heterogeneous media, in general, it can be said that as the level of heterogeneity increases, so do the required number of measured data. This was illustrated by Rehfeldt et al. (1992) who suggested that 10^5 hydraulic conductivity measurements would be required to deterministically model the transport of contaminants in an alluvial aquifer where conductivity was measured to vary over 3 orders of magnitude. This poses a problem, as every data point requires an investment of time and money, which typically leads to sites being characterized based on few measurements. Even in rigorous academic studies that focus on hydraulic characterization, measurements rarely exceed 1,000 points and are commonly well below this number (Eggleston et al., 1996; Rehfeldt et al., 1992; Sudicky, 1986; Zlotnik and Zurbuchen, 2003).

Another complication stems from the selection of a method to estimate the hydraulic properties. It has been shown that when several different methods of K or S_s measurement are tested at a common elevation, or in a common geologic unit, a range of values will be obtained (Bradbury and Muldoon, 1989; Butler, 1998). This phenomenon has to do with the fact that each method samples a certain volume of the porous media and therefore those methods that sample large volumes may interact with a highly conductive zone in the media not 'seen' by a method that samples a smaller volume, as well as the fact that each method employs different mathematical relationships that each make specific assumptions about the system being studied. Furthermore, it was recently shown by Wu et al. (2005) that the hydraulic parameters estimated based on pumping test data may change depending on the portion of the drawdown curve that is analyzed.

There have been a number of studies that have examined the relative abilities of different methodologies to measure aquifer hydraulic properties (Bagarello and Provenzano, 1996; Bradbury and Muldoon, 1989; Butler, 2005; Butler and Healey, 1998; Davis et al., 1999; Dorsey et al., 1990; Gribb et al., 2004; Lee et al., 1985; Paige and Hillel, 1993; Young, 1997; Zlotnik and Zurbuchen, 2003), but only one of these (Davis et al., 1999) has explored the application of estimated parameters to flow prediction. In this study, several point measurements of saturated K were taken using three

different techniques and used as input into a regional, two-layered, shallow flow system model. The authors then assessed the variability in the predicted catchment discharge caused by the range of saturated K values measured. Other studies have recognized the need to incorporate heterogeneity into hydrogeology flow studies, but have used stochastic or geochemical approaches to predict heterogeneity based on few hydraulic field data (Cooley and Christensen, 2005; Moltyaner and Wills, 1993; Yang et al., 2004).

The purpose of this study was to evaluate the ability of selected hydrogeologic site characterization techniques to accurately delineate the distribution of hydraulic properties in a highly heterogeneous aquifer/aquitard system. The success of each characterization technique was evaluated via the simulation of densely monitored pumping tests in *Hydrogeosphere* (Therrien et al., 2005), a transient 3D surface water/groundwater flow model that utilized the various datasets assembled from the measured hydraulic data. This work was designed to answer the question of whether characterization techniques commonly used by hydrogeologists are sufficient in accurately predicting flow through heterogeneous geologic media.

2. Field Site

2.1 Physiography and Geology

The North Campus Research Site (NCRS) is located on the University of Waterloo campus, in Waterloo, Ontario (Figure 2.1). The physiography of the region was largely shaped by the numerous advances and retreats of two primary lobes of the Laurentide ice sheet during the Wisconsin glacial period. Waterloo was essentially the confluence point of the Erie-Ontario lobe, which originated from the east, and the Huron-Georgian Bay lobe, which originated from the north (Karrow, 1993). This complex ice movement deposited the dominant surface feature in the Waterloo region called the Waterloo Moraine (Karrow, 1993). This moraine is a hummocky kettle and kame feature, composed of a somewhat alternating series of till and aquifer units that are well mixed in some areas and show significant erosional discontinuities in others (Karrow, 1993). The moraine reaches a maximum elevation of 381 mASL in the northwest and a minimum of 350 mASL in the southeast (Karrow, 1993), covering an area of approximately 390 km^2. Drainage from the area is conveyed by the Nith and Conestogo rivers, two major tributaries of the Grand River which winds its way south ultimately flowing into Lake Erie. Numerous sections of the moraine are poorly drained, commonly due to the presence of kettle bogs, some of which still contain ponded water (Karrow, 1993). The NCRS lies on the northeastern side of the moraine and is locally drained by a storm water management pond and engineered stream system.

In 1979, the Quaternary geology beneath the University of Waterloo campus was explored by the drilling of a 50 metre deep borehole. Samples collected during drilling reflected the regional model of semi-alternating aquitard-aquifer units (Karrow, 1979). Below the contemporary organic soil is a thin silt section, followed by a sandy to clay silt, identified as the Tavistock Till. This till is underlain by a 3 m glaciofluvial sand sequence, followed by the silty clay Maryhill Till and the stony silty sand Catfish Creek Till, at about 15 meters. This dense, stony till represents the bottom of the NCRS study section. Subsequent work on campus in the immediate vicinity of the NCRS by Sebol (2000) expanded on the Karrow (1979) interpretation of the geology, by drilling and sampling to produce a cross-section that indicates increased heterogeneity (Figure 2.2) (Sebol, 2000). This figure suggests that the geology has a discontinuous nature at the NCRS, with sandy or gravelly lenses being truncated by lower permeability silts and clays. There is some indication of layering, but based on this interpretation, none of the units extend across the entire study site.

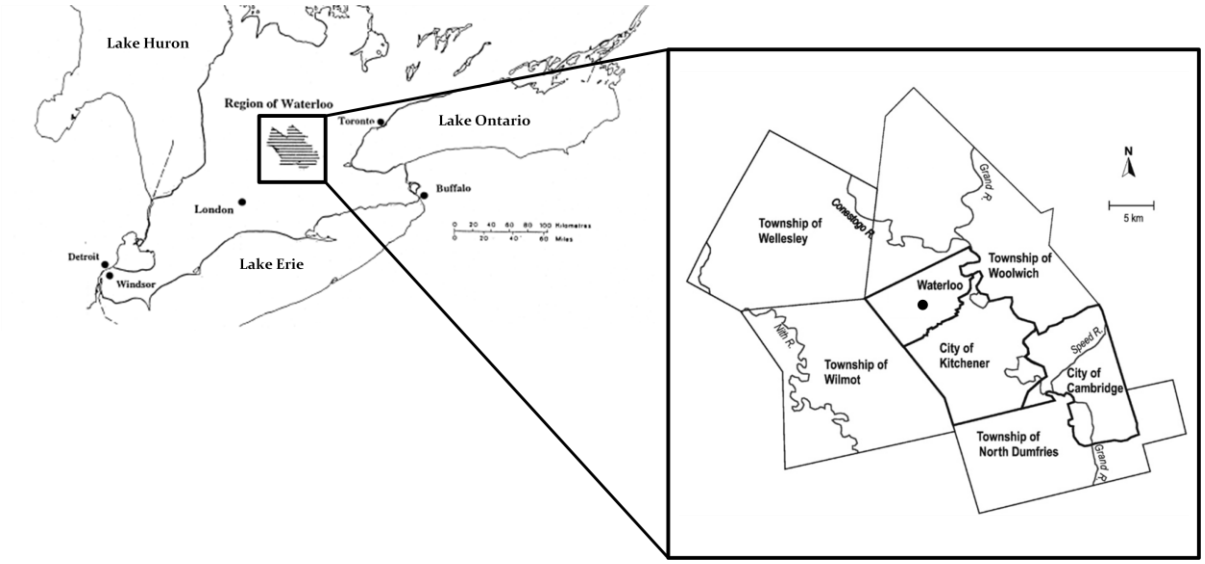

Figure 2.1 Site location map, NCRS denoted by the dot in the City of Waterloo.

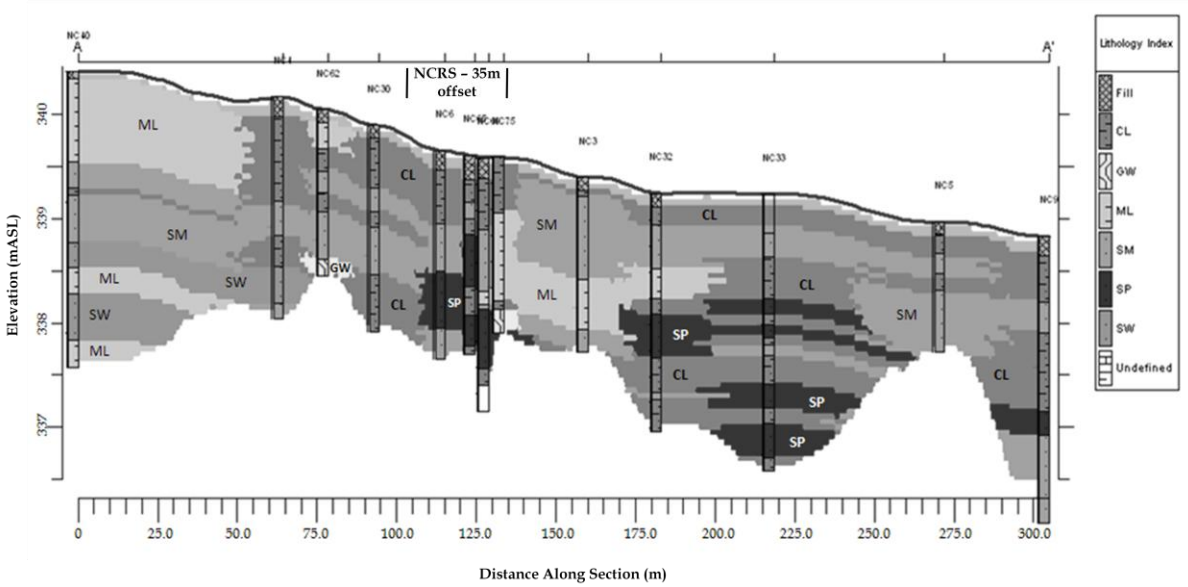

Figure 2.2 East-west geological cross-section immediately south of NCRS (After Sebol, 2000).

2.2 Site Hydrogeology

The shallow groundwater system at the NCRS generally flows towards the southeast, emanating from a groundwater divide located approximately 350 m west of the site (Sebol, 2000). Work done by Sebol (2000) showed that there are two main glaciofluvial aquifer units within the depth of interest for this study, previously referred to as the upper and lower aquifers. They are discontinuous across the site and range in grain size from silty sand/sandy silt (upper aquifer) to sandy gravel/gravelly sand (lower aquifer). The aquitard separating these units also appears to be discontinuous and a hydraulic window connecting the two aquifers may exist in the vicinity of NC6 (Figure 2.2). The lower aquifer is underlain by a thick clay sequence that is truncated by the dense Catfish Creek Till, which likely acts as a hydraulic barrier to underlying units. Water level measurements at the site indicate that the water table fluctuates seasonally by about 1.5 m, with the highest values occurring in the spring when it is located a maximum of 3 m below surface and the lowest in the fall, when it is located a maximum of 1.5 m below the surface (Sebol, 2000). The horizontal hydraulic gradient across the NCRS has a magnitude of approximately 0.029 in the spring and 0.014 in the fall. Within the geologic units at the NCRS, flow is generally horizontal in the aquifer units and vertical through the aquitards.

2.3 Site Instrumentation

In December 2007, four Continuous Multichannel Tubing (CMT) wells with a total of 28 observation ports were installed at the NCRS, with a pumping well added the following spring. The well array is set up in a 5-spot pattern, where the CMT observation wells are equally spaced around the pumping well, forming a square (Figure 2.3). The CMT wells have a diameter of 0.03 m, and contain seven, 0.01 m channels in a circular pattern, each large enough to allow for the installation of a *Micron Systems* pressure transducer, with a range of 0-15 PSI. Screens were constructed for each CMT channel at the desired depth by cutting a 17 cm slot and wrapping the tubing in a fine mesh. The screen elevations were set by evenly distributing them along the length of the tubing, making them independent of the surrounding geology. Field installation was completed by emplacing a 0.3 - 0.6 m filter pack above and below each port and isolating adjacent filter packs with time released bentonite pellets. Bentonite was added above the top filter pack to about 0.3 m below ground surface, where installation was completed by setting a wellhead in concrete.

The pumping well has a diameter of approximately 0.10 m and is screened at 8 different depths with 1 m long screens spaced approximately 2 m apart. During installation, filter packs were

emplaced extending 0.20 m above and below each screen and, as with the CMT wells, each filter pack is isolated from those above and below by time released bentonite pellets (Figure 2.4). The pumping well is designed to facilitate the installation of an inflatable straddle packer system, with the purpose of isolating individual screens and pumping the surrounding geologic unit. A more detailed description of the pump and packer system can be found in Section 3.3. Shortly after their installation, all of the wells were developed until the discharge water was essentially sediment free.

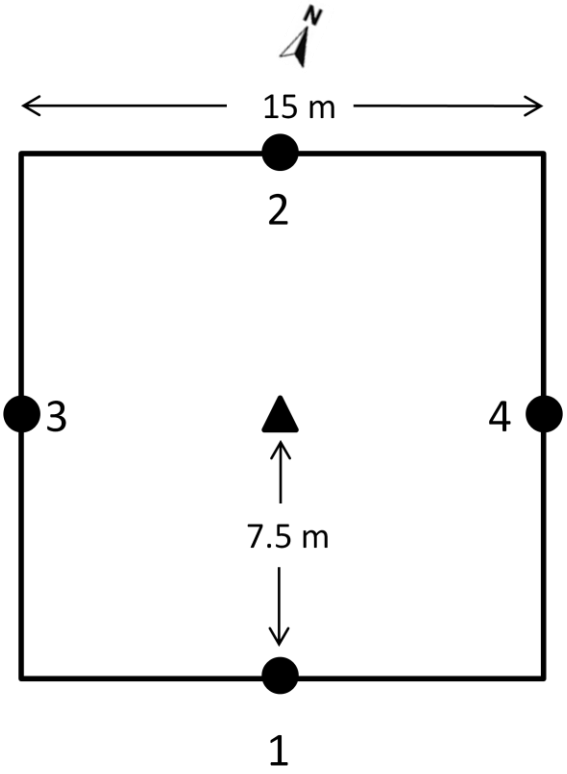

Figure 2.3 Schematic diagram showing well array at the NCRS, circles represent CMT wells and the triangle represents the pumping well.

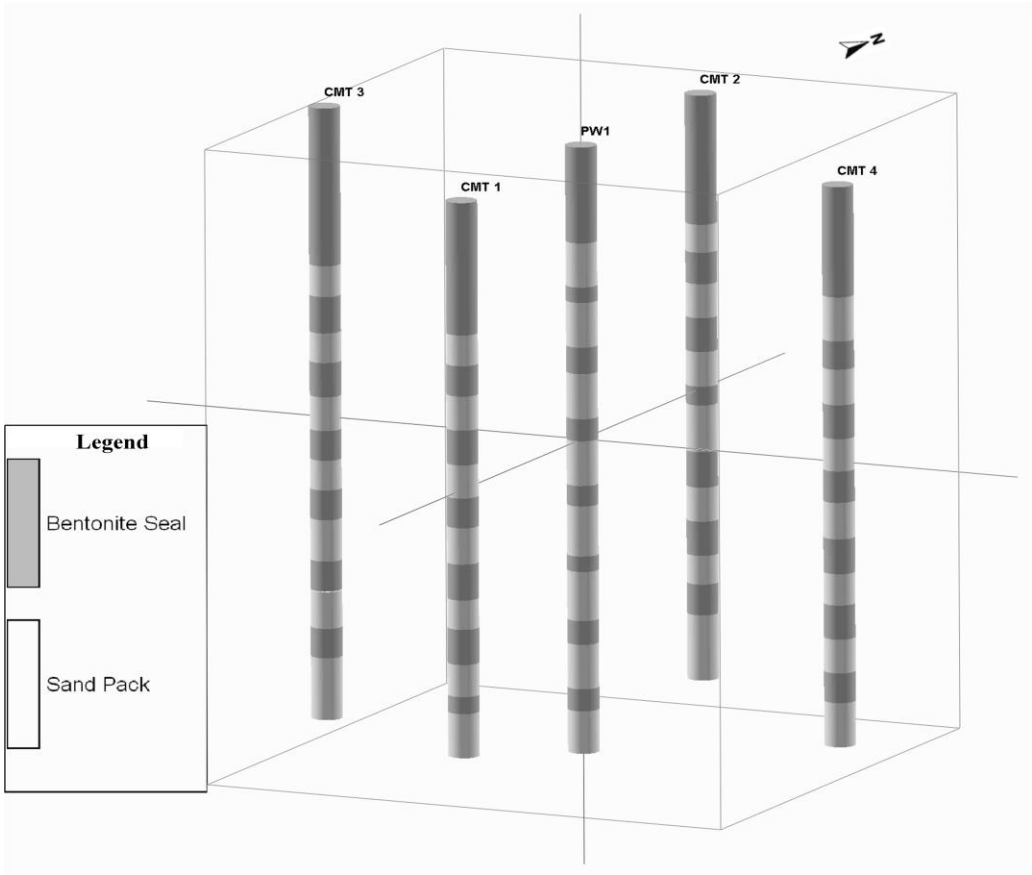

Figure 2.4 Schematic diagram showing the subsurface details of the CMT wells and the pumping well.

3. Characterization Approaches

3.1 Core Analysis

During the drilling of the wells described in the previous section, continuous sampling of the sediment at the NCRS was conducted to help characterize the geology below the site. The core samples were obtained using a 4" split spoon sampler that was driven in front of the drill head in an effort to collect representative samples. Figure 3.1 shows the intervals of successfully recovered core with depth, as well as the overall sample recovery percentage for each of the wells drilled at the NCRS. This figure shows that overall there was good sample recovery, although there are periodic gaps in these profiles that correspond to the elevation of aquifer units. This is a common challenge when using split spoon samplers because of the tendency of non-cohesive soil to fall out of the spoon while it is being raised to the surface. Sand traps installed on the sampler are designed to avoid this problem but are often ineffective in retaining the entire sample. Information about missing intervals was provided by sand and gravel that became lodged on the sampler and made it to surface, and by intact aquifer sections that were retained in the sampler due to the presence of underlying cohesive units.

The sediment core analysis protocol consisted of two major components: traditional soil description (to standardize the field logs) and grain size analysis (for K determinations). The soil description process began by opening the core storage tubes and photographing the sediment while it was relatively undisturbed. An identification card and metre stick were included in the photographs for organizational and scale purposes (Figure 3.2). The core was then halved along its length and identified using the Unified Soil Classification System (ASTM., 1985), along with other pertinent soil descriptors. One grain size analysis sample was extracted from every type of soil identified with intermediate samples being taken when significant changes in physical appearance within a single soil type were observed. If the grain size distribution appeared to remain consistent from the end of one core tube into the top of the following tube, a sample was taken from both tubes. Permeameter samples were extracted at 0.1 m increments for hydraulic conductivity testing, although problems encountered while testing very fine grained materials resulted in the extraction of samples at a reduced frequency for these sediments (see Section 3.1.2).

Grain size analysis of the samples was conducted using the ASTM protocol D 422-63 (ASTM, 2007). This involved passing a known mass of oven dried soil through a series of sieves and recording the mass of sediment retained on each sieve. The fine grained (<75 μm) fraction of the sediment was quantified via hydrometer analysis and combined with the sieve data to produce grain size curves for each soil type. An example grain size distribution from a depth of 4.41 m in CMT-4 is included as Figure 3.3. The results of this grain size analysis, included in Appendix B as Table B1 – Table B5, were used to build cross-sections illustrating the detailed geology of the study site (Figure 3.4).

In general, the grain size analysis results reinforce the existing geologic model for this area. The main units of the system shown in Figure 3.4 are an upper aquitard, upper aquifer, middle aquitard, lower aquifer, thick clay sequence and finally the dense Catfish Creek Till. The upper aquitard, composed of clayey silt, has a base located at approximately 333.5 mASL and is highly variable across the site ranging in thickness from 0.09 – 0.59 m. The base of the upper aquifer is located at approximately 331.5 mASL and is fairly consistent in grain size (silty sand to sand) and in thickness (1.02 – 2.1 m). The base of the middle aquitard is located at 330.5 – 331.0 mASL and is of variable thickness as it ranges from being absent to being 1.23 m thick. The lower aquifer appears to be discontinuous across the site as it was not encountered in CMT-2 and CMT-4, but was present at about 330.0 mASL in the pumping well, CMT-1 and CMT-2. It is a coarser deposit than the upper aquifer having grain size that ranges from sand to gravel as it coarsens downwards. The thick clay deposit below the lower aquifer was present in all wells and below this, the Catfish Creek Till was encountered in the pumping well (324 mASL), in CMT-2 (324.6 mASL) and in CMT-3 (323.3 mASL). Above these major units, additional heterogeneity exists as the geology switches from silt to silt and clay to clayey silt frequently and over short distances (Figure 3.4).

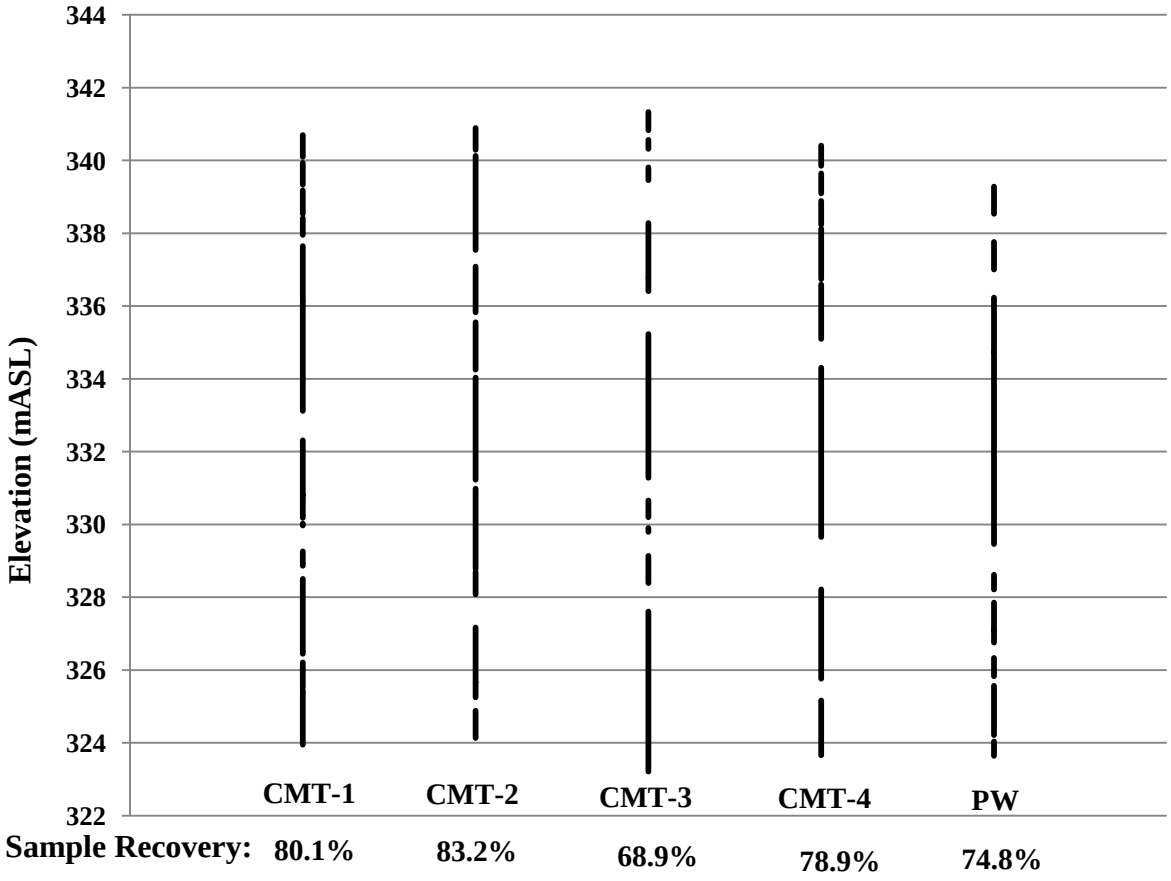

Figure 3.1 Sample recovery details for all wells drilled at the NCRS including the percentage of overall sample recovery for each well. Note the gaps the sampling record thought to correspond to the two aquifer units at the NCRS

Figure 3.2 An example of the sediment core photographs taken during core analysis.

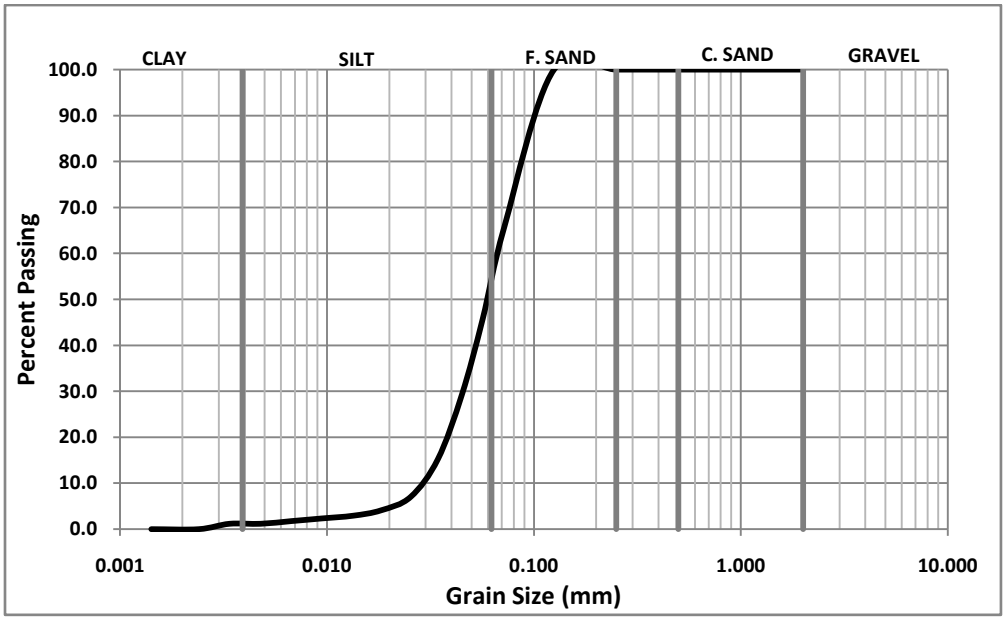

Figure 3.3 Example grain size distribution curve for sample 34b (CMT- 4).

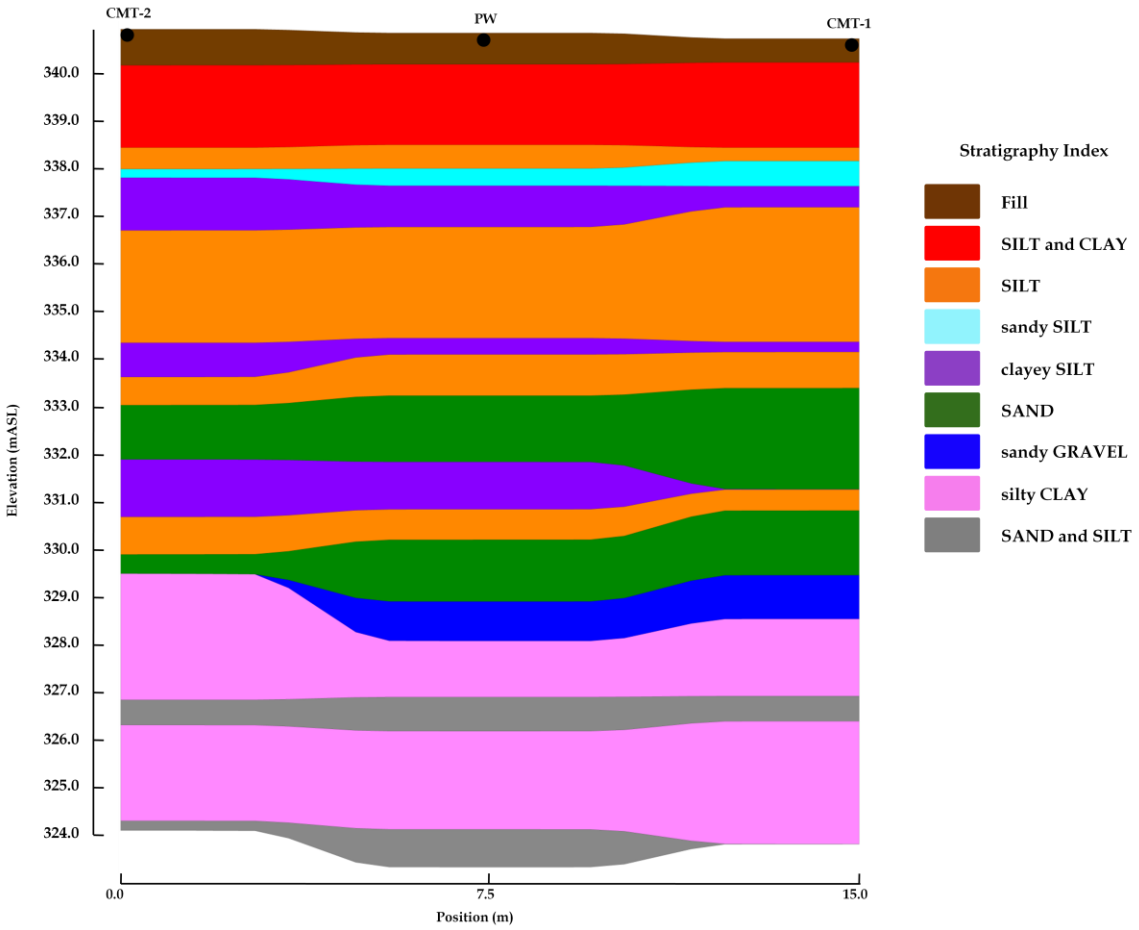

Figure 3.4 North-South cross-Section showing the geology below the NCRS. Well locations are denoted with black circles.

3.1.1 Hydraulic Conductivity Estimation - Grain Size Data

Estimating K from grain size distributions is a convenient approach that has received significant attention in the literature (Alyamani and Sen, 1993; Bear, 1972; Bedinger, 1961; Cosby et al., 1984; Eggleston and Rojstaczer, 2001; Harleman et al., 1963; Hazen, 1911; Kozeny, 1927; Krumbein and Monk, 1943; Puckett et al., 1985; Ross et al., 2007; Shepherd, 1989). The popularity of this method is related to the cost efficiency of obtaining a detailed vertical profile of K estimates by applying empirical relationships to grain size data. This eliminates the need to install, develop and slug test multi-screened wells, which requires man hours, equipment and drilling expertise. However, the heterogeneous nature of the NCRS geology represents a challenge when applying this estimation technique, as a majority of the equations presented in the literature were derived based on samples with a grain size of coarse silt or larger (see above references). As one would expect, an analysis of several of these equations by Bradbury and Muldoon (1989) suggested that a given equation tends to work best for the soil it was derived for and not necessarily very well for other types. Therefore, in order to characterize the range of hydraulic conductivities at the NCRS, two equations were selected to estimated K values: Hazen (1911) for coarse grained material and Puckett et al. (1985) for fined grained soil, with the expectation of assembling a dataset for each well where K was estimated specifically for each soil type. These equations are as follows:

Hazen: $$K = C(d_{10}^2) \text{ (cm/s)} \quad (1)$$

where *C* is a coefficient based on grain properties and d_{10} is the grain size where 10% of the sample is finer.

Puckett et al.: $$K = 4.36x10^{-5} * e^{(-0.1975*\%cl)} \text{ (m/s)} \quad (2)$$

where *%cl* is the percentage of the total sample finer than 0.002 mm. Both of these equations were utilized to estimate K from 269 grain size distributions. The physical location of each sample is shown on Figure 3.5. As a first approach to investigate the range of grain sizes that each equation could be reliably applied to, both equations were used to estimate K for each grain size distribution. The extension of the Puckett et al. equation beyond its intended range was straight forward because it only depends on the percentage of clay in the sample; however, the *C* coefficient in Hazen's equation creates difficulty in extending this equation. The appropriate use of *C* can be found in Table B6 in Appendix B. This shows that information on an appropriate value for *C* is not available for grain sizes finer than very fine sand. Therefore, for the purpose of this initial approach the minimum value

of C = 40 was used for all silt and clay samples. The results of these calculations are presented as log10 K (m/s) in Figure 3.6 and in Appendix B as Table B7 – Table B11. These estimates reflect the highly variable geology described in Section 3.1, demonstrated by the range in $\log_{10}$ K and variance values from -3 to -11 and -4 to -10.5 and 2.74 and 1.94 for the Hazen and Puckett datasets, respectively (Table 3.1). This variability in K values is reflected over short distances in places, where K changes several orders of magnitude within a 1 metre elevation change, likely at the transition between an aquifer and aquitard. The discontinuous nature of the alternating aquifer/aquitard pattern is also reflected in this data as no two datasets have the same pattern of variation with depth (Figure 3.6). Between equations, the datasets are clearly independent as the Puckett et al. equation, with a mean of -5.69 consistently estimates higher conductivity than those made by the Hazen equation, which yielded a mean of -7.63. It should be noted that the high values at the bottom of the PW, CMT-2 and CMT-3 datasets are likely artificially high, as the dense, partially saturated Catfish Creek Till was located at this elevation. Also included in these plots are the K estimations from the permeameter tests for comparison purposes (a full explanation of how these data were obtained can be found in the subsequent section). The permeameter data suggest that the Hazen equation provides reasonable estimates of K beyond the sandy material from which it was derived. The evidence for this can be seen above approximately 328 mASL, in each of these figures, where the pattern of change in the permeameter and Hazen datasets is very similar, despite the fact that there are several units above this elevation that contain a significant amount of silt and clay. Below 328 mASL, the permeameter data is much better approximated by the Puckett et al. estimations and in general, the Hazen estimations appear to be under estimations (Figure 3.6). Based on the grain size distributions, the geology below 328 mASL is predominantly clay and above this elevation clay is largely present as a secondary or tertiary percentage in the overall grain size distribution, suggesting that the Puckett et al. equation works most effectively when clay is the main component of a soil. The possibility was considered that the Hazen equation best represents K for all of the soil types at NCRS and that the estimations from the Puckett et al. equation and the permeameter tests are erroneous. However, the analysis of slug test data presented in Section 0 indicated that the values below 328 mASL from the permeameter test data are more realistic than those from the Hazen equation and therefore the Puckett et al. values were considered to be more representative for the clay-rich samples. Based on this analysis, datasets were built for each well using values estimated from Hazen's equation for all samples where clay constituted a minority

component and estimations from the Puckett et al. equation were used for the samples where clay was the majority component.

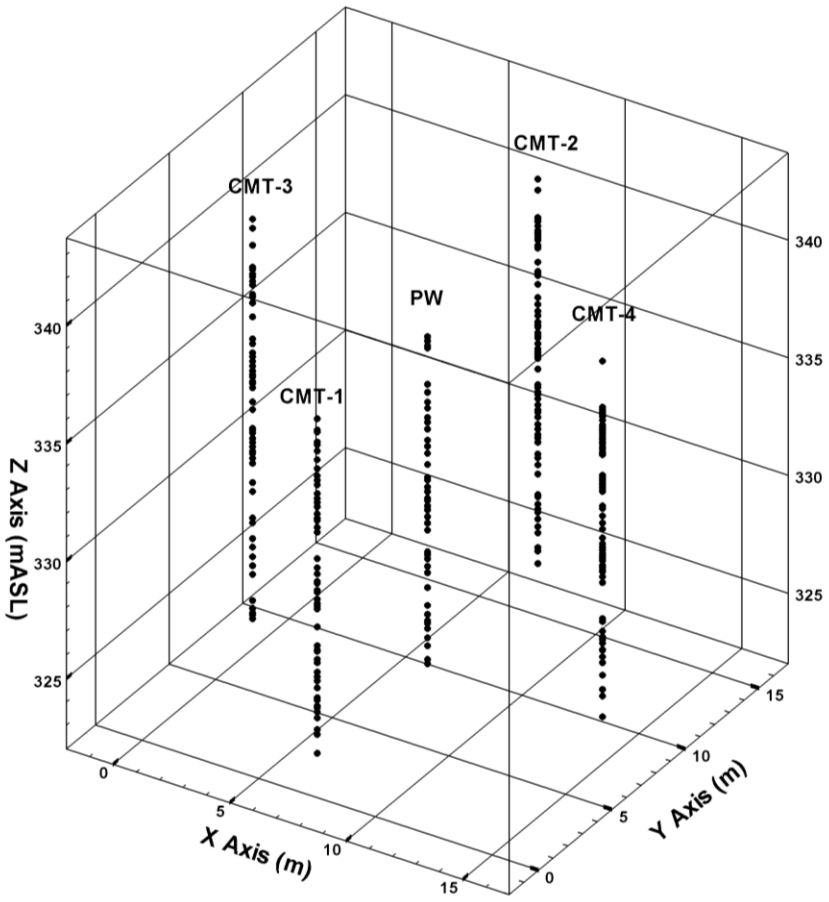

Figure 3.5 Distribution of grain size samples used to estimate K from empirical equations.

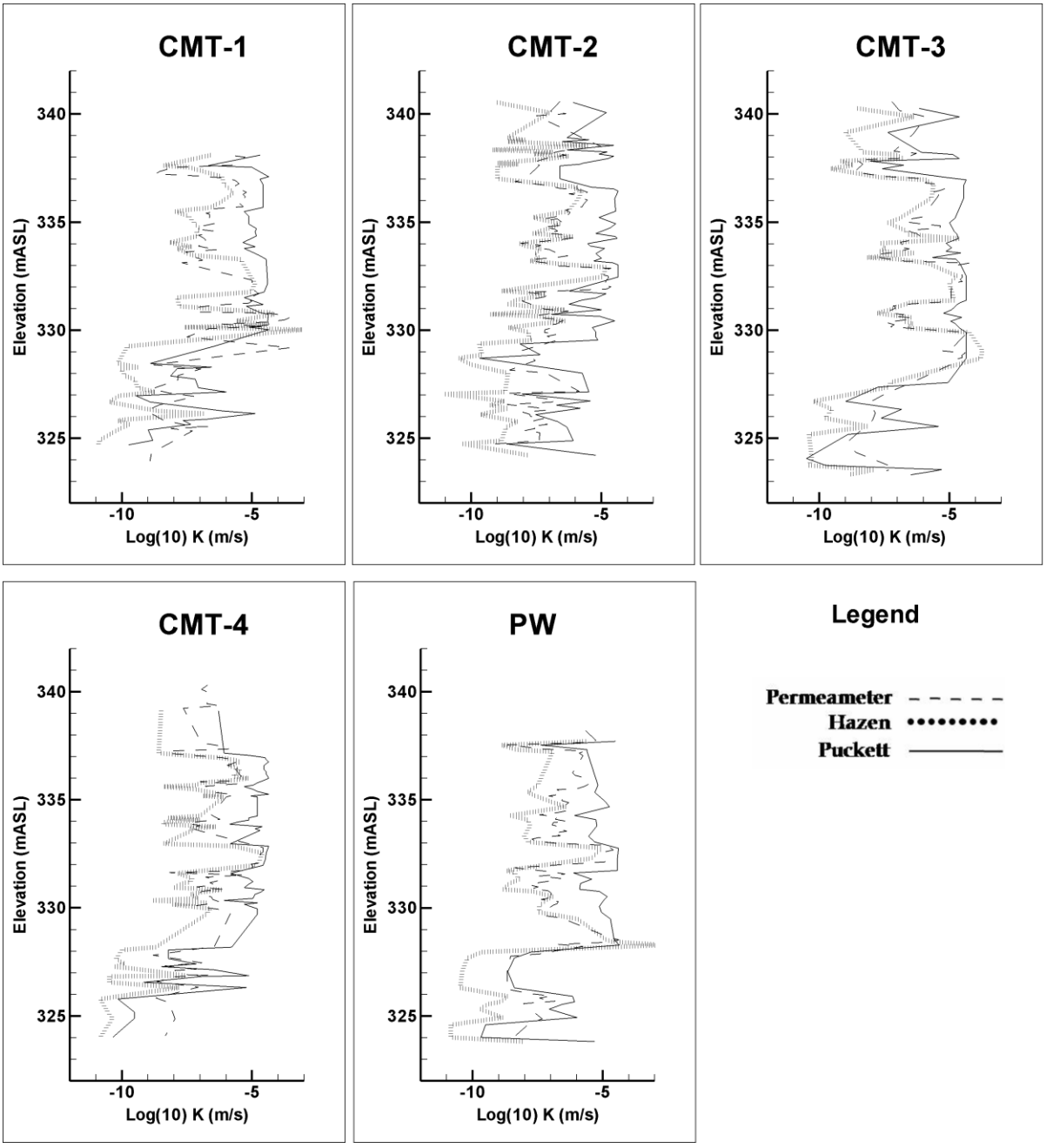

Figure 3.6 Hydraulic conductivity estimates from empirical equations and falling head permeameter tests for all wells at the NCRS.

Table 3.1 Descriptive statistics calculated for K values estimated using empirical equations.

Statistical Parameter	Hazen Log_{10} K (m/s)	Puckett et al. Log_{10} K (m/s)
Geometric Mean	-7.63 (2.3E-08)	-5.69 (2.0E-06)
Median	-7.64 (2.3E-08)	-5.13 (7.4E-06)
Standard Deviation	1.69 (1.6E-04)	1.45 (1.4E-05)
Sample Variance	2.85 (2.7E-08)	2.09 (2.0E-10)
Kurtosis	-0.35 (213.6)	1.32 (-0.458)
Skewness	0.13 (14.22)	-1.45 (0.936)
Range	8.40 (2.5E-03)	6.13 (4.4E-05)
Minimum	-11.00 (1.0E-11)	-10.50 (3.2E-11)
Maximum	-2.60 (4.2E-03)	-4.36 (4.4E-05)
n	269	269

3.1.2 Hydraulic Conductivity Estimation – Permeameter Tests

The falling head permeameter testing followed the ASTM protocol D 5084-03 (ASTM, 2003) and Oldham (1998). The first step in the procedure was to weigh the oven dried sediment sample and then load it into the permeameter cell (1), ensuring even grain size distribution (Figure 3.7). Carbon dioxide was then passed through the sample to displace the oxygen in the sediment pores. This gas is much more soluble then oxygen, so its presence ensures that full saturation of the sample occurs. Wetting of the sample was initiated by pumping de-aired water through the bottom of the permeameter cell (4). After passing through the sample, the water filled the remaining space in the permeameter cell and was raised to a selected point in the manometer tube, suspended above the permeameter cell (5). Each trial began by opening the outlet valve (6), allowing water to flow through the permeameter cell via gravity drainage. The time required for the water level to fall a set distance in the manometer tube was recorded and the test was repeated in triplicate. The test results were translated into a hydraulic conductivity estimate using the following equation (Freeze and Cherry, 1979):

$$K = \frac{aL}{At} ln \frac{H_0}{H_1} \quad (3)$$

where a is the cross-sectional area of the manometer, L is the sample thickness, A is the cross-sectional area of the sample tube, t is the average time of three trials, H_0 is the total head at the start of the test and H_1 is the total head at the end of the test.

The periodic presence of very fine grained sediments in the NCRS soil cores caused difficulties during permeameter testing. Soil having a d_{10} grain size of silt or larger ran well in the permeameter, but soils with a d_{10} in the clay range became problematic. In these cases, pressure tended to build up in the line between the pump and the sample cell (Figure 3.7) eventually causing the sample to breach the upper confining plate. This was avoided by using a low flow pump to saturate the clay samples, which extended the saturation process from approximately 30 minutes to upwards of 6 hours (or longer). There was also a corresponding increase in the test times. In an effort to complete the testing in a reasonable amount of time, testing of the clay-rich samples was done in duplicate, rather than in triplicate and the testing frequency was reduced from every 0.1 m to once per core tube containing a clay soil. Multiple samples were taken from tubes that contained clay soils with an observable change in the grain size distribution along its length.

Results from the permeameter tests were temperature corrected from the lab ambient temperature of ~17°C to the mean annual groundwater temperature of ~7ºC, for the Waterloo area (Environment Canada, 2009). This is necessary when one considers the standard equation for hydraulic conductivity:

$$K = \frac{k\rho g}{\mu} \quad (4)$$

where k is the permeability, ρ is the fluid density, g is gravitational acceleration and μ is fluid viscosity. Two parameters in this equation, density and viscosity, are affected by temperature change and therefore the final result must be adjusted by the factor of change observed in density and viscosity. Under these conditions, this factor is given by the CRC handbook as 1.28 (Chemical Rubber Company, 1977).

The temperature adjusted results of the permeameter tests are presented as Figure 3.6 and as Table B 12-Table B 15 in Appendix B and the distribution of the permeameter data points are shown on Figure 3.8. These data follow a very similar pattern to that of the grain size K data.

The heterogeneity of the geology is well reflected, although the range in $\log_{10}$ K values is slightly narrower at -3 to -9 (m/s), the variance is smaller at 1.22 and the mean value (-6.64) falls between the Hazen and Puckett datasets (Table 3.2). As with the grain size K datasets, K values change several orders of magnitude within the space of 1 metre, at the boundary between geologic units. Considering the continuity between data sets, it could be said that these data reflect a somewhat alternating series of aquifer/aquitard units that are discontinuous across the NCRS.

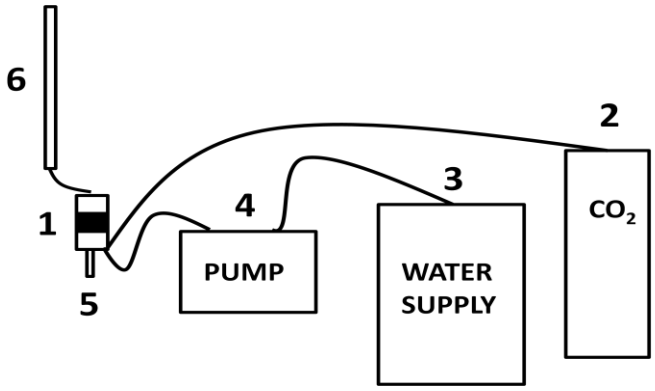

Figure 3.7 Schematic diagram of a falling head permeameter apparatus.

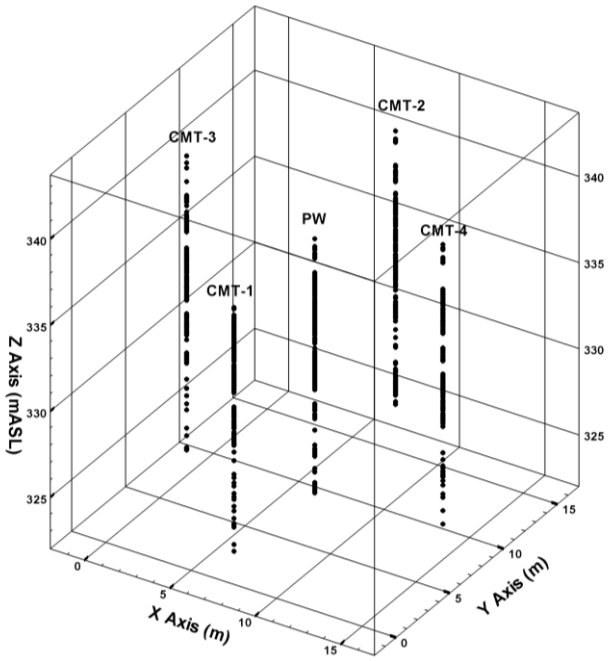

Figure 3.8 Orientation of wells at the NCRS showing the distribution of samples used for K measurements.

Table 3.2 Descriptive statistics calculated for K estimations from falling head permeameter tests.

Statistical Parameter	**Value** $\mathbf{Log_{10}}$ **K**
Geometric Mean	-6.52 (3.0E-07)
Median	-6.67 (2.2E-07)
Standard Deviation	1.14 (2.3E-05)
Sample Variance	1.29 (5.4E-10)
Kurtosis	-0.46 (96.9)
Skewness	0.15 (9.30)

Statistical Parameter	Value Log_{10} K
Range	5.69 (2.8E-04)
Minimum	-9.24 (5.75E-10)
Maximum	-3.55 (2.8E-04)
n	471

3.2 Hydraulic Conductivity and Specific Storage Estimates from Slug Tests

Slug testing the extensive network of 28 monitoring ports at the NCRS allowed for the rigorous characterization of K and S_s. Slug test data collection was fully automated using *Micron Systems* pressure transducers (accurate to approximately 0.01 m) that were wired into a central data collection/storage unit. Tests commenced following transducer emplacement, only after transducer readings indicated that water levels had returned to static conditions. A slug of water was injected into each port using a syringe containing a pre-measured 60 mL volume of water which, based on the diameter (0.01 m) of each CMT channel, corresponded to a 0.5 m rise in the static water level. A typical example of the data collected during the slug tests, taken from CMT-1.3, is presented as Figure 3.9. Slug test analysis was performed with *AQTESOLV 4.5 PRO* (Duffield, 2007), utilizing the Kansas Geological Survey (KGS) model for confined cases (Hyder et. al., 1994) and the Dagan (1978) solution for cases where the water table intersected the sand pack. By applying of these solutions the assumption is made that flow to the CMT well screens is radial in nature, despite the fact that the screen geometry is not the typical cylindrical shape. It is acknowledged that flow to the CMT's may deviate from the radial pattern; however it is assumed that this does not affect the results to the extent that these results cannot be used to characterize the NCRS geology. The KGS model is equivalent to the Dougherty-Babu (1984) solution for partially penetrating wells in a confined aquifer and it yields estimations of K and S_s. The Dagan (1978) solution, used in the unconfined zone does not provide an estimate of S_s. The K and S_s estimates from the slug tests are presented as Figure 3.10.

The slug test $\log_{10}$ K estimates range from -5 to -9, a narrower range then that of the detailed datasets obtained from grain size calculations and permeameter testing. This is reflected in the variance (1.66), which is the smallest of the three datasets, whereas the mean (-6.91) falls between the two values calculated for the grain size datasets. Some of the heterogeneity detail is lost as well, largely due to the fewer number of data points and because K values from slug tests are essentially an average value for the sediment adjacent to the screen. The aquifer/aquitard layering is somewhat discernible on Figure 3.10 but again, not to the degree observed with the large grain size and permeameter datasets (Figure 3.6). The $\log_{10}$ S_s estimates range from -2 to -7, a larger range than expected based on tabulated values for the types of soil present at the NCRS (see Section 3.4). When comparing S_s values between CMT wells, there is an absence of correlation between units. Portions of each dataset reflect the geologic heterogeneity, but no one well captures the heterogeneity like the detailed K datasets (Figure 3.6).

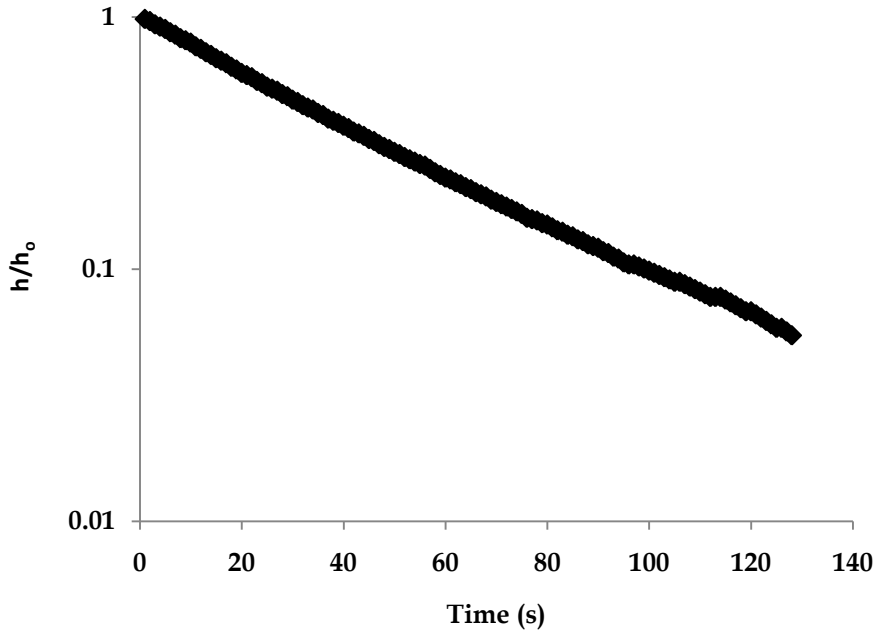

Figure 3.9 An example of slug test data collected from CMT-1.3. Slug tests were conducted on all 28 CMT ports and were used to estimate K and S_s.

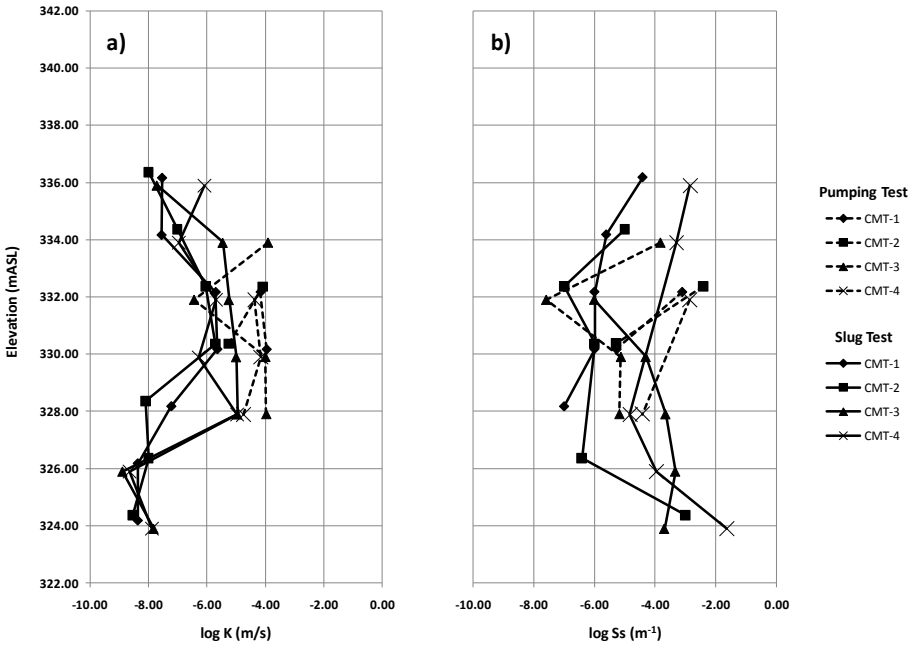

Figure 3.10 Hydraulic conductivity a) and specific storage b) estimates calculated for all CMT wells from slug and pumping test data.

3.3 Hydraulic Conductivity and Specific Storage Estimates from Pumping Tests

The pumping tests at the NCRS were conducted over a two week period in October, 2008. A total of seven tests were run, each test isolating and stressing a specific zone using an inflatable straddle packer system (Figure 3.11). The pump is situated between the packers and can draw water through the target screen when activated, discharging this water at surface through discharge piping. Tests were run for an average of 10 hours with an equal recovery period prior to the next test. The response to pumping in the various units is measured using pressure transducers installed in all 28 CMT ports, as well as above, below and in between the packers (Figure 3.11). Three of the six zones pumped (Zones 3, 4, and 5) produced an appreciable amount of water and sufficient drawdown to allow for analysis (Table 3.3). The Zone 3 screen bridges the upper aquitard and upper aquifer, Zone 4 is screened entirely in the upper aquifer, and Zone 5 is screened almost entirely in the lower aquifer.

The responses recorded for each CMT port by the pumping in these three zones are shown on Figure 3.12 - Figure 3.14. Each of the three tests produced a unique pattern of drawdown throughout

the NCRS subsurface. The pumping in Zone 3 indicated that the geology between CMT ports 1-3 in all of the wells is hydraulically connected, suggesting that the low conductivity clayey silt layer above

the upper aquifer, does little to isolate the units. This may simply be because it is acting as a 'leaky aquitard' or because it is discontinuous across the NCRS. There was evidence to support this second hypothesis during the drilling, as the thickness of this layer varied from a few centimeters thick to almost 0.5 m, suggesting the presence of discontinuity in this unit. This test also showed that the geology below approximately 326 mASL is hydraulically isolated from the above aquifer units. Drawdown responses below this elevation were either on the order of a few centimeters or were below the measurement threshold, a pattern that was consistent for all three pumping tests.

Pumping in Zone 4 caused a response in both the upper and lower aquifer units, likely because the aquitard separating these units was bridged by the Zone 4 pumping well screen, although like the aquitard above the upper aquifer, the presence of this low permeability unit across the NCRS was inconsistent. The largest drawdown values in response to this pumping were recorded in CMT-2.4 and CMT-3.3, two locations where relatively low K values were measured for this aquifer unit, when compared to CMT-1 and CMT-4. The ports that responded in CMT-1 and CMT-4 are screened in sediment with a higher measured K, likely causing the dampened response.

The most interesting aspect of the data from Zone 5 pumping was the lack of response recorded in all of the CMT ports. Based on the elevation of this zone, this test isolated the lower aquifer unit, which was absent in CMT-2 and CMT-4. It is believed that CMT-1 and CMT-3 intersect the edge of this high K gravel aquifer unit, which extends from these wells at least as far as pumping well NC17 (approximately 25 m to the south and not used for this study). Several ports responded quickly to the pumping of Zone 5 but did not exhibit large drawdown, indicating that the geology is hydraulically connected and capable of yielding sufficient water to meet the demand of the pump.

One additional pattern observed in the drawdown data from all tests, but most pronounced in the Zone 3 test was the increase in aquitard hydraulic head, in response to pumping, or 'reverse water level fluctuation'. The phenomenon was first observed by Verruijt (1969), who named it Noordbergum, after the area in the Netherlands where he was working. It is caused by the

difference in the pore elasticity between aquifer and aquitard units and is not accounted for in any of the conventional pumping test analysis solutions. Therefore, the data from these ports could not be analyzed for K and S_s values.

AQTESOLV 4.5 PRO (Duffield, 2007) was again used to calculate K and S_s estimates for the zones screened by the CMT ports, based on the drawdown data. A majority of the estimates were calculated using the Hantush leaky aquitard solution, which considers storage in the aquitard (Hantush, 1960). This aquifer geometry can be explained by the results of the drilling program where it was shown that the aquitard units were discontinuous across the NCRS and were clay-poor in many locations. This aquitard pattern unfortunately violates the assumption in Hantush's solution that the aquitard is competent and infinite in extent; however, the complex nature of the geology does not fully satisfy any of the solutions. This method was therefore considered the best available approach for analyzing this dataset. Estimates were not calculated for every port, as the Noordbergum and other irregular responses yielded poor matches to the theoretical curves available in *AQTESOLV*. The resulting K and S_s estimates are included with the slug test estimates on Figure 3.10. The sparse nature of this data makes it difficult to directly compare these data to the values calculated from the previous methods discussed, although it is obvious that the K estimates are consistently larger than those from the slug tests. There is no clear pattern between the pumping test K values and the grain size data. In general, the Hazen equation appears to predict values close to those from the pumping test more consistently, but there are several instances where the pumping test values are either significantly larger or smaller than those from the Hazen dataset. When compared to the permeameter data, the pumping test K values are consistently higher, commonly by a few orders of magnitude. This pattern of K increasing with measurement scale has been observed previously in studies evaluating the different methods of K measurement in a variety of geologic settings (Bradbury and Muldoon, 1989; Butler, 2005; Clauser, 1992; Guimerà et al., 1995; Illman, 2006; Illman and Neuman, 2001, 2003; Martinez-Landa and Carrera, 2005; Schulze-Makuch and Cherkauer, 1998; Zlotnik et al., 2000). The S_s data all fall within the range of values calculated from the slug test data, but again, the sparse nature prevents quantitative comparison of values or qualitative comparison of patterns with depth.

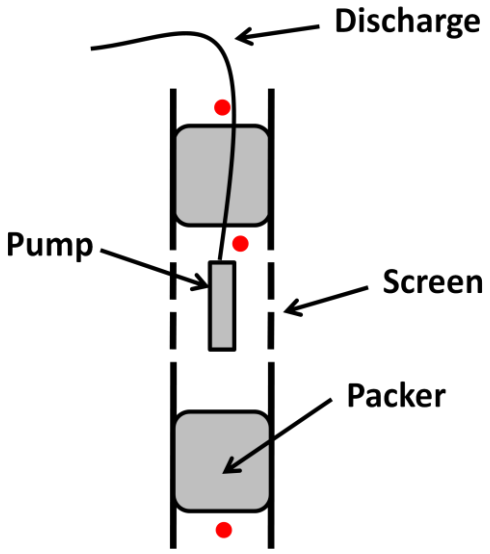

Figure 3.11 Schematic of pump and packer system. Dots indicate the position of pressure transducers used to measure pressure changes resulting from pumping.

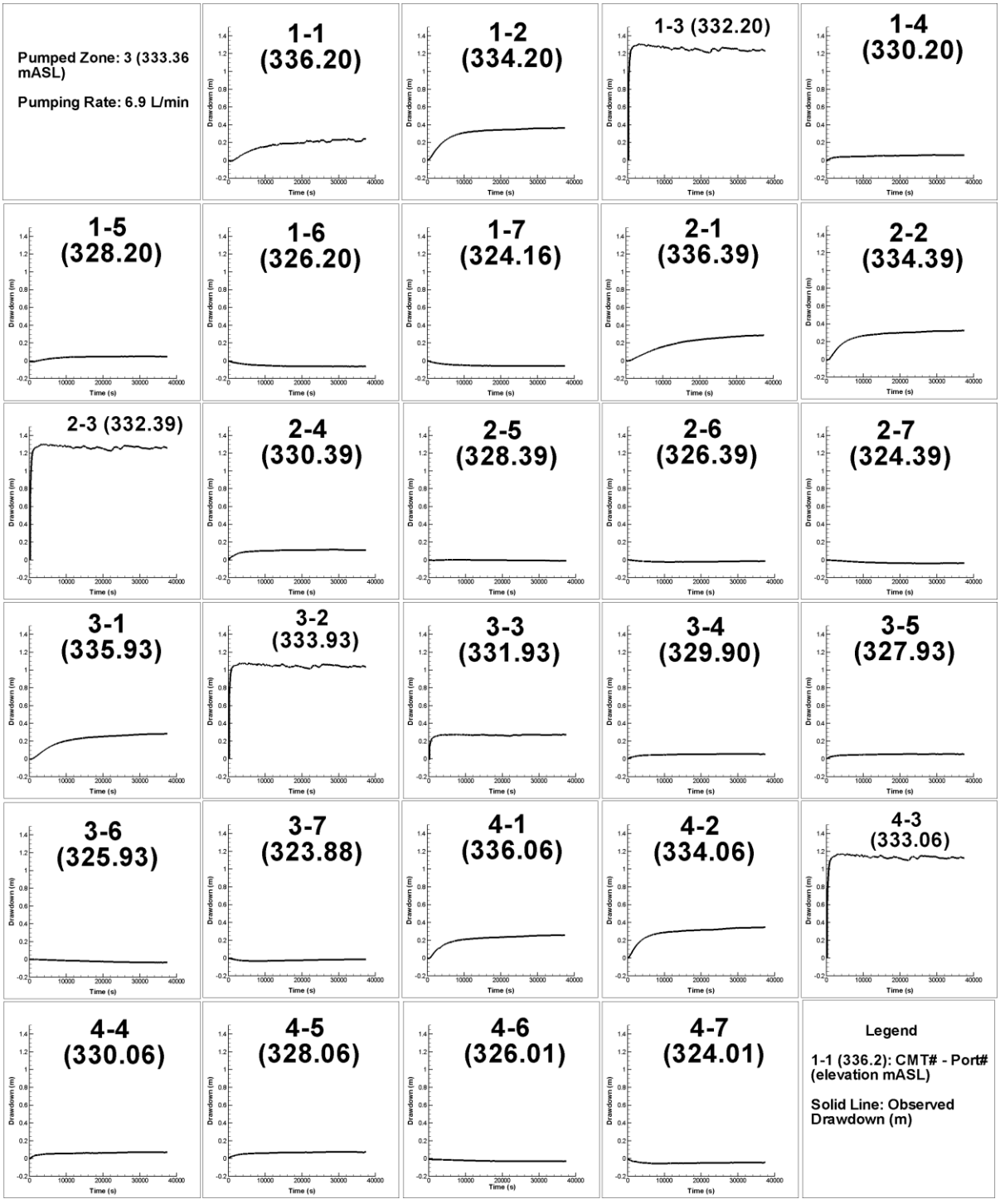

Figure 3.12 Drawdown observations in each CMT port during the Zone 3 pumping test. Time (s) is on the X-Axis and drawdown (m) is on the Y-Axis.

Figure 3.13 Drawdown observations in each CMT port during the Zone 4 pumping test. Time (s) is on the X-Axis and drawdown (m) is on the Y-Axis.

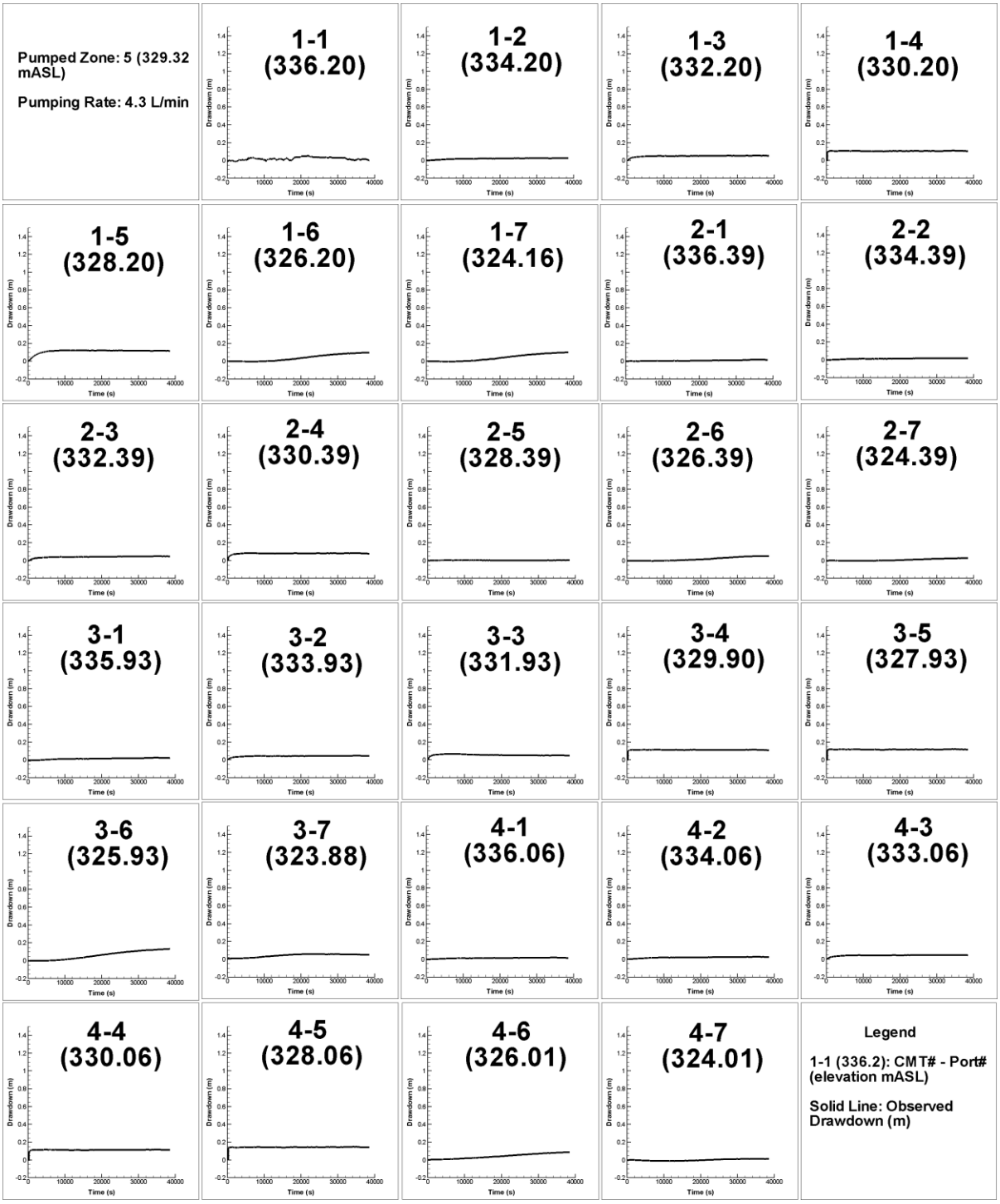

Figure 3.14 Drawdown observations in each CMT port during the Zone 5 pumping test. Time (s) is on the X-Axis and drawdown (m) is on the Y-Axis.

Table 3.3 Details of the pumping tests conducted at the NCRS.

Zone Number	Elevation of Screen Midpoint (mASL)	Pumping Rate (L/min)	Maximum Drawdown (m)
2	335.25	0.166	0.065
3	333.14	6.905	1.260
4	331.11	4.143	0.682
5	329.15	4.440	0.145
6	327.06	0.132	0.068
7	325.01	1.200	0.206

3.4 Comparison of the Characterization Techniques

Hydraulic conductivity values were obtained for the NCRS via four different techniques: pumping test analysis, slug test analysis, permeameter tests and empirical equations using grain size data. For any one geologic unit, the methods produced a range of values (Figure 3.15). Attempting to use these data to assess the tendencies of the individual techniques is difficult, as there are no patterns that fully characterize their behavior, however there are trends. In the high K zones, the most notable pattern is the high estimation by the Puckett et al. method. These values are considered to be poor estimates, and this is expected when this equation is used for analysis of clay-poor samples. In all of the high K zones considered, pumping test values are one of the top three highest estimates. This is commonly reported in studies comparing K estimation methods (Bradbury and Muldoon, 1989; Butler, 2005). In three of the five sub-datasets, the slug test estimate is the lowest value, which contradicts both Bradbury and Muldoon (1989) and Butler (2005), who reported that slug test values were larger than those estimated from both permeameter tests and grain size empirical equations. The permeameter tests yield the lowest estimation in the remaining two elevations, which is expected based on these previous studies.

In the case of the low K units, there is far more agreement between methodologies, with the exception of the analysis at 326 mASL where the Puckett et al. equation produced an outlier (Figure 3.15). At the other two elevations, the Puckett et al. estimation is very close to that from the falling head permeameter. This reinforces the decision to use the Puckett et al. values for the

clay-rich samples; however it should be noted that the estimates from the Hazen equation are not significantly different at the three selected elevations.

Recognizing the inconsistency in K estimates between methods, Muldoon and Bradbury (1989) suggest that a method which fits the scale of a study should be selected in order to obtain the most representative values. In this case, where the goal is to simulate pumping tests using a transient flow model, this rule of thumb would select the pumping test K values as being most appropriate. However, the pumping tests do not provide data at the level of detail likely required to simulate the heterogeneous flow at the scale being investigated here. Furthermore, in a non-academic study, pumping tests would not yield a detailed set of hydraulic parameters as they can only be determined for units that are screened by an observation well and, outside of research studies, a given study site would not likely be this heavily instrumented. In a typical sparsely instrumented site, pumping test analysis would normally only be able to produce enough hydraulic data for a homogeneous, or at best a coarsely layered model.

The pumping and slug tests were the two sources of specific storage estimates for this study. As with the pumping test K estimates, S_s values were obtained for those units that produced drawdown data that could be accurately analyzed. With the slug test data, S_s estimates were available for screens that were fully saturated and could be analyzed using the KGS model. The S_s estimates from both methods are tabulated, along with common values from the literature in Table 3.4. This comparison indicates that these estimates do not match well with expected values based on typical tabulations, a result that has been documented previously by Butler (1998), stating that S_s estimates can be very difficult to obtain from slug test analysis. The accuracy of these estimates was further evaluated through flow modeling in *Hydrogeosphere* (see Section 5.).

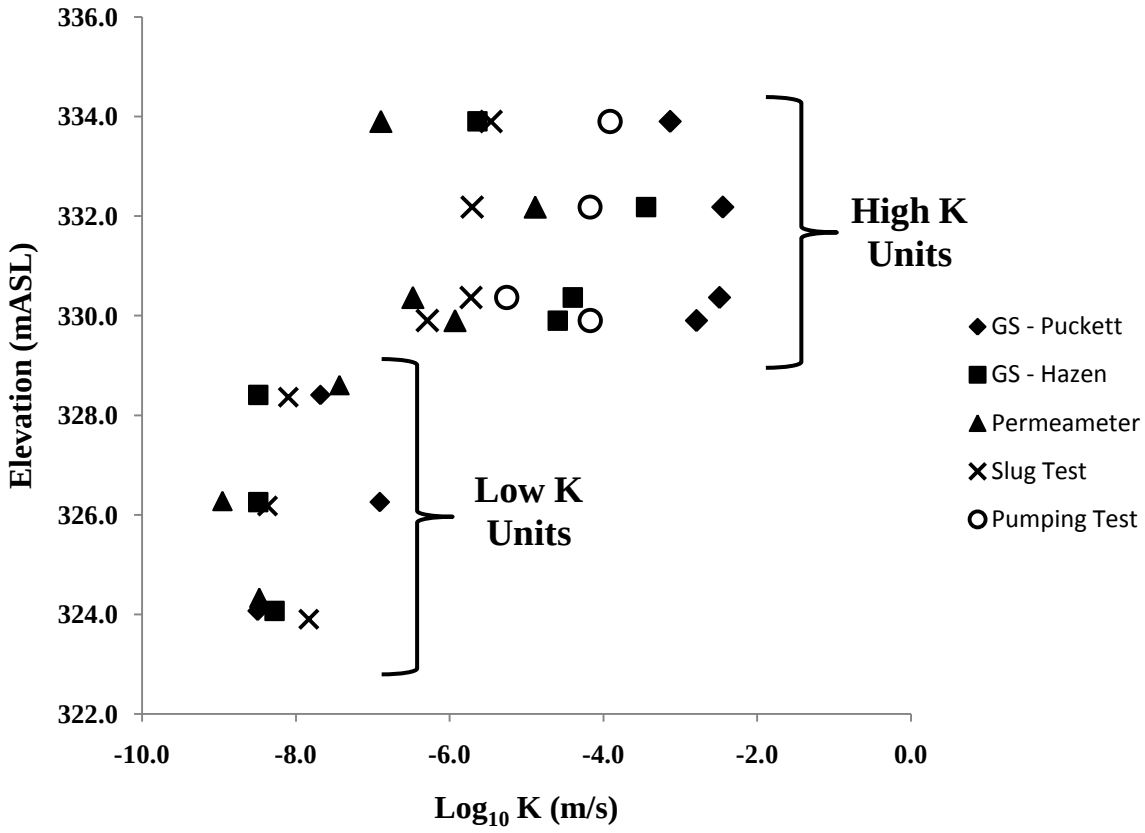

Figure 3.15 Comparison of K values obtained via the four selected methods in both high and low K units. Note that GS stands for grain size method.

Table 3.4 Comparison of slug and pumping test S_s values to tabulated values.

Port	Elevation (mASL)	Log_{10} Specific Storage			Corresponding Soil Type
		Slug Test	Pumping Test	Tabulated Range*	
CMT-1.1	336.176	-4.41 (3.9E-05)	-	-2.99 to -3.31 (1.0E-03 to 4.9E-04)	loose sand
CMT- 1.2	334.176	-5.61 (2.5E-06)	-		
CMT- 1.3	332.18	-6.00 (1.0E-06)	-3.11 (7.8E-04)	-3.69 to -3.89 (2.0E-04 to 1.3E-04)	dense sand
CMT- 1.4	330.18	-6.00 (1.0E-06)	-5.28 (5.2E-06)		
CMT- 1.5	328.176	-7.00 (1.0E-07)	-		
CMT- 2.2	334.36	-5.00 (1E-05)	-		
CMT- 2.3	332.363	-7.00 (1.0E-07)	-2.42 (3.8E-03)		
CMT- 2.4	330.363	-6.00 (1.0E-06)	-5.30 (5.0E-06)	-2.99 to -3.31 (1.0E-03 to 4.9E-04)	loose sand
CMT- 2.6	326.363	-6.42 (3.8E-07)	-	-3.69 to -3.89 (2.0E-04 to 1.3E-04)	dense sand
CMT- 2.7	324.363	-3.00 (1.0E-03)	-	-1.69 to -2.59 (2.0E-02 to 2.6E-03)	plastic clay
CMT- 3.2	333.903	-	-3.82 (1.5E-04)	-3.69 to -3.89 (2.0E-04 to 1.3E-04)	dense sand
CMT- 3.3	331.903	-6.00 (1.0E-06)	-7.59 (2.6E-08)		
CMT- 3.4	329.903	-4.31 (4.9E-05)	-5.12 (7.5E-06)	-3.99 to -4.31 (1.0E-04 to 4.9E-05)	dense sandy gravel
CMT- 3.5	327.903	-3.66 (2.2E-04)	-5.17 (6.7E-06)		
CMT- 3.6	325.903	-3.34 (4.6E-04)	-	-1.69 to -2.59 (2.0E-02 to 2.6E-03)	plastic clay
CMT- 3.7	323.903	-3.70 (2.0E-04)	-		

Port	Elevation (mASL)	Slug Test	Pumping Test	Tabulated Range*	Corresponding Soil Type
CMT- 4.1	335.898	-2.85 (1.4E-03)	-	-3.69 to -3.89 (2.0E-04 to 1.3E-04)	dense sand
CMT- 4.2	333.898	-3.30 (5.0E-04)	-	-1.69 to -2.59 (2.0E-02 to 2.6E-03)	plastic clay
CMT- 4.3	331.898	-	-2.87 (1.4E-03)	-3.69 to -3.89 (2.0E-04 to 1.3E-04)	dense sand
CMT- 4.5	327.898	-4.84 (1.5E-05)	-4.43 (3.7E-05)		
CMT- 4.6	325.898	-3.96 (1.1E-04)	-		
CMT- 4.7	323.898	-1.64 (2.3E-02)	-	-1.69 to -2.59 (2.0E-02 to 2.6E-03)	plastic clay

*** Duffield, 2004 (p.510) (After Batu, 1998)**

4. Geostatistical Analysis of Hydraulic Conductivity Data

4.1 Descriptive Statistics

The ultimate goal of the geostatstical analysis of the hydraulic conductivity data was to use kriging to produce a continuous K field for use as input in a transient flow model used to evaluate the various characterization techniques. The kriging process works optimally when two criteria are satisfied: the datasets are normally distributed and the data are stationary within the domain of interest (Gringarten and Deutsch, 2001). This section will evaluate the detailed permeameter and empirical equation K datasets based on these criteria.

Previous studies have shown that hydraulic conductivity datasets follow a log-normal probability distribution, although sometimes the correlation is somewhat weak (Freeze, 1975; Turcke and Kueper, 1996; Woodbury and Sudicky, 1991). The distribution of the data in this study was investigated by plotting histograms for both datasets (Figure 4.1, Figure 4.2). The independence of the data included in the histograms was ensured by calculating the average vertical correlation length for each individual well dataset through an autocorrelation analysis. The result of these calculations was that that the average correlation length is 0.15 m, so this distance was used as the minimum separation distance for the histogram datasets. It was noted during the histogram analysis that the number of bins selected can have a significant influence on the shape of the histogram, so an effort was made to present the data in an efficient and unbiased way by calculating the appropriate number of bins using the method given by Scott (1979). A visual inspection of the resulting histograms (Figure 4.1, Figure 4.2) indicates that they follow a Gaussian distribution, but in order to assess the validity of this assumption, a Kolmogorov-Smirnov goodness-of-fit test (Massey, 1951) was performed on random sub-samples of the log-transformed datasets. This test computes the Maximum Absolute Difference (d) statistic that is compared with critical Kolmogorov-Smirnov values to determine whether or not the theoretical normal distribution is matched. The tests run for both datasets showed that at the 95% confidence level, the null-hypothesis stating that the data is *not* log-normally distributed could be rejected 100% percent of the time. Therefore, it is appropriate to analyze these datasets under the assumption that they are log-normally distributed.

The stationarity of the datasets was the second property to be investigated prior to kriging. A stationary dataset is one that has a mean and variance that are invariant of space. Table 4.1 shows that the permeameter dataset has a geometric mean that is within the same order of magnitude at each well location and that the variance has a maximum difference between well datasets of 0.9. The same

is true of the geometric means of the empirical equation well datasets, although the maximum difference in the variance values is slightly larger at 1.2. The question of whether these differences in the calculated mean and variance values are statistically significant was addressed by evaluating the mean and variance values of several random sub-samples taken from each dataset using T and F-tests. The results of these tests showed that at the 95% level of confidence, the differences in the mean and variance values were not statistically significant. Based on this result, the next stage in the geostatistical analysis was performed assuming stationarity in the datasets.

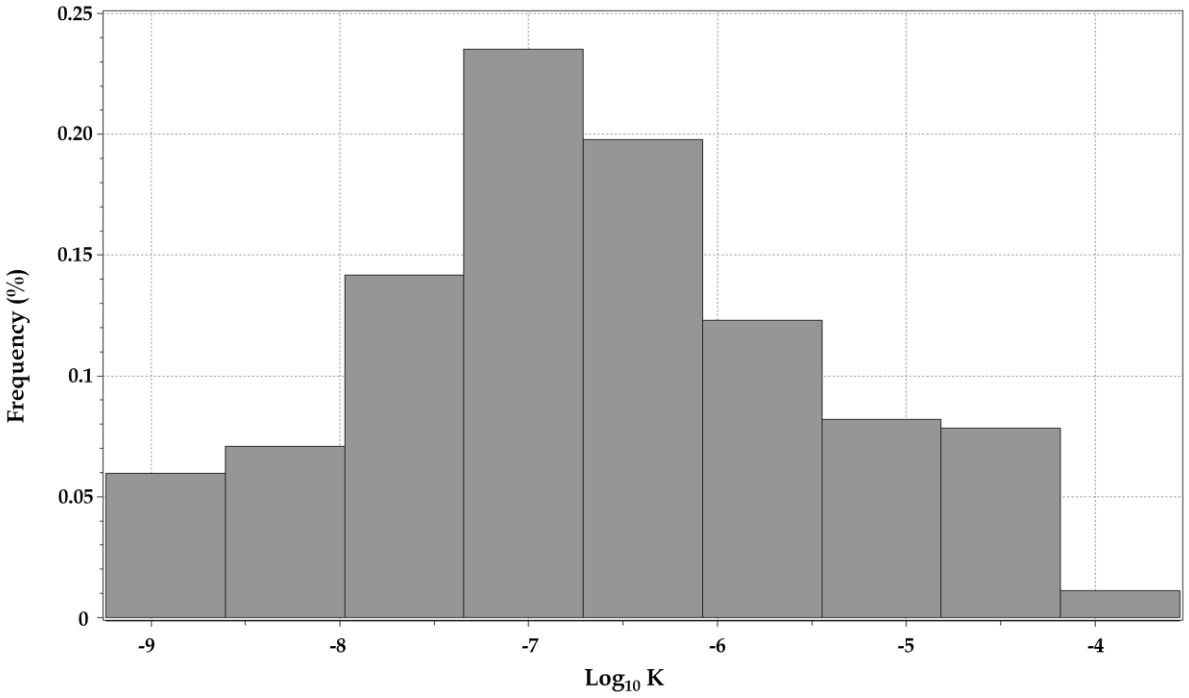

Figure 4.1 Frequency histogram of log-transformed permeameter hydraulic conductivity data.

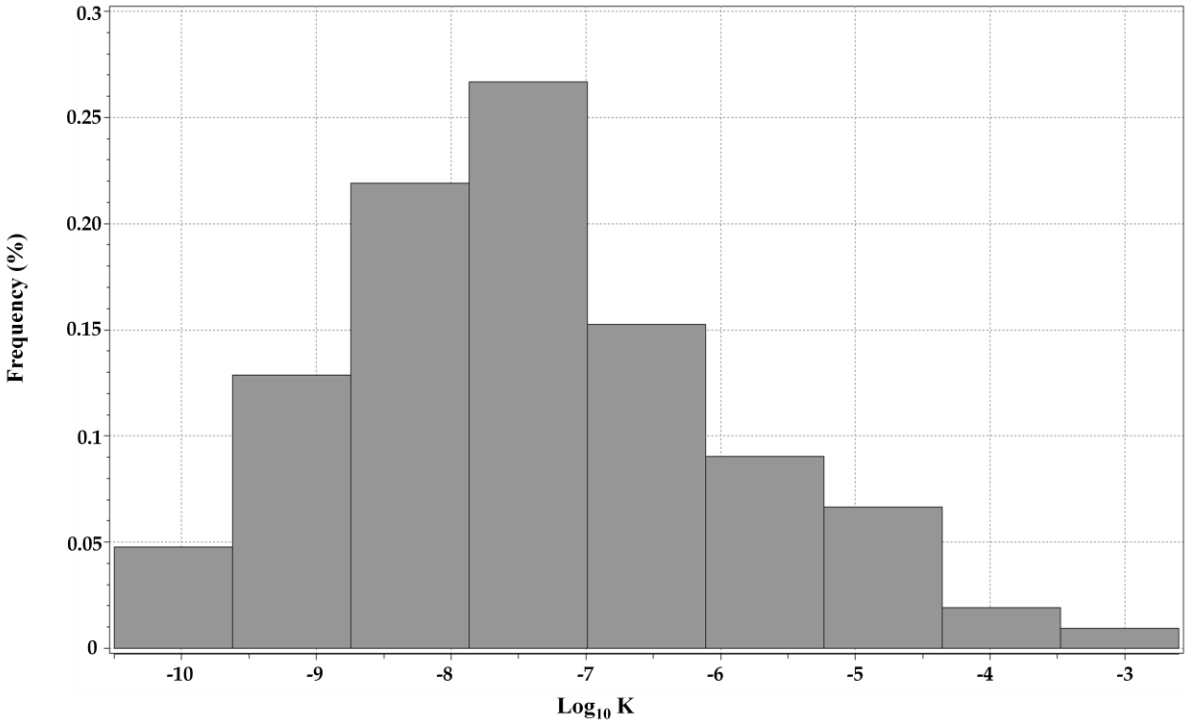

Figure 4.2 Frequency histogram of log-transformed empirical equation hydraulic conductivity data.

Table 4.1 Geometric mean and variance values for individual well datasets.

Well	Permeameter Data		Empirical Equation Data	
	Mean (m/s)	Variance	Mean (m/s)	Variance
PW	2.4E-07	0.97	4.8E-08	2.55
CMT 1	4.1E-07	1.83	2.7E-08	1.31
CMT 2	1.7E-07	1.00	9.8E-08	2.15
CMT 3	5.3E-07	1.43	4.5E-08	2.06
CMT 4	3.2E-07	1.12	9.9E-09	2.52

4.2 Variogram Modeling

The variogram, also referred to as the semi-variogram, is a popular and powerful tool in geostatistical analysis. It provides a method to investigate the manner in which a random variable of interest changes in a given domain as well as a systematic method of interpolating values for this variable where measurements are not available (Davis and Borgman, 1979). It was first described for geostatistical purposes by Matheron (1962) and has the general form:

$$\gamma(h) = \frac{1}{2N(h)} \sum_{\alpha=1}^{N(h)} [z(u_\alpha + h) - z(u_\alpha)]^2 \quad (5)$$

where *h* is the lag distance used to evaluate the data, *N(h)* is the number of pairs separated by lag *h*, u_α are the vector spatial coordinates, $z(u_\alpha)$ is the variable under consideration as a function of location and $z(u_\alpha+h)$ is the lagged version of the variable under consideration.

The variogram modeling process begins by constructing the experimental variogram, which is a measure of the dissimilarity in the variable with increasing distance between measurements (Cressie, 1993). Based on the implicit assumption of stationarity mentioned previously, the variogram further assumes that the variable under consideration can be expressed at any point in the domain as the mean value, plus a random fluctuation. In this study, the process of constructing experimental variograms, selecting the appropriate variogram models and kriging the continuous K fields was automated using a computer program called *Stanford Geostatistical Earth Modeling Software* (*SGEMS*) (Remy et al., 2008). Based on the distribution of data at the NCRS (Figure 3.5, Figure 3.8) the vertical experimental variogram was significantly more useful than the horizontal for modeling the variogram. As is commonly the case in geologic studies, the horizontal data distribution was too sparse to properly construct a horizontal variogram, unfortunately eliminating the ability to investigate the possibility of anisotropy in the dataset. The variability in the vertical direction was analyzed in *SGEMS* by calculating experimental variograms for all of the individual well datasets separately, as well as a variogram that considered all of the data in each dataset simultaneously. All of the variograms, showing the best-fit models, for the permeameter and empirical equation datasets are included as Figure A 1 - Figure A 12. The details of the best-fit models for all of the experimental variograms are included in Table 4.2, Table 4.3.

Focusing first on the permeameter variograms, it can be seen that each sub-dataset has a unique variogram based on the variation within the respective data however, there are properties

that are shared between variograms. One property shared by all variograms with the exception of CMT-1, is the cyclic pattern in the data with increasing lag distance. This pattern is commonly referred to as a 'hole effect' as it is often encountered when data is acquired 'down a borehole' (Gringarten and Deutsch, 2001). It is caused by the layered nature of the geology, which results in layers with similar K being separated by layers with distinctly different K. A second property shared by these variograms, as well as the empirical equation variograms, is the increase in data dispersion with increasing lag distance. This feature is a result of there being fewer data pairs available as input in the variogram calculation as lag distance increases, resulting in the pattern of change not being as well represented at these distances (Journel and Huijbregts, 1978). This dispersion introduces difficulty into the model fitting process, as the standard models reach a sill value that largely remains constant past the range value. This was overcome by using a truncated model fitting procedure, where data beyond the 'distance of reliability' is not considered in the modeling step. This distance of reliability is typically taken to be half of the maximum lag distance, a rule of thumb that was used here (Journel and Huijbregts, 1978). Table 4.2 shows that the models fit to the permeameter variograms were variable between the well datasets, although the exponential model was the most common choice.

The variograms calculated from the empirical equation datasets were not as well defined as the permeameter variograms, the main cause of this being the fewer number of data pairs available as input into the variogram calculation at each lag distance. It is likely that another factor of the dispersed nature of these variograms is the error in this empirical estimation technique and the fact that the equations were extended beyond the ranges of grain size that their original datasets were based on. These variograms show little, if any, indication of the hole-effect present in the permeameter variograms. Again, this may be related to the low number of pairs factored into the calculation or error in the technique. The result of these less well defined variograms is that the model fitting process is more challenging and the resulting sill estimation does not come as close to the sample variance as was seen in the permeameter variograms. In the case of both permeameter and empirical equation variograms, the model fit to the experimental variogram that considered all of the data simultaneously was selected to be the kriging model, as it was felt that these variograms best captured the overall pattern of change in the data, within the NCRS. Both of these final variograms were fit with exponential models, a model that has previously shown to be the most appropriate in other studies of hydraulic conductivity variation in aquifers (Goltz, 1991; Sudicky, 1986). The exponential model is defined as:

$$\gamma(h) = c\left[1 - \exp\left(\frac{-3h}{a}\right)\right] \quad (6)$$

where *c* is the sill, the point where the variogram stops increasing and *a* is the range, the lag distance at which the sill is reached.

As an aside, the CMT-4 variogram from the empirical equation dataset showed indications of having a trend with increasing lag distance (Figure A 10). This suggests non-stationarity in the domain, however, it is thought that this pattern is a reflection of the measurement technique rather than the geology, due to the fact that none of the other variograms showed any indication of having a trend, and T and F-tests performed suggested that the data is stationary. The kriging was therefore carried out with the assumption if stationarity in place.

Table 4.2 Details of permeameter data experimental variogram models

Dataset	Permeameter Experimental Variograms				
	Nugget	**Sill**	**Range**	**Sample Variance**	**Best Fit Model**
CMT-1	0.25	2	7	1.83	Exponential
CMT-2	0.2	0.97	1	0.97	Spherical
CMT-3	0.2	1.7	1.5	1.43	Spherical
CMT-4	0.3	1	2	1.13	Gaussian
PW	0.1	1	4	0.97	Exponential
All	0.35	1.08	4	1.29	Exponential

Table 4.3 Details of empirical equation data experimental variogram models

Dataset	Empirical Equation Experimental Variograms				
	Nugget	**Sill**	**Range**	**Sample Variance**	**Best Fit Model**
CMT-1	0.5	2	3.5	2.55	Exponential
CMT-2	0.5	0.95	3.5	1.31	Exponential
CMT-3	0.5	1.2	3.5	2.15	Exponential
CMT-4	-	-	-	2.06	-
PW	0.5	1.8	3.0	2.52	Exponential
All	0.6	1.9	10	2.09	Exponential

4.3 Kriging

Kriging, pioneered by D.G. Krige, is a geostatistical interpolation technique where a variable of interest is estimated at a specific point in space (Sen and Subyani, 1992). This is done via a regression calculation where the variogram model is used to assign weights to the surrounding points and the sum of these weights provides the estimate. There are many interpolation equations under the umbrella of kriging, including several available through *SGEMS* such as simple, ordinary, and kriging with a trend. Ordinary kriging was used for the K data in this study, in order to capture the heterogeneity of the NCRS. Ordinary kriging assumes that the statistics defining the dataset are stationary overall, however, it considers the mean in the local neighborhood of a given point in space as being constant and representative of that neighborhood (Cressie, 1993). Two continuous K fields were kriged in *SGEMS* using Ordinary Kriging, with the exponential models fit to the experimental variograms and the two detailed K datasets as input (Figure 4.3, Figure 4.4). Prior to kriging, the issue of data scarcity in some of the aquifer units was addressed. It was noted previously that several sections of core, assumed to be aquifer material were missing from the recovered samples (see Section 3.1). Consequently, K values could not be estimated at these depths via either the permeameter or empirical equation methods. In cases where there was sufficient evidence that measured values above and below the missing core were representative of the absent samples, these

values were used to interpolate the missing values. Any cases where there wasn't any direct evidence of the absent soil type, no value was included in the dataset for kriging.

The kriging process utilizes a search ellipsoid in order to identify appropriate known K data points for the algorithm and in this case the search ellipsoids were both defined by parameters of x, y = 45m, z = 4m. The results of the *SGEMS* kriging using the permeameter and empirical equation datasets are shown in Figure 4.3 and Figure 4.4, respectively. These two fields share many of the same attributes such as moderate K values from surface to approximately 5 m, the depth of the upper aquifer, where the K values increase. K then declines and reaches its lowest value in the thick clay sequence encountered in all of the boreholes. The two kriged fields also exhibit several differences with the most noticeable being the lack of a well defined upper and lower aquifer system in the empirical equation field (Figure 4.4). In fact, both aquifers are nearly absent in the vicinity of CMT-2 and CMT-4. This lack of detail is likely due to the problems encountered during sampling at this depth, mentioned previously, which led to the aquifer units being under-represented in the empirical equation dataset. Beyond the samples that couldn't be obtained, there were fewer data points in the empirical equation K dataset due to the fact that sampling for grain size analysis was done less frequently than the permeameter sampling. This likely led to the poor representation of other structures in the geology on the empirical equation K field relative to the permeameter field. The other major difference between the two K fields is the larger range of K values predicted by the empirical equation kriging, as this ranges from 10^{-4} - 10^{-11} m/s compared to the permeameter range of 10^{-4} to 10^{-9} m/s.

Also included are the variance maps that correspond to the two kriged domains (Figure 4.5, Figure 4.6). These figures show that kriged K values in the domain are less certain the further a point is from the known points measured at the wells. The variance is very low in the immediate vicinity of the wells, and remains fairly low throughout the area where the pumping test drawdown values were simulated in the modeling step. If one were to simulate drawdown outside of the square formed by the distribution of the wells, these values would have to be considered very uncertain.

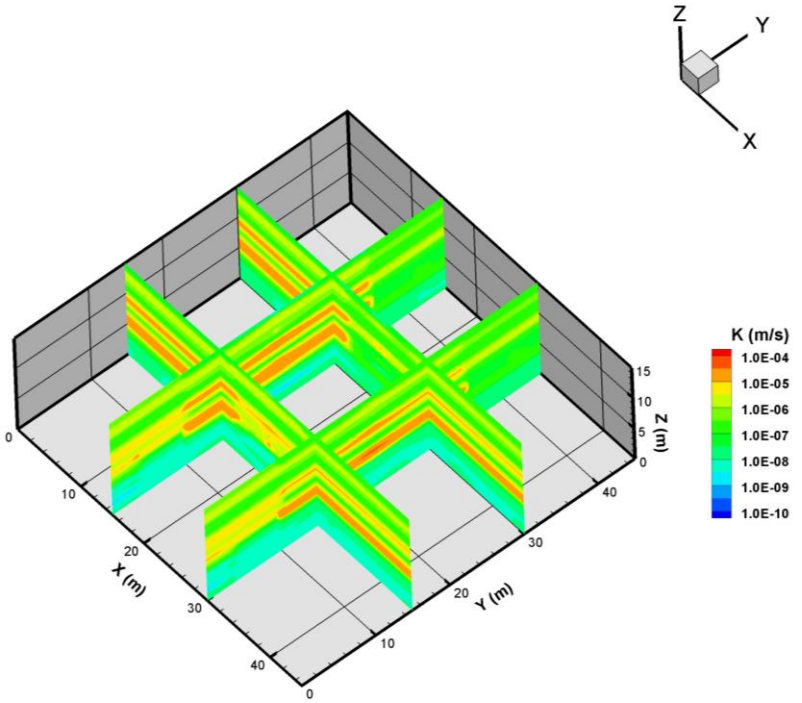

Figure 4.3 Fences showing the detail of the NCRS kriged K field, constructed using the permeameter dataset.

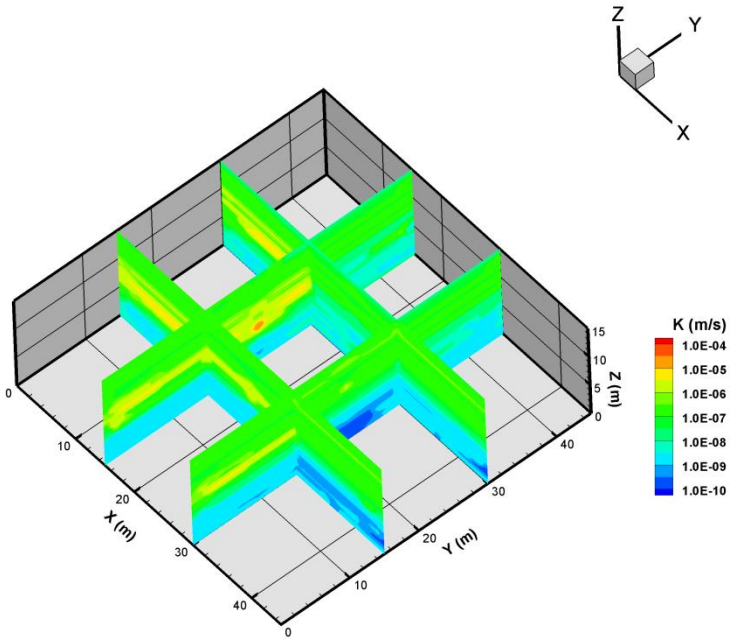

Figure 4.4 Fences showing the detail of the NCRS kriged K field, calculated using the empirical equation K dataset.

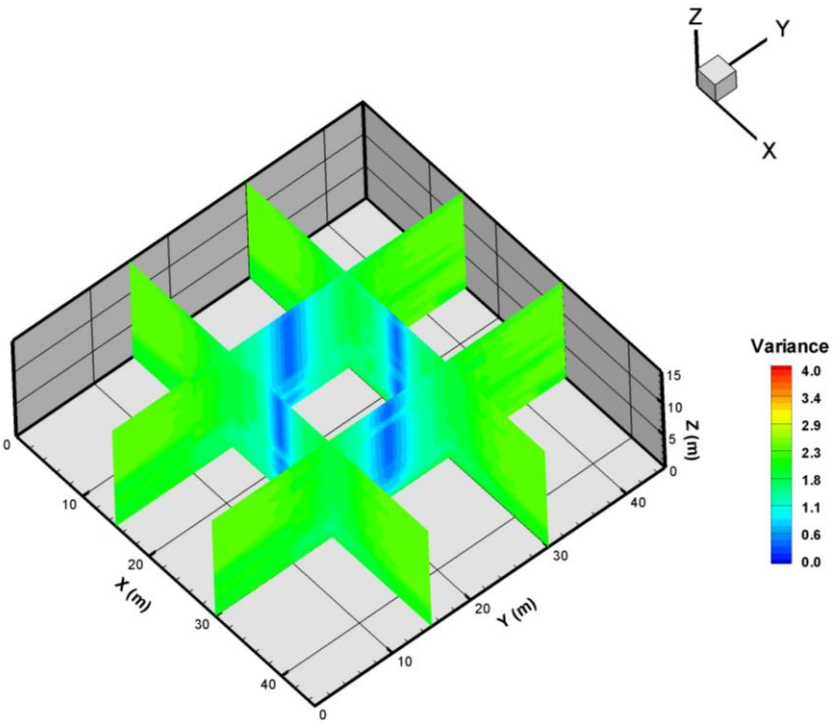

Figure 4.5 3-D variance map corresponding to kriged K field (permeameter data).

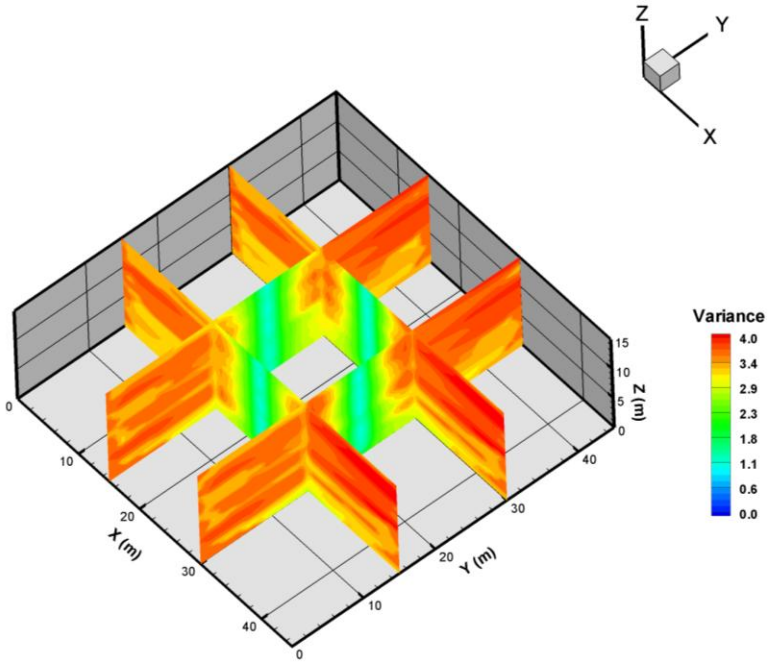

Figure 4.6 3-D variance map corresponding to kriged K field (empirical equation data).

5. Evaluation of Various Site Characterization Techniques Using Groundwater Modeling

5.1 Hydrogeosphere

The ability of the various characterization techniques to estimate hydraulic properties that could accurately predict groundwater flow in the highly heterogeneous NCRS was evaluated by simulating the selected pumping tests with a 3D forward numerical model, built using *Hydrogeosphere* (*HGS*) (Therrien et al., 2005). *HGS* is an integrated surface water/groundwater flow model, with the surface water module based on the Surface Water Flow Package of the *MODHMS* simulator and the groundwater component based on the University of Waterloo and University of Laval *FRAC3DVS* transport code (Therrien et al., 2008). Surface water flow was ignored in these simulations as there are no rivers in the close vicinity of the site.

5.1.1 Domain Size and Boundary Conditions

The focus when designing the domain size for the NCRS flow model was to capture the entire zone of interest, while avoiding any error in the hydraulic head calculations induced by the boundary conditions infringing on the CMT wells. The unsaturated zone was not modeled in this study, so the water table was set as the upper boundary of the domain. Water level measurements suggest the presence of a slight dip in the water table towards the east across the site, but the magnitude of the elevation change (~0.20 m) was smaller than the height of a single element (0.5 m), so the water table was modeled as a flat surface. A zero flux (Neumann) boundary condition was assigned to the water table, as no significant precipitation fell before or during the pumping test period.

The bottom of the domain was set at the upper surface of the Catfish Creek Till, encountered at the bottom of PW, CMT-2 and CMT-3. Karrow (1993) described this unit as a dense stony sand and silt till, with little clay, and it became the base of the study area when it could not be penetrated by the drill augers. The nature of this till suggests that it acts as a hydraulic barrier, preventing any significant flux of groundwater to the units above and below. A second zero flux (Neumann) boundary condition was assigned to the Catfish Creek Till surface, to reflect this expected hydraulic barrier condition.

The horizontal extent of the domain was determined based on historical pumping test data from a well (NC 17) located 25 m southwest of the NCRS (Alexander, 2008). NC 17 is screened in a glaciofluvial sand and gravel aquifer, and was pumped at a significantly higher rate than the tests run

at the NCRS for this study. Drawdown from the NC17 test was observed up to 100 m away. In order to strike a balance between the maximum possible domain size based on computing power, and the expected extent of drawdown, the sides of the domain were set at 22.5 m from the pumping well and constant head (Dirichlet) boundary conditions were assigned to these boundaries. Using these dimensions there was a total of 243,000 elements in the model of uniform 0.5 x 0.5 m size.

5.1.2 Model Cases

When selecting the hydraulic properties for each trial, an attempt was made to represent several of the 'typical' approaches used by hydrogeologists when modeling groundwater flow at a given field site. Four cases were designed and employed in *HGS*: 1) a homogeneous case with K and S_s estimates obtained by taking the geometric average of equivalent K and S_s values from the cross-hole pumping tests, 2) a layered heterogeneous case with strata determined from site geology, K and S_s estimates from the slug tests, 3) two heterogeneous cases with the kriged K data (permeameter and grain size) and S_s from the slug tests assigned to layers defined based on the geology, and 4) a mixed case with kriged K data (permeameter) and a homogeneous S_s value from the pumping tests. All of these approaches were applied to each of the chosen pumping tests (Zone 3, Zone 4 and Zone 5: see Table 3.3) and the complete details of all trials run in *HGS* are presented in Table 5.1, Table 5.2.

The questionable accuracy of the slug test S_s data (See Section 3.4) caused a deviation from the planned modeling approach for the heterogeneous cases. Originally, these values were assigned to the various layers by averaging the slug test results that fell within the defined extent of each layer. However, based on the comparison in Table 3.4 and the model results, it appears that the slug test S_s estimates are poor (ex. Figure). The possibility that poor S_s estimates were resulting in erroneous overall simulation results was investigated by abandoning the layered S_s approach and utilizing homogenous S_s values from the geometric means of the slug and pumping tests. Both of these approaches produced similarly poor drawdown predictions (Figure A 14, Figure A 17). Therefore, S_s values were obtained for each layer from tabulated values that represented the soil type of each layer (Batu, 1998).

Table 5.1 Details of the K values and boundary conditions used in all cases modeled using *Hydrogeosphere*.

					Boundary conditions		
Field Type	**Layer Number**	**Layer Thickness (m)**	**K Value Used (m/s)**	**Source**	**Top**	**Bottom**	**Sides**
Homogeneous	1	15	3.4E-05	pumping tests	zero flux	zero flux	constant head
Heterogeneous - Layered	1	3	1.10E-07	slug tests	zero flux	zero flux	constant head
	2	2	9.00E-07	slug tests	zero flux	zero flux	constant head
	3	9	4.80E-08	slug tests	zero flux	zero flux	constant head
Heterogeneous - Kriged	-	15	one per element	permeameter tests/ empirical equation calculation	zero flux	zero flux	constant head
Heterogeneous - Kriged (2)	1	15	one per element	permeameter tests	zero flux	zero flux	constant head

Table 5.2 Details of the S_s values used in all cases modeled using *Hydrogeosphere*.

Field Type	**Layer Number**	**Layer Thickness (m)**	**S_s Value (m^{-1})**	**Source**
Homogeneous	1	15	4.7E-04	pumping tests
Heterogeneous - Layered	1	3	1.10E-02	Batu, 1998
	2	2	1.02E-04	Batu, 1998
	3	9	1.28E-03	Batu, 1998
Heterogeneous - Kriged	1	4.5	1.10E-02	Batu, 1998
	2	2.5	4.92E-05	Batu, 1998
	3	0.5	9.18E-04	Batu, 1998
	4	3.5	1.28E-04	Batu, 1998
	5	4	1.28E-03	Batu, 1998
Heterogeneous - Kriged (2)	1	15	3.4E-05	pumping tests

6. Results and Discussion

The results of all trials run in *HGS* are included as Figure A 13 - Figure A 32 in Appendix A. A visual inspection of these figures indicates that there was a wide range in the ability of the different modeling approaches to simulate matching drawdown values to those observed in the field. Each approach had its strengths and weaknesses, and no one approach proved to be the clear best choice for modeling all three of the selected pumping tests. The task of evaluating the complex nature of the various model results and determining the approach that proved the most successful is broken into two sections: qualitative and quantitative analysis. The qualitative analysis involves a visual inspection of the results, highlighting the strengths and weaknesses of each approach and suggesting why each approach produced these results. The quantitative portion of the analysis evaluates the actual differences between observed and simulated drawdown in order to determine the best approach in an unbiased fashion.

6.1 Qualitative Analysis

A qualitative view of the results produced by the homogeneous modeling approach suggests that the moderate K and S_s values used for these trials were effective at accurately simulating drawdown in ports where very little (<0.1 m) drawdown was observed (Figure A 13, Figure A 21, Figure A 27). This was also the weakness of this approach, as it predicted moderate drawdown throughout the domain, completely missing the high drawdown values observed in ports screened in the hydraulically active units (Figure A 13, Figure A 21). It is important to note that negative drawdown was observed in several ports completed in aquitard units, most noticeably during pumping in Zone 3. This phenomenon is known as the Noordbergum Effect (Verruijt, 1969) and is caused by differences in pore elasticity between aquifer and aquitard units. The Noordbergum Effect is not accounted for in *HGS* and consequently positive or zero drawdown values are predicted in all of the ports where this phenomenon was observed.

The second modeling approach was the heterogeneous layered approach, with the K and S_s parameters taken from slug test measurements. This method produced simulated drawdown values for all three pumping tests that were very poor matches of the observed data (Figure A 14, Figure A 22, Figure A 28). One possible reason for these poor results are the K values, which were obtained by taking the geometric average of the slug test values from ports screened within the defined layers. The resulting values were several orders of magnitude lower than those

estimated from the pumping tests, a common phenomenon discussed previously. Rather than being bulk aquifer parameters, these lower K values more accurately represent the geology immediately adjacent to the slug tested screens. An analysis of the S_s values used in these simulations suggests that they play a more important role in the over prediction of the observed drawdown values than the K values do. As was shown previously in Table 3.4, the S_s values obtained from the slug test analysis vary quite significantly from tabulated S_s values from similar soil types. In order to investigate the quality of these S_s values, the next modeling approach replaced these measured values with tabulated values, commonly accepted in the literature. This produced significantly improved drawdown predictions, suggesting that the model is quite sensitive to S_s and that the slug test S_s values may not be representative (Figure A 15, Figure A 23, Figure A 29).

The incorporation of heterogeneity into the model for the layered approach is reflected in Figure A 15, Figure A 23, Figure A 29, especially in the Zone 3 and 4 pumping tests, where there are signs of the model discerning between the hydraulically isolated and hydraulically connected zones in the subsurface. Even with the more accurate S_s values, the simulated drawdown values are far from perfect. Of particular interest are the values in ports that were accurately simulated by the homogeneous approach and show poorer matches using this approach (See ports 1-4, 1-5, 3-4 and 3-5). The major weakness of introducing the layered zones into the model is the fact that the layering was incorporated by defining flat, continuous borders to each layer. This is difficult to do accurately, given the nature of the discontinuous geology at the NCRS (Figure 3.4Figure 3.4). Another aspect of the simulated drawdown values that requires improvement are the shape of the drawdown curves. While these trials predicted increased drawdown in the appropriate ports, the pattern of drawdown is very different than observed in the field, with the rising limb of the simulated drawdown curve being much longer in many cases (See Figure A 15, 1-2, 1-3, 2-2 etc.).

The simulations utilizing the K field kriged from the permeameter data are presented in Appendix A as Figure A 18, Figure A 19, Figure A 24, Figure A 25, Figure A 30, and Figure A 31. There were three simulations in this category for each pumping test, one that used the slug test S_s values, a second that used tabulated values and a third that used a homogeneous S_s value from the pumping tests. The simulations using the slug test S_s values generally over predicted drawdown, however, there were several ports where drawdown was predicted nearly perfectly (See Figure A 18 port 2-3, Figure A 24 ports 1-6, 4-5, etc.). The moderate success of this approach suggests that the failure of the

heterogeneous layered simulations using the slug test parameters was due to errors in both the K and the S_s values. In some cases, the S_s values may have been close to reflecting in situ values, but the simulations were affected by incorrect K values. Where this is the case, the S_s values are likely very specific to the aquifer unit they were measured in, and the process of applying these values to a thick layer of geology introduced a source of error into the model.

In the second trial using the K field kriged from the permeameter data, the slug test S_s values were replaced by accepted literature values, resulting in many improved drawdown correlations. However, the near perfect matches mentioned previously were lost suggesting that a more heterogeneous, or detailed S_s field may be required to achieve good matches in all CMT ports. That being said, this approach was the most successful at predicting the heterogeneous response to pumping, as well as matching the shape of the drawdown curves and final drawdown values. The exception is the Zone 5 pumping test, where little drawdown was observed, resulting in the homogeneous approach producing the best match.

The final group of simulations used the K field kriged from the permeameter dataset in conjunction with a homogeneous Ss value from the pumping tests (Table 5.1, Table 5.2). This model predicted a heterogeneous response to pumping however; the results were not as accurate as those predicted by the model using the same K field with heterogeneous S_s values. This suggests that in order to make accurate prediction of flow in a heterogeneous environment, multiple estimates of both K and Ss values are required to effectively characterize the heterogeneity of the system.

A qualitative analysis of the *HGS* simulations using the K field kriged from the empirical equation dataset suggests that this approach was somewhat less successful than the same approach using the permeameter data (Figure A 20, Figure A 26, Figure A 32). In general, this approach did a poorer job of predicting the pattern as well as the total magnitude of drawdown in the CMT ports. The root of the difference between predictive capabilities appears to be the kriged K fields used as input for these simulations (Figure 4.3, Figure 4.4). Much like with the simulations using the K field kriged from permeameter data, these simulations predict a heterogeneous response to pumping, but due to the lower level of detail in the empirical equation K field, the predictions are not as accurate. It would be incorrect to assume that this approach would always produce poorer results than the kriged (permeameter) approach, because with a more detailed dataset, matches at several of the ports may improve.

6.2 Quantitative Analysis

The quantitative step in this analysis utilized two numerical tools: scatter plots comparing simulated and observed drawdown at three different time steps within each test and the L_1 and L_2 norms. The scatter plots are presented as Figure 6.1 - Figure 6.3, and a set of statistics based on the error between the simulated and observed drawdown were also calculated for all of the plots to aid in the interpretation of the scatter plots and are included in Table 6.1. This table shows that, while the maximum average under prediction for all trials was 0.23 m (Zone 3 – heterogeneous layered approach) and the maximum over prediction was 0.22 m (Zone 5 – empirical equation kriged K approach), on average more than half of the errors are less than 0.1 m from the observed drawdown. The error means in this table also indicate that, on average, a large majority of the observed drawdown values were under predicted by the models and this is reflected in the scatterplots where data points sit below the 1:1 line (Figure 6.1 - Figure 6.3). This is especially true in the homogeneous cases for each pumping test, which show definite bias to under prediction. When the homogeneous approach is used, the moderate S_s and K values used to represent the entire domain cause the model to 'miss' the increased drawdown observed in the coarse-grained zones with reduced storage. When increased complexity is introduced into the model the points on the scatter plots are closer to the 1:1 line and some over predictions are made, suggesting that these lower storage zones are now being represented and, overall, the predictions are better.

A majority of the large error mean values are associated with the pumping in Zone 3, where the highest discharge occurred and, consequently, highest drawdown values were observed. The correlation coefficient column in Table 6.1 indicates that for two of the modeling approaches in Zone 3, the error between the simulated and observed drawdown values decreased through time. This pattern also occurred for two of the approaches in Zone 4. This appears to result from a delay between the time a response to pumping is predicted to occur in a given port, compared to the observed time until a response occurs, especially in the ports where significant drawdown was observed. Therefore, at late time when the predicted drawdown approaches a maximum value in the CMT port, the correlation coefficient improves. As mentioned previously, the necessity to define layers in the model in order to distribute the S_s values is likely a contributor to this error. The different geologic units were shown to vary significantly in thickness across the NCRS (Figure 3.4), but these units were represented as having a uniform thickness in the model. The reality of variability in the thickness of geologic units is that the storage in the aquifer is less than what is

represented in the model and therefore a faster response to pumping is observed in the field than is predicted in the model.

With respect to the model predictions at late time, it should be noted that during the latter part of all pumping tests, drawdown in a majority of the CMT's was observed to level off significantly, and in some cases it could be said that steady state was reached. Longer pumping tests would be required to confirm this, but it is an important factor as this suggests that there is some source of recharge in the domain that was not encountered during the drilling and, consequently, was not built into the model. This highlights a short coming of the detailed characterization approaches used in this study, as hydraulic parameters could only be confidently assigned to the geology that was directly sampled, or in the case of the slug and pumping tests, directly monitored during the characterization stage. If the recharge is due to a leaky aquitard, as suggested by the slug test analysis, the level of detail used to construct these models did not adequately capture this feature of the system.

The second quantitative approach used to evaluate the success of each simulation employed two goodness-of-fit statistical parameters: the average absolute error norm (L_1 norm) and the mean squared error norm (L_2 norm). Correlation coefficients ($\rho_{x,y}$) were also calculated again, as this time they apply to the drawdown predictions in the final time step of the simulation (Table 6.1). The L_1 and L_2 norms are calculated as follows:

$$L_1 = \frac{1}{n}\sum_{i=1}^{n}\left|h_{s,i} - h_{m,i}\right| \quad (8)$$

$$L_2 = \frac{1}{n}\sum_{i=1}^{n}(h_{s,i} - h_{m,i})^2 \quad (9)$$

where $h_{s,i}$ is the simulated value of hydraulic head at port i and $h_{m,i}$ is the measured value of hydraulic head at port i. The L_1 and L_2 norms reflect agreement between simulated and measured values, such that low L_1 and L_2 values indicate good matches.

There were two approaches taken to compare the modeling results in an unbiased way. First, the L_1 and L_2 norms were calculated for all of the CMT ports to provide a basis for ranking the approaches in terms of their overall ability to make accurate drawdown predictions. Based on these rankings, each approach received a score for its performance in simulating drawdown for each pumping test, such that the approach performing the best received a score of 5, down to a score of 1 for the poorest approach. The second element of this analysis focused on the most hydraulically active zones in the system (Figure 4.3), defined in this case as zones where >0.1 m

of drawdown was observed. These hydraulically active units were isolated in this analysis as they are the ones that control the bulk of fluid movement in the subsurface and therefore must be understood in order to make accurate contaminant migration or water resource predictions. In the final step of this analysis, the scores achieved by each approach in the two scenarios outline above were summed in order to identify the modeling approach that preformed best overall.

A plot of the L_1 and L_2 values calculated for all CMT ports provides some insight into the success of the pumping test simulations for the various trials (Figure 6.4,Figure 6.5). As was determined in the qualitative analysis process, it is clear from this figure that no one approach can be considered as being the outright best. The heterogeneous layered approach was rated the highest for Zone 3, the kriged (permeameter data) approach performed best for Zone 4 and the homogeneous approach worked best for Zone 5. It could be said that the Zone 3 pumping test was most difficult to simulate, as it was pumped at the highest rate, and produced the greatest variability in drawdown values. It is clear from the Zone 3 results (Figure 6.4,Figure 6.5) that incorporating heterogeneity into the model produced better results as the heterogeneous layered approach was ranked the highest, followed by the kriged K (permeameter) approach.

The results of the second L_1 and L_2 analysis, which just considered the ports where drawdown was >0.1 m, are presented as Figure 6.5. The L_1 and L_2 values rank the modeling approaches for the Zone 3 and 4 tests in the following order: kriged K field (permeameter data)> kriged K field (empirical equation data) > heterogeneous layered approach > kriged K field (permeameter data, homogeneous S_s) > homogeneous approach and kriged K field (permeameter data)> kriged K field (permeameter data, homogeneous S_s) > kriged K field (empirical equation data) > heterogeneous layered approach > homogeneous. This suggests that the more heterogeneity incorporated into the model the better the ability of the model to simulate groundwater flow in the highly conductive zones. The results were opposite for modeling of the Zone 5 pumping test, where the approaches were ranked homogeneous > heterogeneous layered > kriged K (permeameter data) > kriged K field (permeameter data, homogeneous S_s) > kriged K (empirical equation data). In this case, increasing the detail level in the model resulted in poorer drawdown predictions. This appears to be related to the complexity of the lower coarse-grained, high yielding aquifer that is discontinuous across the site, and therefore poorly represented in the kriged datasets (Figure 4.3, Figure 4.4). The significant amount of gravel present in the samples from this aquifer also brings into question the accuracy of the permeameter test results for this unit, as it is known to introduce error in these tests (ASTM, 2003).

The final stage in this analysis summed the rankings from stages one and two, in an attempt to quantitatively select the site characterization approach that was most successful overall (Table 6.3). Based on this scoring system the approaches are ranked as: kriged K (permeameter data) > heterogeneous layered > homogeneous > kriged K (empirical equation data) > kriged K field (permeameter data, homogeneous S_s), suggesting that increasing the number of points used to characterize this highly heterogeneous aquifer system results in more accurate simulations.

These observations raise two important issues. First, examining the results for Zone 3 (Figure A 13 - Figure A 20) where the most variability in drawdown was observed, it can be seen that increased characterization does improve the estimation ability of the model, but there are significant shortfalls in the predictions for several of the ports (see 1-3, 1-4, 2-4, 3-2 and 4-3). This highlights the need for even more comprehensive characterization, to further the ability to simulate flow in systems with similar levels of heterogeneity. One approach which has received considerable attention is hydraulic tomography [e.g., *Yeh and Liu,* 2000; *Liu et al*., 2002; *Zhu and Yeh,* 2005, 2006; *Illman et al*., 2007, 2008, 2009; *Liu et al*., 2007; *Yin and Illman*, 2009]. The second issue revolves around the challenges surrounding existing and new approaches. The most detailed approach here was the kriged K approach using permeameter data, which required significant time, effort and therefore cost to produce. This amount of time and effort is not realistic in a non-academic project, yet better results are imperative. New techniques must improve overall hydraulic characterization, while being less invasive, and minimizing the associated cost.

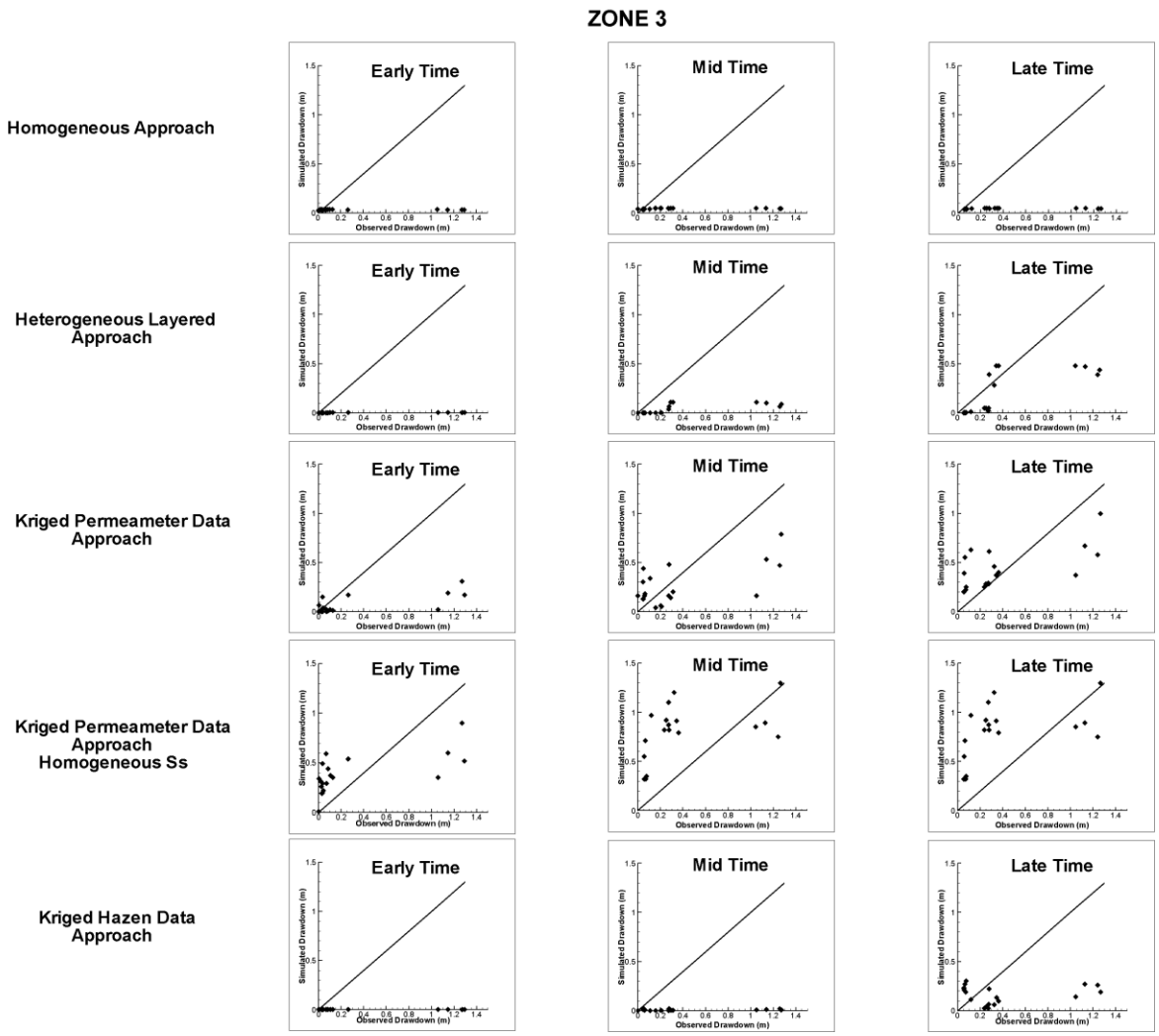

Figure 6.1 Scatter plot of observed (x-axis) versus simulated (y-axis) drawdown during the Zone 3 pumping test for three time steps (early, mid and late), for each modeling approach. The solid line in the plots represents a perfect match between data, all drawdown values are in metres.

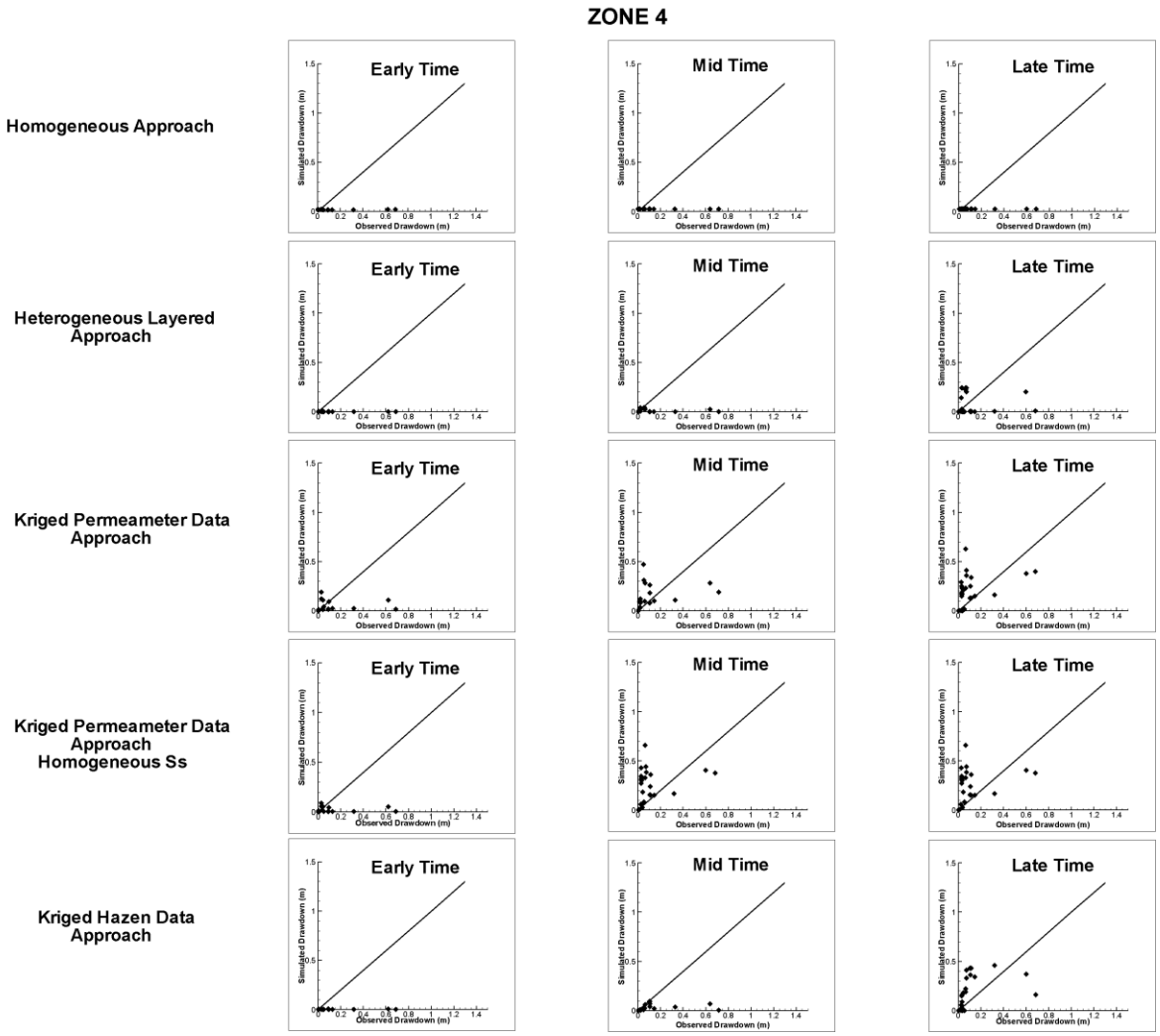

Figure 6.2 Scatter plot of observed (x-axis) versus simulated (y-axis) drawdown during the Zone 4 pumping test for three time steps (early, mid and late), for each modeling approach. The solid line in the plots represents a perfect match between data, all drawdown values are in metres.

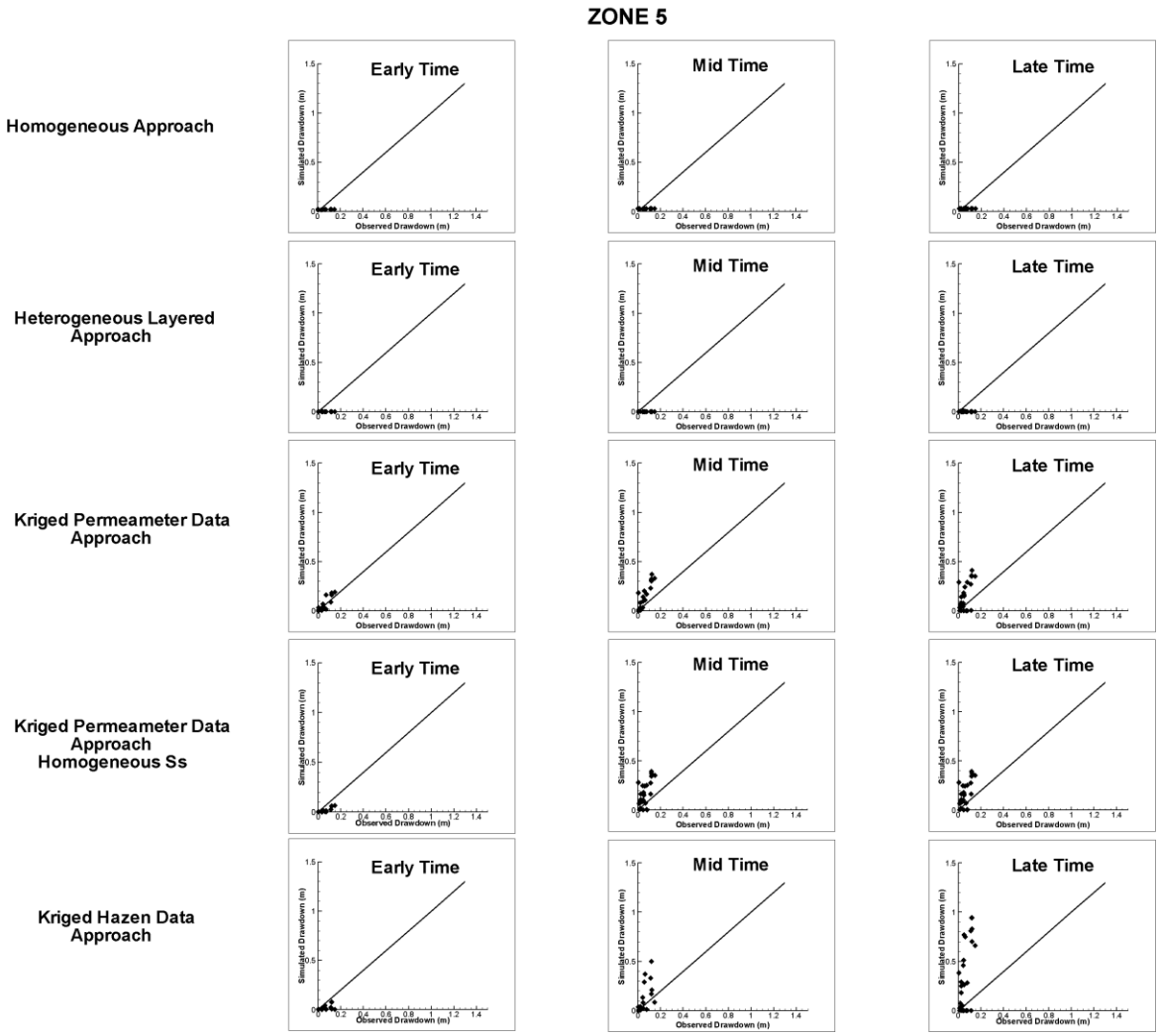

Figure 6.3 Scatter plot of observed (x-axis) versus simulated (y-axis) drawdown during the Zone 5 pumping test for three time steps (early, mid and late), for each modeling approach. The solid line in the plots represents a perfect match between data, all drawdown values are in metres.

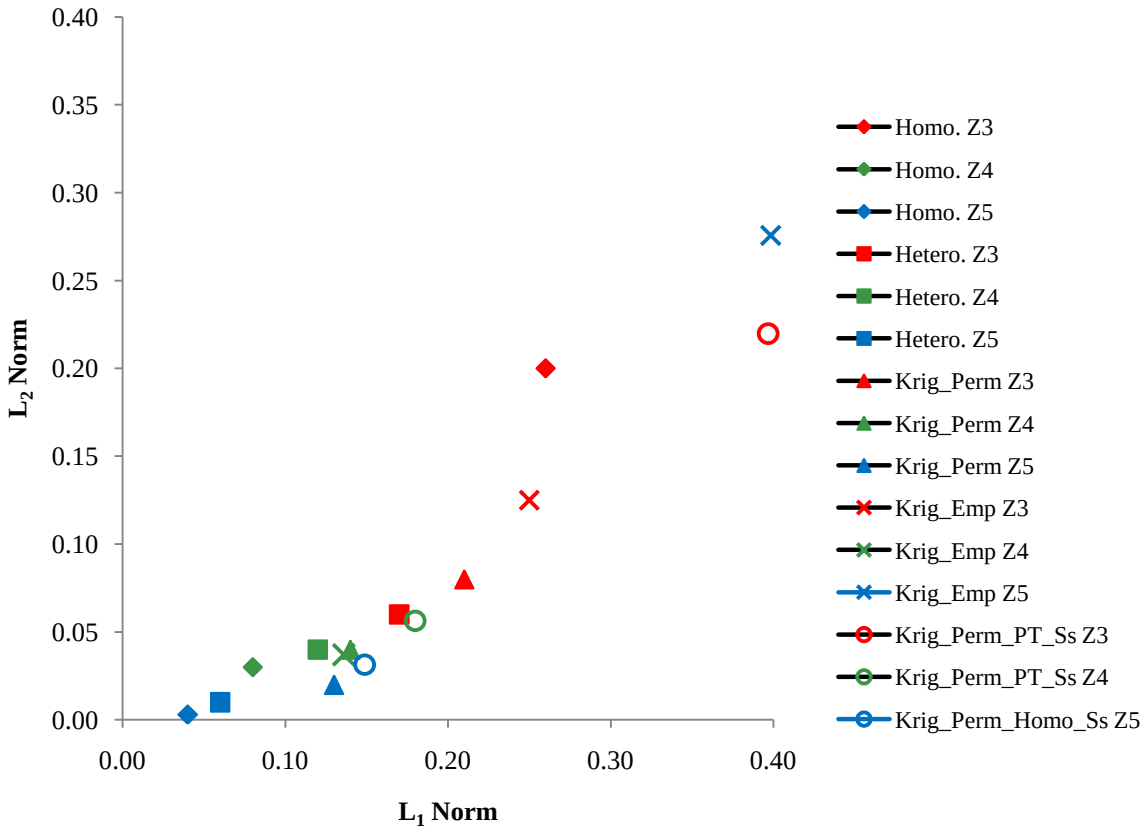

Figure 6.4 Plot of L_1 and L_2 norms for all trials modeled in *Hydrogeosphere*. The following short forms are used: Zones 3, 4, 5 coded as Z3, Z4, Z5, homogeneous K field as Homo., heterogeneous layered K field as Hetero., heterogeneous kriged K field using permeameter data as Krig_Perm, and heterogeneous kriged K field using empirical equation data as Krig_Emp.

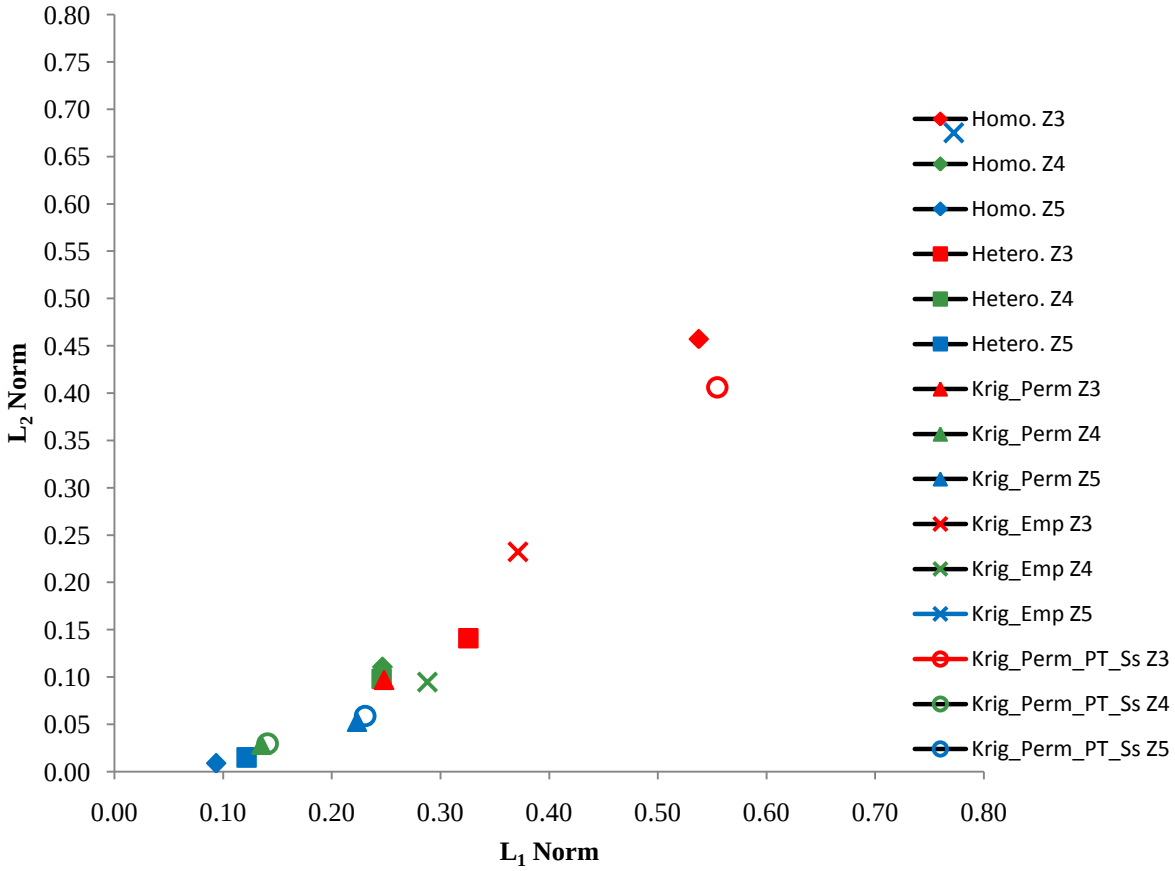

Figure 6.5 Plot of L_1 and L_2 norms for all trials modeled in *Hydrogeosphere*. Only ports where 0.1 m or more of drawdown was observed, were used for the calculation. The following short forms are used: Zones 3,4,5 coded as Z3, Z4, Z5, homogeneous K field as Homo., heterogeneous layered K field as Hetero., heterogeneous kriged K field using permeameter data as Krig_Perm, and heterogeneous kriged K field using empirical equation data as Krig_Emp.

Table 6.1 Mean, variance and correlation coefficient of error dataset for each modeling approach at three times during each pumping test.

		Pumping Test Time	Error Mean	Error Variance	Error Correlation
Zone 3	Homogeneous	Early	-0.171	0.173	0.420
		Mid	-0.199	0.163	0.555
		Late	-0.216	0.160	0.607
	Heterogeneous Layered	Early	-0.199	0.174	0.660
		Mid	-0.216	0.141	0.768
		Late	-0.129	0.073	0.810
	Heterogeneous Kriged (Permeameter)	Early	-0.155	0.132	0.750
		Mid	-0.063	0.089	0.712
		Late	0.041	0.077	0.732
	Heterogeneous Kriged (Permeameter) Homogeneous Ss (Pumping Test Value)	Early	-0.198	0.172	0.785
		Mid	-0.109	0.078	0.818
		Late	0.442	0.141	0.804
	Heterogeneous Kriged (Hazen)	Early	-0.200	0.174	0.622
		Mid	-0.230	0.158	0.567
		Late	-0.085	0.114	0.564

		Pumping Test Time	Error Mean	Error Variance	Error Correlation
Zone 4	Homogeneous	Early	-0.060	0.031	0.351
		Mid	-0.066	0.032	0.339
		Late	-0.075	0.027	0.345
	Heterogeneous Layered	Early	-0.078	0.031	-0.075
		Mid	-0.082	0.032	0.024
		Late	-0.036	0.035	0.052
	Heterogeneous Kriged (Permeameter)	Early	-0.049	0.029	0.230
		Mid	0.014	0.030	0.397
		Late	0.087	0.031	0.419
	Heterogeneous Kriged (Permeameter) Homogeneous Ss (Pumping Test Value)	Early	-0.065	0.030	0.196
		Mid	0.007	0.032	0.287
		Late	0.132	0.041	0.289
	Heterogeneous Kriged (Hazen)	Early	-0.078	0.031	0.039
		Mid	-0.075	0.031	0.220
		Late	0.087	0.036	0.425

		Pumping Test Time	Error Mean	Error Variance	Error Correlation
Zone 5	Homogeneous	Early	-0.016	0.002	0.551
		Mid	-0.016	0.002	0.429
		Late	-0.033	0.002	0.673
	Heterogeneous Layered	Early	-0.034	0.002	-0.133
		Mid	-0.043	0.002	-0.072
		Late	-0.058	0.002	-0.325
	Heterogeneous Kriged (Permeameter)	Early	0.006	0.001	0.909
		Mid	0.063	0.007	0.930
		Late	0.083	0.014	0.614
	Heterogeneous Kriged (Permeameter) Homogeneous Ss (Pumping Test Value)	Early	-0.023	0.001	0.897
		Mid	0.035	0.003	0.931
		Late	0.107	0.011	0.657
	Heterogeneous Kriged (Hazen)	Early	-0.033	0.002	0.396
		Mid	0.002	0.006	0.524
		Late	0.223	0.099	0.523

Table 6.2 L_1 and L_2 norms and correlation coefficients ($\rho_{x,y}$) for all trials modeled in *Hydrogeosphere*.

	Homogeneous			Heterogeneous - Layered		
	L1	**L2**	**Corr. Coeff.**	**L1**	**L2**	**Corr. Coeff.**
Zone 3	0.260	0.200	0.615	0.170	0.060	0.815
Zone 4	0.080	0.030	0.345	0.120	0.040	0.052
Zone 5	0.040	0.003	0.696	0.060	0.010	-0.354
	Heterogeneous - Kriged (Permeameter)			**Heterogeneous - Kriged (Empirical)**		
	L1	**L2**	**Corr. Coeff.**	**L1**	**L2**	**Corr. Coeff.**
Zone 3	0.210	0.080	0.738	0.250	0.125	0.465
Zone 4	0.140	0.040	0.419	0.136	0.037	0.419
Zone 5	0.130	0.020	0.467	0.398	0.276	0.471
	Heterogeneous - Kriged (Permeameter) Homogeneous Ss (Pumping Test Value)					
	L1	**L2**	**Corr. Coeff.**			
Zone 3	0.397	0.220	0.635			
Zone 4	0.180	0.056	0.289			
Zone 5	0.149	0.031	0.512			

Table 6.3 Scoring system used to evaluate the various modeling approaches.

	All Units			High K Zones			
Approach	**Zone 3 Test**	**Zone 4 Test**	**Zone 5 Test**	**Zone 3 Test**	**Zone 4 Test**	**Zone 5 Test**	**Total Score**
Homogeneous	2	5	5	1	1	5	19
Heterogeneous Layered	5	4	4	3	2	4	22
Kriged - Permeameter	4	3	3	5	5	3	23
Kriged - Hazen	3	2	1	4	3	1	14
Kriged - Permeameter (Homogeneous PT Ss)	1	1	2	2	4	2	12

7. Conclusions

Several traditional aquifer characterization techniques were utilized to estimate the hydraulic properties of a complex, thoroughly instrumented, highly heterogeneous aquifer/aquitard system. The techniques selected were, empirical equations using grain size data to calculate K, falling head permeameter tests to estimate K, slug tests to measure K and S_s and pumping tests to measure K and S_s. A geostatistical analysis was conducted on the detailed K datasets, which included histogram analysis, the selection of a variogram model based on experimental variograms of the data, and kriging to interpolate K values for the entire domain being studied. The resulting datasets were used to build 3D transient groundwater flow models in *Hydrogeosphere* that were tested by simulating three pumping tests that had been conducted at the research site. The output was analyzed against the observed drawdown in the four CMT monitoring wells screened at 28 locations in the study section. The results suggest that no one method stands out as being the absolute best choice for modeling flow in this complex system. The approach of treating the domain as having homogeneous properties resulted in good prediction of all the hydraulically isolated ports that experienced little drawdown. This method proved to be poor at accurately predicting drawdown in the ports that were hydraulically connected to the zone being stressed. As the level of detail included in the model increased, in general, so did the quality of the predictions. This was especially true in cases where there were large differences in observed drawdown over short vertical distances. The pumping test in the coarse-grained lower aquifer proved to be difficult to model, especially with the heterogeneous approaches, as sparse sampling of this unit led to the poor representation of it in kriged K fields.

This study highlighted the difficulty of measuring S_s using traditional slug test techniques. When the values estimated from the slug tests were incorporated into the HGS models, the drawdown values were significantly over-predicted. There were a few rare examples where the S_s did produce acceptable matches, particularly in the aquifer units where significant drawdown was observed, but overall the slug test S_s values could not be used in the heterogeneous models. When these were replaced with accepted literature values, the simulated drawdown values were greatly improved. This brings into question the validity of using S_s values to model transient groundwater flow.

Overall, this work has shown that it is extremely difficult to accurately predict flow in heterogeneous aquifer systems, but that increasing the detail level of hydraulic characterization will generally improve predictions. It has also highlighted an area that has significant room for improvement, as the very properties essential to making accurate predictions of flow in these complex systems were proven difficult to measure precisely. This indicates the need for methodology that improves the accuracy and spatial coverage of K and S_s prediction, while minimizing the invasiveness and cost of the procedure.

References

Alexander, M. 2008. Pumping test field notes. Department of Earth Science Field School, University of Waterloo. Unpublished Data.

Alyamani, M.S. and Z. Sen. 1993. Determination of hydraulic conductivity from complete grain-size distribution curves. *Ground Water* 31, no. 4: 551-555.

American Society for Testing and Materials (ASTM). *Annual book of ASTM standards, Classification of Soil for Engineering Purposes*. Philadelphia: ASTM, 1985.

American Society for Testing and Materials (ASTM). *Annual book of ASTM standards, ASTM D 5084 Standard Test Methods for Measurement of Hydraulic Conductivity of Saturated Porous Materials Using a Flexible Wall Permeameter*. Philadelphia: ASTM, 2003.

American Society for Testing and Materials (ASTM). *Annual book of ASTM standards, Standard Test Method for Particle-Size Analysis of Soils,* Philadelphia: ASTM, 2007.

Bagarello, V. and G. Provenzano. 1996. Factors affecting field and laboratory measurement of saturated hydraulic conductivity. *Transactions of the ASAE,* 39 no. 1: 153-159.

Batu, V. 1998. *Aquifer Hydraulics: A Comprehensive Guide to Hydrogeologic Data Analysis.* New York: John Wiley & Sons.

Bear, J. 1972. *Dynamics of Fluids in Porous Media*. New York: American Elsevier.

Bedinger, M.S. 1961. Relation between median grain size and permeability in the Arkansas River Valley. U.S. Geological Society Professional Papers, 292: C31-C32.

Bradbury, K.R. and M. A. Muldoon. "Hydraulic Conductivity Determinations in Unlithified Glacial and Fluvial Materials." In: *Ground Water and Vadose Zone Monitoring*. Philadelphia, PA: American Society for Testing and Materials, 1989.

Butler, J.J. Jr. 1998. *The Design, Performance, and Analysis of Slug Tests.* Boca Raton: Lewis Publishers.

Butler, J.J. Jr., and J.M. Healey. 1998. Relationship between pumping-test and slug-test parameters: Scale effect or Artifact? *Ground Water* 36, no. 2: 305-314.

Butler, J.J. Jr. "Hydrogeological Methods for Estimation of Spatial Variations in Hydraulic Conductivity." In: *Hydrogeophysics*. The Netherlands: Springer, 2005.

Clauser, C., 1992. Permeability of crystalline rocks. Eos Transactions, American Geophysical Union, 73, 233.

Cooley, R.L. and S. Christensen. 2006. Bias and uncertainty in regression-calibrated models of groundwater flow in heterogeneous media. *Advances in Water Resources* 29: 639-656.

Cosby, B.J., G.M. Hornberger, R.B. Clapp, and T.R. Ginn. 1984. A statistical exploration of the relationships of soil moisture characteristics to the physical properties of soils. *Water Resources Research,* 20(6): 682-690.

CRC Press. *CRC handbook of chemistry and physics*. Boca Raton: Chemical Rubber Company, 1977.

Cressie, N.A.C. 1993. *Statistics for spatial data*. New York: Wiley Interscience.

Dagan, G., 1978. A note on packer, slug, and recovery tests in unconfined aquifers. *Water Resources Research* 14, no. 5: 929-934.

Davis, B.M. and L.E. Borgman. 1979. Some exact sampling distributions for variogram estimators. *Mathematical Geology*, 11(6): 643-654.

Davis, S.H., R.A. Vertessy, and R.P. Silberstein. 1999. The sensitivity of a catchment model to soil hydraulic properties obtained by using different measurement techniques. Hydrological Processes, 13: 677-688.

Dorsey, J.D., A.D. Ward, N.R. Fausey, and E.S. Bair. 1990. A comparison of 4 field methods for measuring saturated hydraulic conductivity. *Transactions of the ASAE* 33, no. 6: 1925-1931.

Dougherty, D.E. and D.K. Babu. 1984. Flow to a partially penetrating well in a double-porosity reservoir. Water Resources Research, 20(8): 1116-1122.

Duffield, G.M. 2007. *AQTESOLV for Windows Version 4.5 User's Guide.* Reston, VA: HydroSOLVE, Inc.

Eggleston, J.R., S.A. Rojstaczer, and J.J. Peirce. 1996. Identification of hydraulic conductivity structure in sand and gravel aquifers: Cape Cod data set. *Water Resources Research* 32, no. 5: 1209-1222.

Eggleston, J. and S. Rojstaczer. 2001. The value of grain-size hydraulic conductivity estimates: Comparison with high resolution in-situ field hydraulic conductivity. *Geophysical Research Letters* 28, no. 22: 4255-4258.

Environment Canada. "National Climate Data and Information Archive." Environment Canada. http://www.climate.weatheroffice.ec.gc.ca/Welcome_e.html

Freeze, R.A. 1975. Stochastic-conceptual analysis of one-dimensional groundwater flow in non-uniform homogeneous media. *Water Resources Research* 11, no. 5: 725-741.

Goltz, I. 1991. Spatial variability of hydraulic conductivity in a sand aquifer at North, Bay, Ontario. MSc. Thesis. Department of Earth Sciences. University of Waterloo.

Gribb, M.M., R. Kodesova, and S.E. Ordway. 2004. Comparison of soil hydraulic property measurement methods. *Journal of Geotechnical and Geoenvironmental Engineering* 130, no. 10: 1084-1095.

Gringarten, E. and C.V. Deutsch. 2001. Variogram interpretation and modeling. *Mathematical Geology* 33, no. 4: 507-534.

Guimerà, J., L. Vives, J. Carrera, 1995. A discussion of scale effects on hydraulic conductivity at a granitic site (El Berrocal, Spain), Geoph. Res. Lett., 22, 1449-1452.

Hantush, M.S. 1960. Modification of the theory of leaky aquifers. *Journal ofGeophysical Research* 65, no. 11: 3713-3725.

Harleman, D.R.F., P.F. Melhorn, and R.R. Rumer. 1963. Dispersion-permeability correlation in porous media. *Journal of the Hydraulic Division of the American Society of Civil Engineers,* 89(HY.2): 67-85.

Hazen, A. 1911. Discussion: Dams on sand foundations. *Transactions, American Society of Civil Engineers* 73: 199.

Hyder, Z., J.J. Butler, Jr., C.D. McElwee and W. Liu. 1994. Slug tests in partially penetrating wells. *Water Resources Research* 30, no. 11: 2945-2957.

Kozeny, J. 1927. Ueber kapillare leitung des Wassers im boden. Wien, Akad. Wiss., 136(2a): 271.

Krumbein, W.C. and G.D. Monk. 1943. Permeability as a function of the size parameters of unconsolidated sands. *Transactions of the Petroleum Division, American Institute of Mining and Metallurgical Engineering,* 151: 153-163.

Illman, W. A., X. Liu, S. Takeuchi, T. J. Yeh, K. Ando, and H. Saegusa (2009), Hydraulic tomography in fractured granite: Mizunami Underground Research site, Japan, *Water Resour. Res*., 45, W01406, doi:10.1029/2007WR006715.

Illman, W. A., A. J. Craig, and X. Liu, (2008), Practical issues in imaging hydraulic conductivity through hydraulic tomography, *Ground Water*, 46(1), 120-132.

Illman, W. A., X. Liu, and A. Craig (2007), Steady-state hydraulic tomography in a laboratory aquifer with deterministic heterogeneity: Multi-method and multi-scale validation of hydraulic conductivity tomograms, *J. of Hydrol.*, 341(3-4), 222-234.

Illman, W.A. 2006. Strong field evidence of directional permeability scale effect in fractured rock. *Journal of Hydrology*, 319(1-4): 227-236.

Illman, W. A. and S. P. Neuman, 2003. Steady-state analyses of cross-hole pneumatic injection tests in unsaturated fractured tuff, J. Hydrol., 281, 36-54.

Illman, W. A. and S. P. Neuman, 2001. Type-curve interpretation of a cross-hole pneumatic injection test in unsaturated fractured tuff, Water Resour. Res. 37, 583-603.

Journel, A.G. and CH. J. Huijbregts. 1978. *Mining Geostatistics*. London: Academic Press.

Karrow, P.F., 1979. Geology of the University of Waterloo Campus, Department of Earth Sciences.

Karrow, P.F., 1993. Quaternary geology, Stratford-Conestogo area. Ontario Geological Survey report.

Kitanidis, P.K. 1997. *Introduction to Geostatistics: Applications in Hydrogeology*.New York: Cambridge University Press.

Lee, D.M., W.D. Reynolds, and D.E. Elrick. 1985. A comparison of 3 field methods for measuring saturated hydraulic conductivity. *Canadian Journal of Soil Science*, 65(3): 563-573.

Liu, X., W. A. Illman, A. J. Craig, J. Zhu, and T.-C. J. Yeh (2007), Laboratory sandbox validation of transient hydraulic tomography, *Water Resour. Res*., 43, W05404, doi:10.1029/2006WR005144.

Liu, S., T. -C. J. Yeh, and R. Gardiner (2002), Effectiveness of hydraulic tomography: sandbox experiments. *Water Resour. Res.* 38(4): 10.1029/2001WR000338.

Martinez-Landa, L., and J. Carrera (2005), An analysis of hydraulic conductivity scale effects in granite (Full-scale Engineered Barrier Experiment (FEBEX), Grimsel, Switzerland), Water Resour. Res., 41, W03006, doi:10.1029/2004WR003458.

Massey, F.J., 1951. The Kolmogorov-Smirnov test for goodness of fit. *Journal of the American Statistical Association* 46, no. 253: 68-78.

Matheron, G. 1962. Traite de Geostatistique Appliquee. Memoires du Bereau de Recherches Geologiques et Minieres.

Mohanty, B.P., R.S. Kanwar, and C.J. Everts. Comparison of saturated hydraulic conductivity measurement methods for a glacial-till soil. *Soil Science Society of America Journal* 58, no. 3: 672-677.

Moltyaner, G.L. and C.A. Wills. 1993. Characterization of aquifer heterogeneity by in situ sensing. *Water Resources Research* 29, no. 10: 3417-3431.

Oldham, T.L. 1998. Use of Falling Head Permeameters to Determine Hydraulic Conductivity. Department of Earth Sciences, University of Waterloo.

Paige, G.B. and D. Hillel. 1993. Comparison of 3 methods for assessing soil hydraulic properties. *Soil Science*, 155(3): 175-189.

Puckett, W.E., J.H. Dane, and B. F. Hajek. 1985. Physical and Mineralogical Data to Determine Soil Hydraulic Properties. *Soil Science Society of America Journal* 49: 831-836.

Rehfeldt, K.R. and J.M. Boggs. 1992. Field study of dispersion in a heterogeneous aquifer. 3. Geostatistical analysis of hydraulic conductivity. *Water Resources Research* 28, no. 12: 3309-3324.

Remy, N., A. Boucher and J. Wu. 2008. *Applied Geostatistics with SgeMS: A Users Guide.* New York: Cambridge University Press.

Ross, J., M. Ozbek, and G.F. Pinder. 2007. Hydraulic conductivity estimation via fuzzy analysis of grain size data. *Mathematical Geology* 39, no. 8: 765-780.

Schulze-Makuch, D. and D. S. Cherkauer, 1998. Variations in hydraulic conductivity with scale of measurements during aquifer tests in heterogeneous, porous carbonate rock. Hydrogeol. J. 6, 204-215.

Scott, D. 1979. On optimal and data-based histograms. *Biometrika* 66**:**605-610.

Sebol, L.A., 2000. Determination of Groundwater Age Using CFC's in Three Shallow Aquifers in Southern Ontario. Ph.D. diss., Department of Earth and Environmental Science, University of Waterloo, Waterloo.

Sen, Z. and A. Subyani. 1992. Review of geostatistics in geohydrology. 1: Basic Concepts - Discussion. *Journal of Hydraulic Engineering* 118, no. 4: 638-640.

Shepherd, R.G. 1989. Correlations of grain size and permeability. Ground Water, 27(5): 633-638.

Sudicky, 1986. A natural gradient experiment on solute transport in a sand aquifer: spatial variability of hydraulic conductivity and its role in the dispersion process. *Water Resources Research* 22, no. 13: 2069-2082.

Therrien, R., R.G. McLaren, E.A.Sudicky, and S.M. Panday. (2005). HydroGeoSphere: A Three-dimensional Numerical Model Describing Fully-integrated Subsurface and Surface Flow and Solute Transport. Groundwater Simulations Group, Waterloo, Ontario.

Turcke, M.A. and B.H Kueper. 1996. Geostatistical analysis of the Borden aquifer hydraulic conductivity field. *Journal of Hydrology* 178, no. 1-4: 223-240.

Verruijt, A., 1969. Elastic Storage of Aquifers. In: *Flow Through Porous Media.* New York: Academic Press.

Woodbury, A.D. and E.A. Sudicky. 1991. The geostatistical characteristics of the Borden aquifer. Water Resources Research, 27(4): 533-546.

Wu, C.M., T.C.J. Yeh, J. Zhu, T.H. Lee, N.S. Hsu, C.H. Chen, and A.F. Sancho. 2005. Traditional analysis of aquifer tests: Comparing apples to oranges? *Water Resources Research* 41: W09402.

Yang, Y.S., A.A. Cronin, T. Elliot, and R.M. Kalin. 2004. Characterizing a heterogeneous hydrogeological system using groundwater flow and geochemical modeling. *Journal of Hydraulic Research* 42, extra: 147-155.

Yeh, T.-C. J., and S. Y. Liu (2000), Hydraulic tomography: development of a new aquifer test method, *Water Resour. Res*., 36(8), 2095-2105.

Yin, D., and W. A. Illman (2009), Hydraulic tomography using temporal moments of drawdown recovery data: A laboratory sandbox study, *Water Resour. Res*., 45, W01502, doi:10.1029/2007WR006623.

Young, S.C. 1997. Application of aquifer tests and sedimentological concepts to characterize the hydrological properties if a fluvial deposit. Ph.D. Diss. Department of Earth Sciences, University of Waterloo.

Zhu, J., T.-C. J. Yeh (2006), Analysis of hydraulic tomography using temporal moments of drawdown recovery data, *Water Resour. Res*., 42, W02403, doi:10.1029/2005WR004309.

Zhu, J., and T.-C. J. Yeh (2005), Characterization of aquifer heterogeneity using transient hydraulic tomography, *Water Resour. Res*., 41, W07028, doi:10.1029/2004WR003790.

Zlotnik, V. A., B. R. Zurbuchen, T. Ptak, and G. Teutsch, 2000. Support volume and scale effect in hydraulic conductivity: experimental aspects, in Zhang, D., and C. L. Winter, eds., Theory, Modeling, and Field Investigation in Hydrogeology: A Special Volume in Honor of Shlomo P. Neuman's 60th Birthday: Boulder, Colorado, Geological Society of America Special Paper 348, 191–213.

Zlotnik, V.A. and B.R. Zurbuchen. 2003. Field study of hydraulic conductivity in a heterogeneous aquifer: Comparison of single-borehole measurements using different instruments. *Water Resources Research* 39, no. 4: SBH8.

Appendix A

Additional Figures

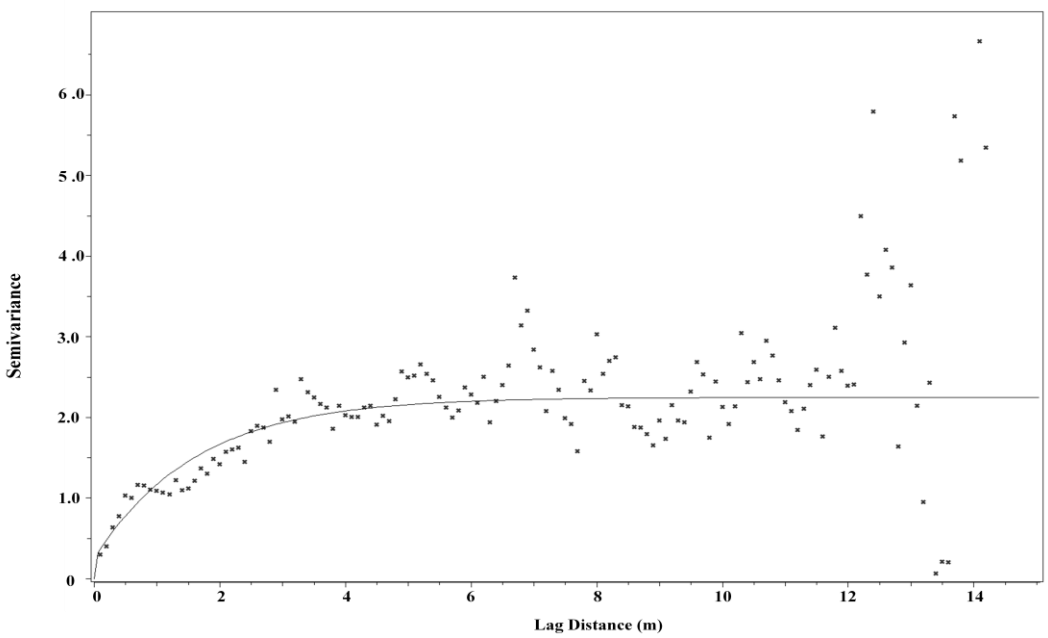

Figure A 1 Experimental vertical variogram of CMT-1 falling head permeameter K data.

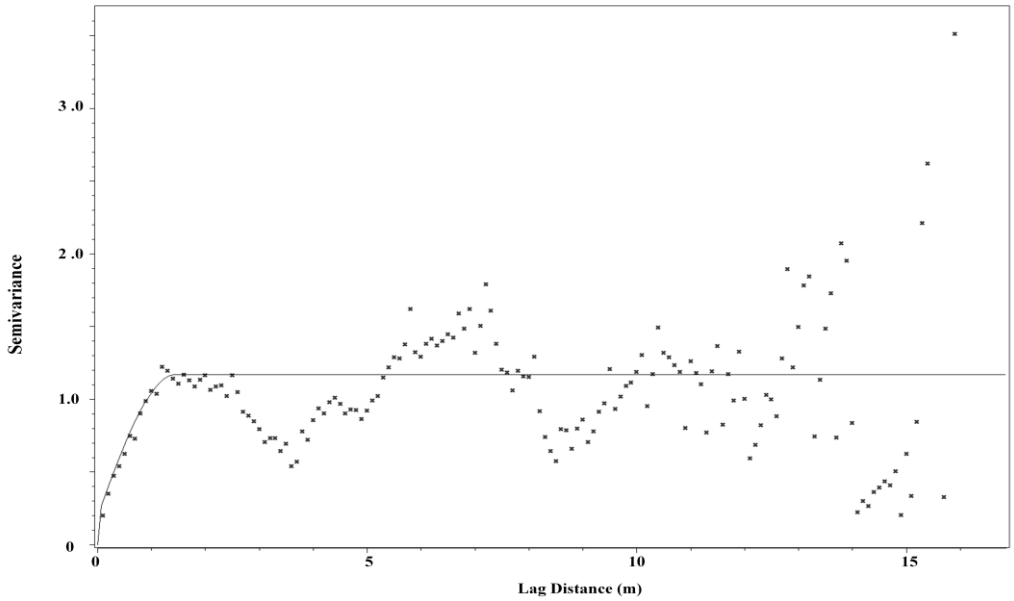

Figure A 2 Experimental vertical variogram of CMT-2 falling head permeameter K data.

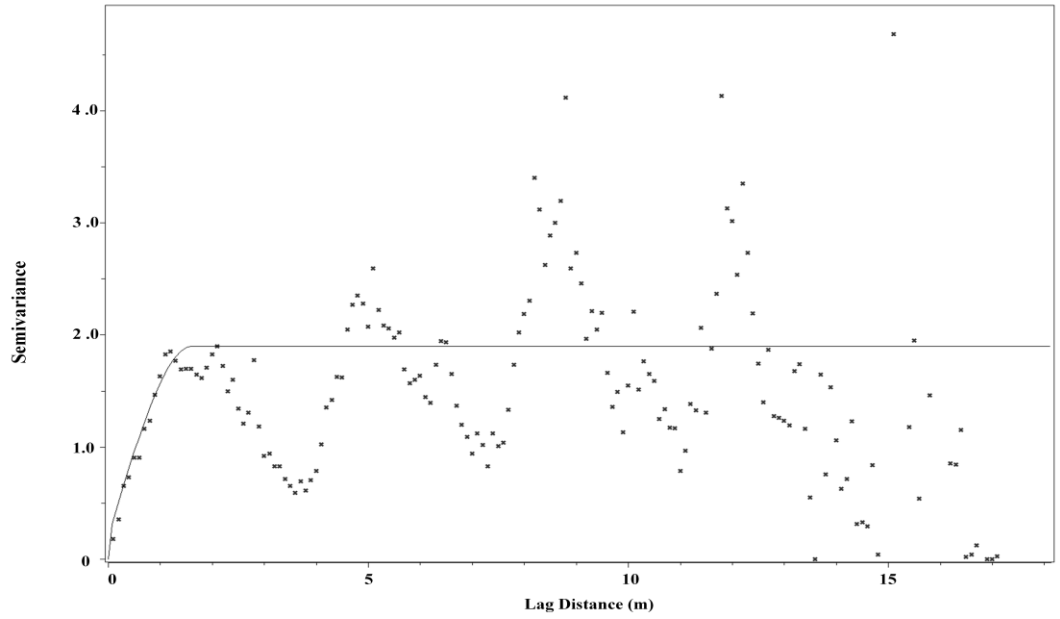

Figure A 3 Experimental vertical variogram of CMT-3 falling head permeameter K data.

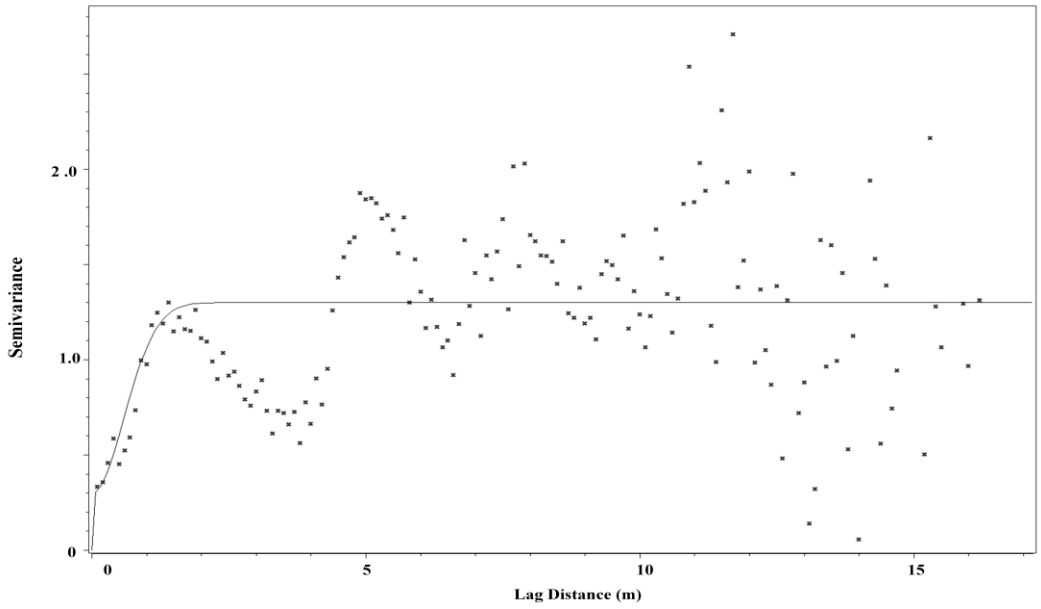

Figure A 4 Experimental vertical variogram of CMT-4 falling head permeameter K data.

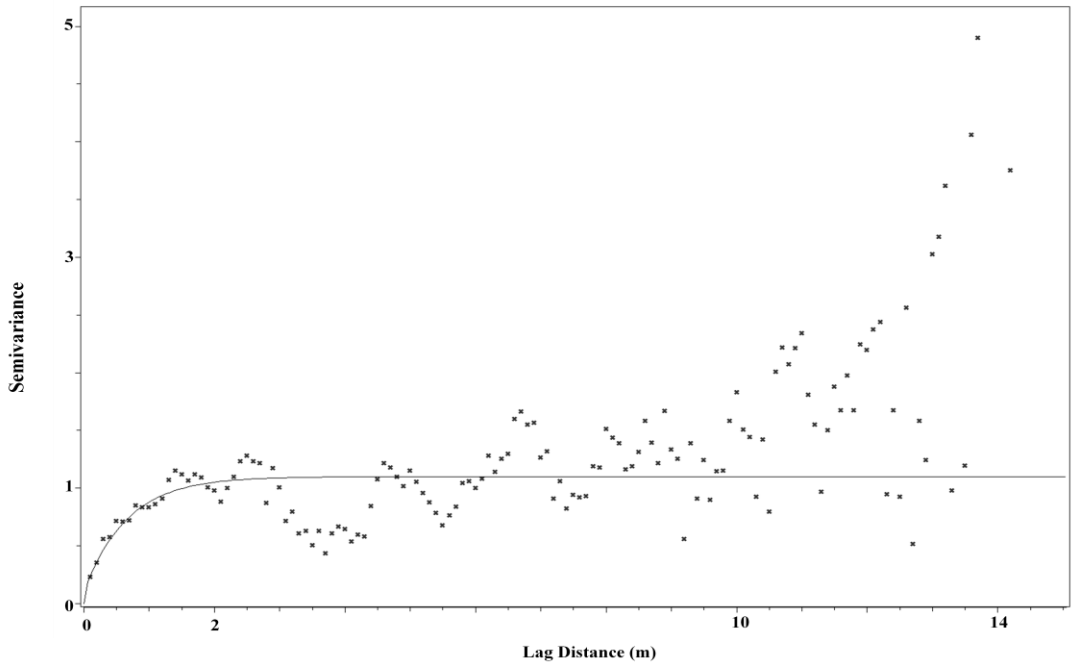

Figure A 5 Experimental vertical variogram of PW falling head permeameter K data.

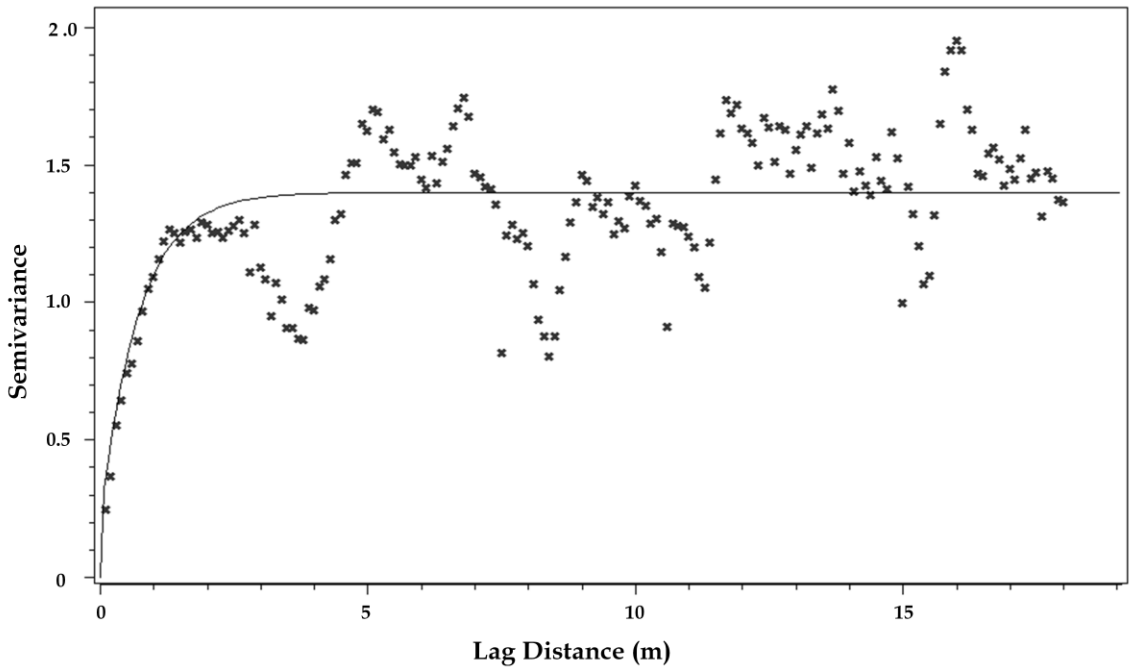

Figure A 6 Experimental vertical variogram calculated using all of the falling head permeameter K data.

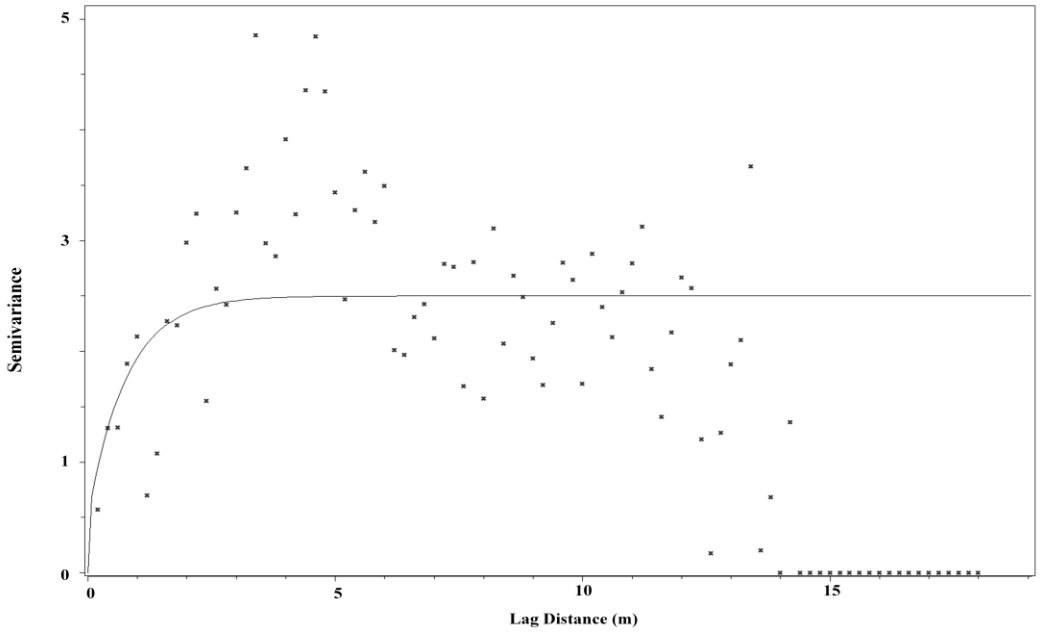

Figure A 7 Experimental vertical variogram of CMT-1 empirical equation K data.

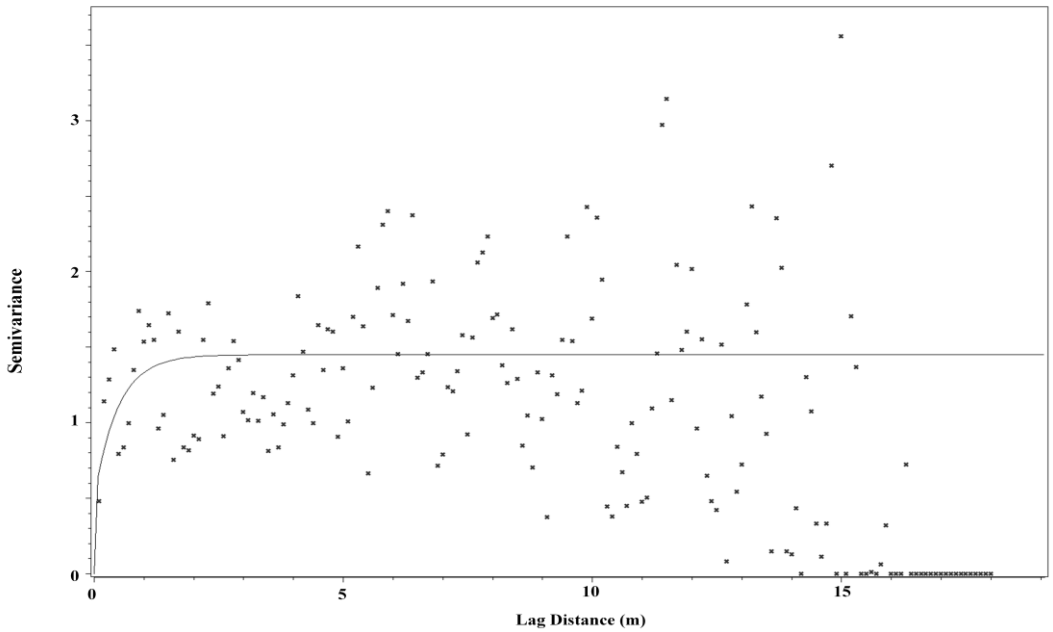

Figure A 8 Experimental vertical variogram of CMT-2 empirical equation K data.

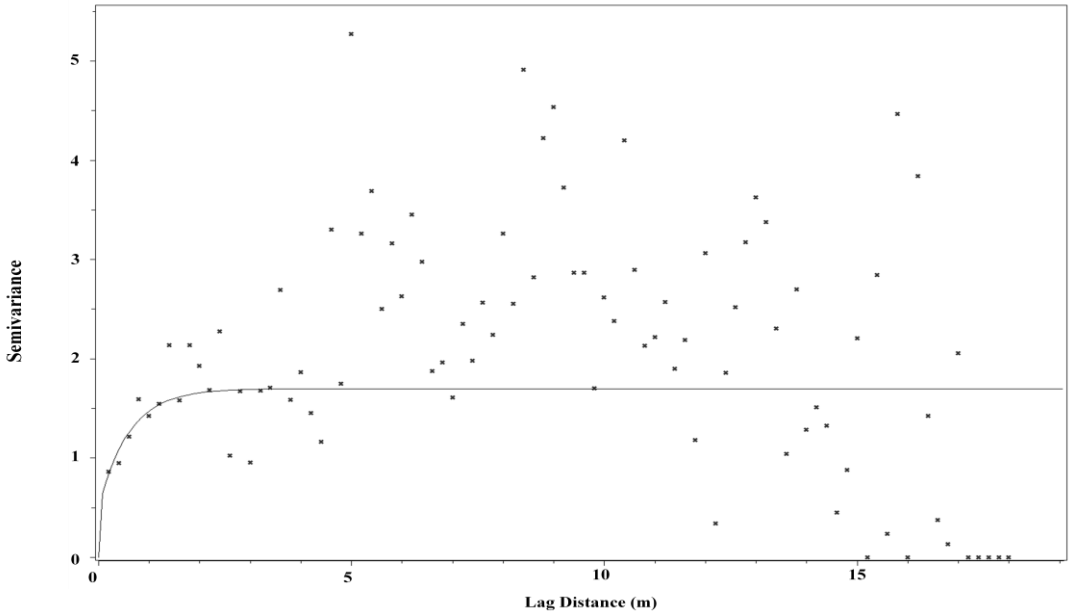

Figure A 9 Experimental vertical variogram of CMT-3 empirical equation K data.

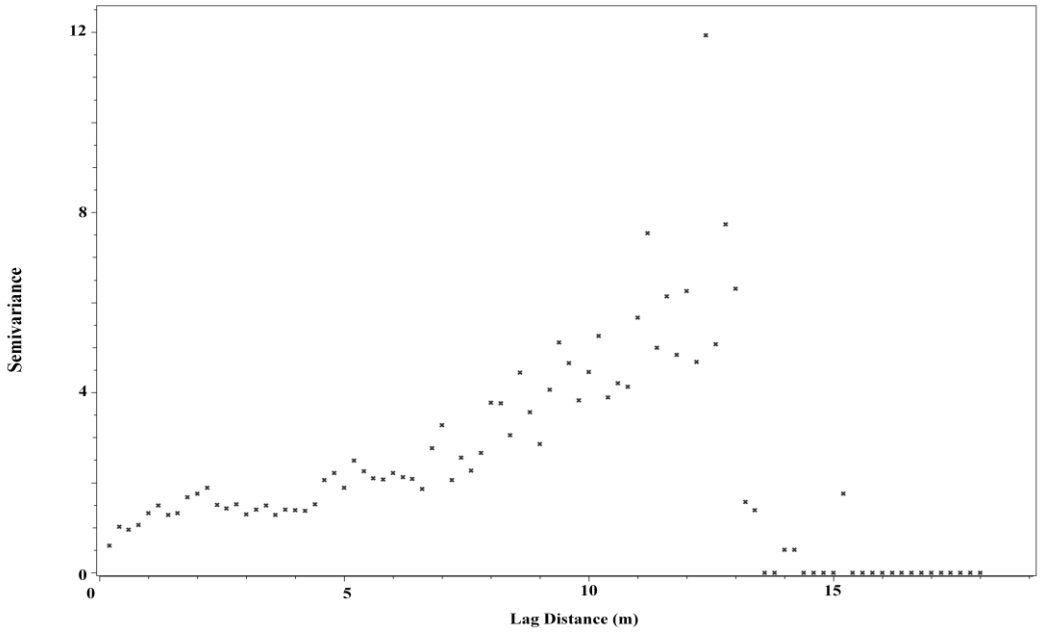

Figure A 10 Experimental vertical variogram of CMT-4 empirical equation K data.

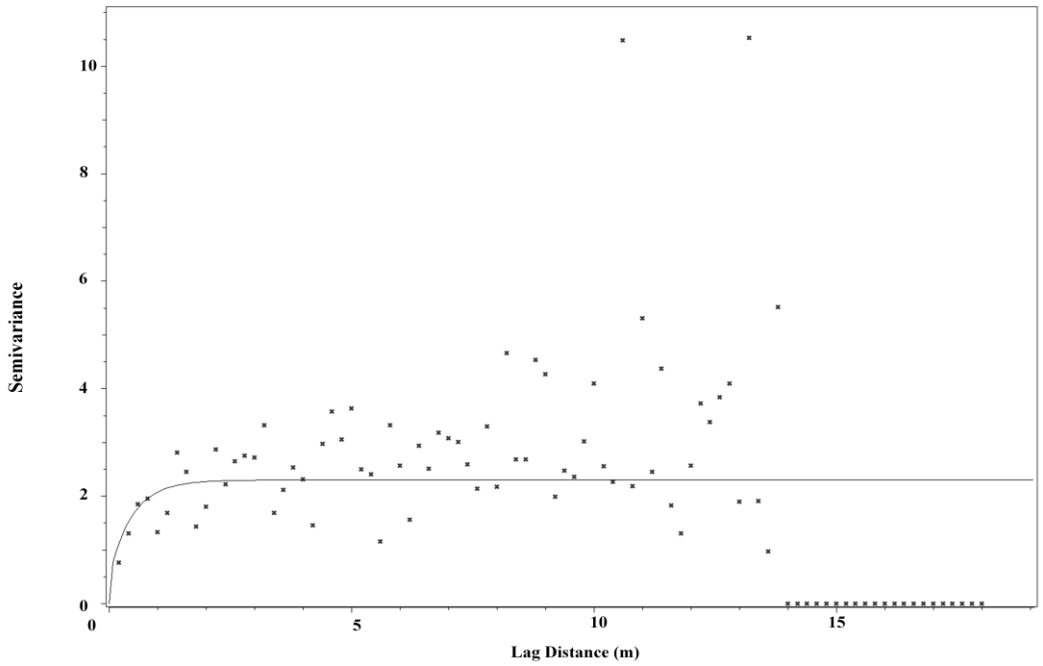

Figure A 11 Experimental vertical variogram of PW empirical equation K data.

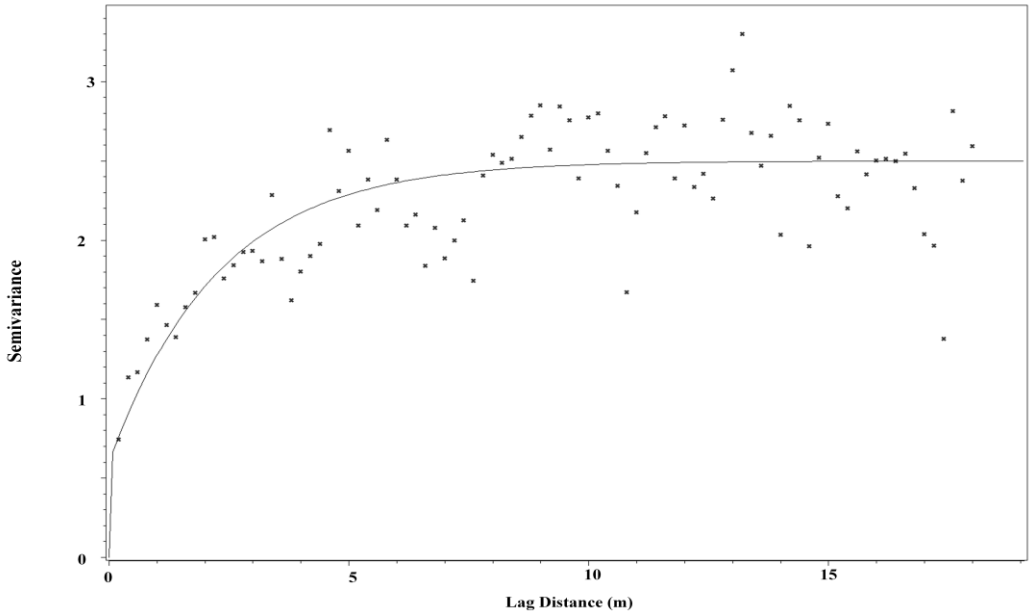

Figure A 12 Experimental vertical variogram calculated using all empirical equation K data.

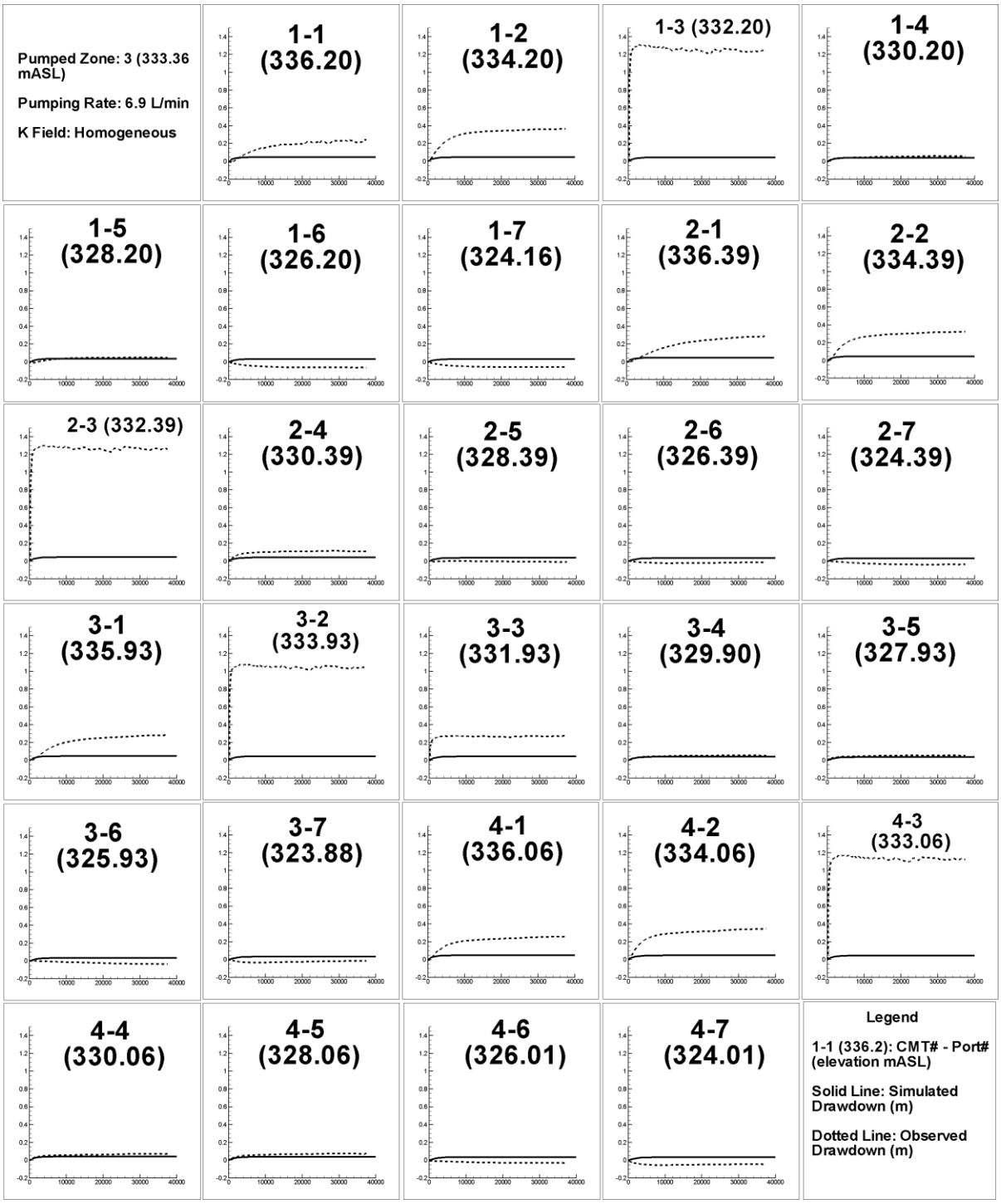

Figure A 13 Zone 3 *HGS* simulation results (homogeneous case). X-Axis is time in seconds and Y-Axis is drawdown in metres.

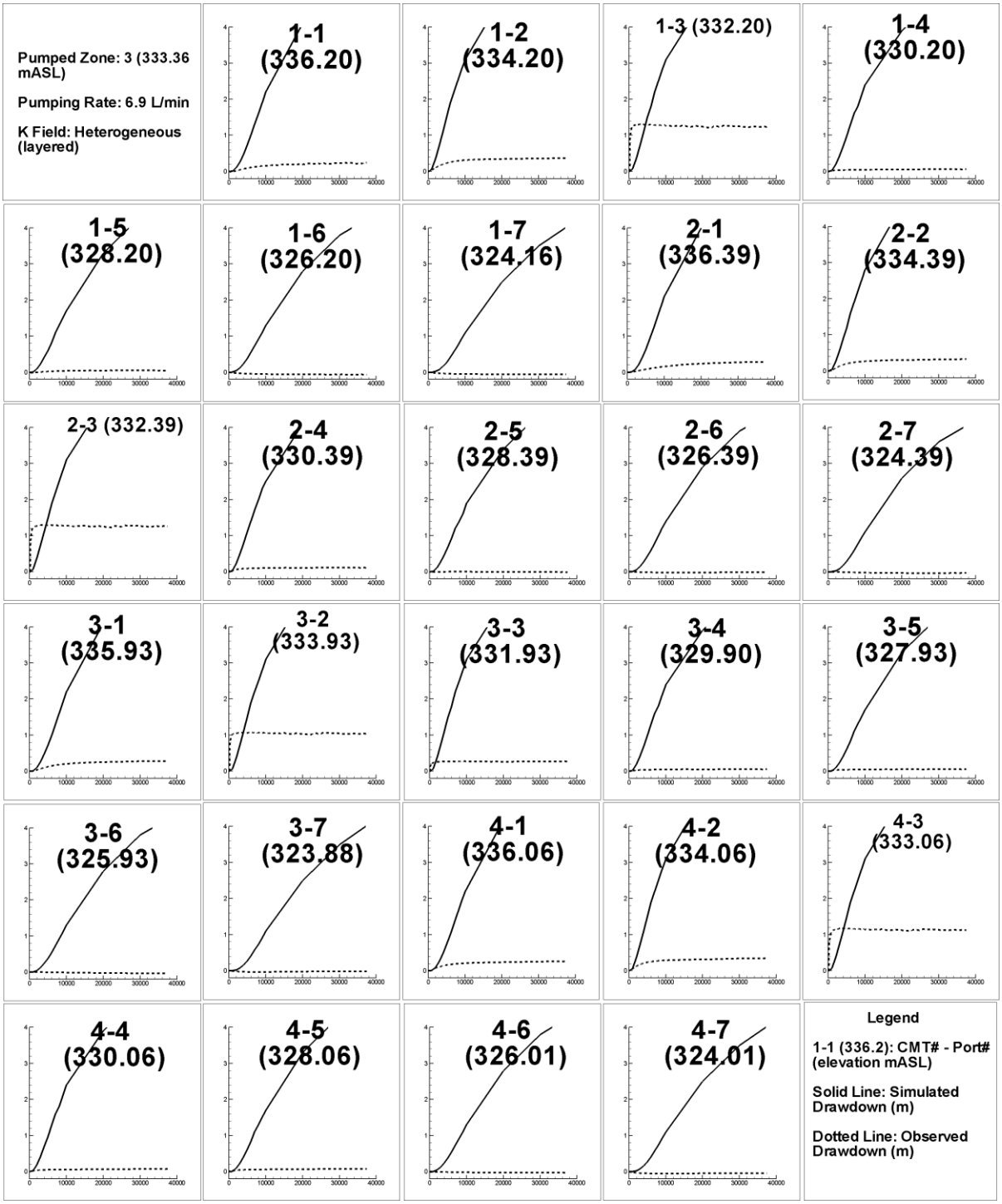

Figure A 14 Zone 3 *HGS* simulation results (heterogeneous layered case, slug test S_s values). X-Axis is time in seconds and Y-Axis is drawdown in metres.

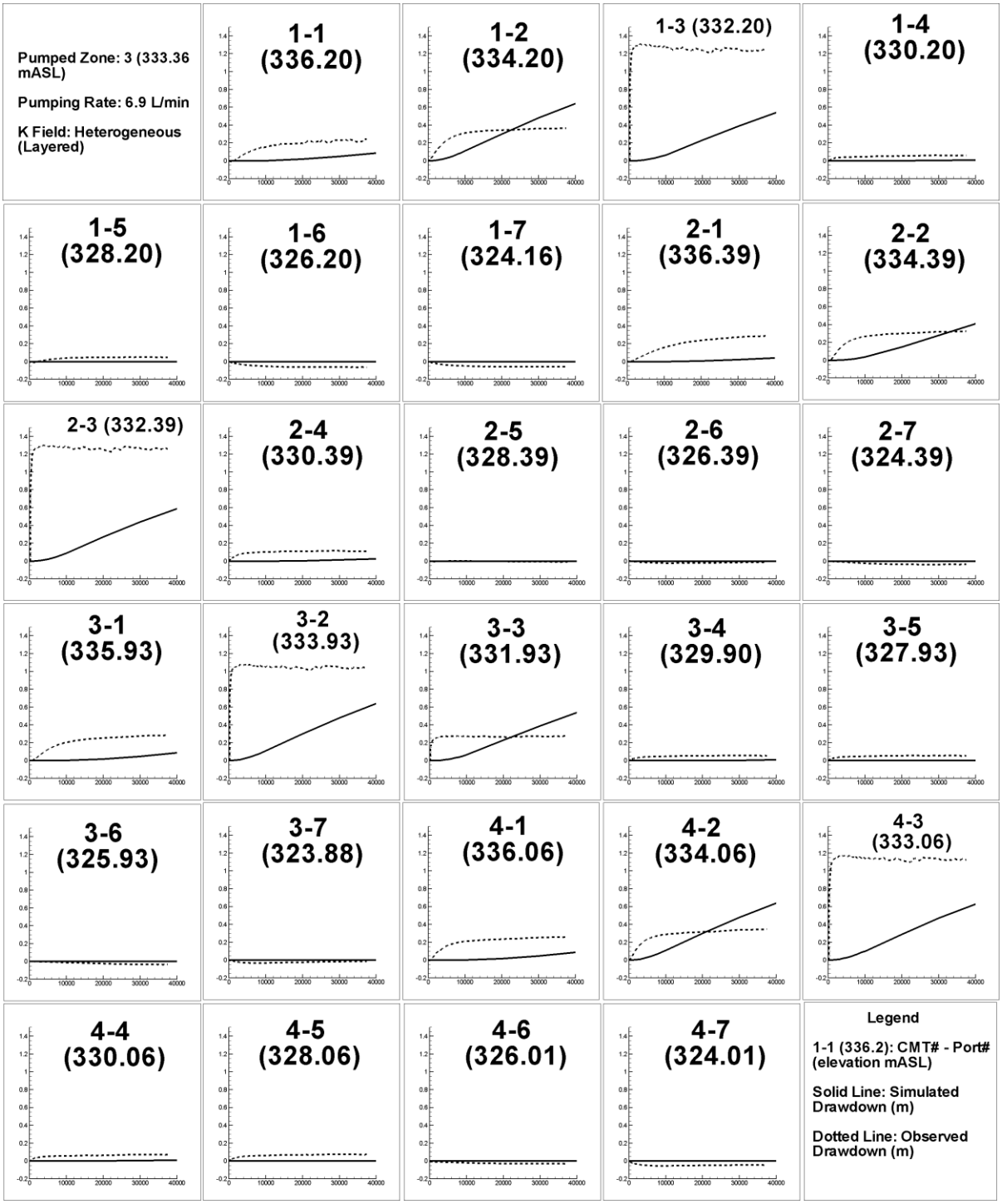

Figure A 15 Zone 3 *HGS* simulation results (heterogeneous layered case, tabulated S_s values). X-Axis is time in seconds and Y-Axis is drawdown in metres.

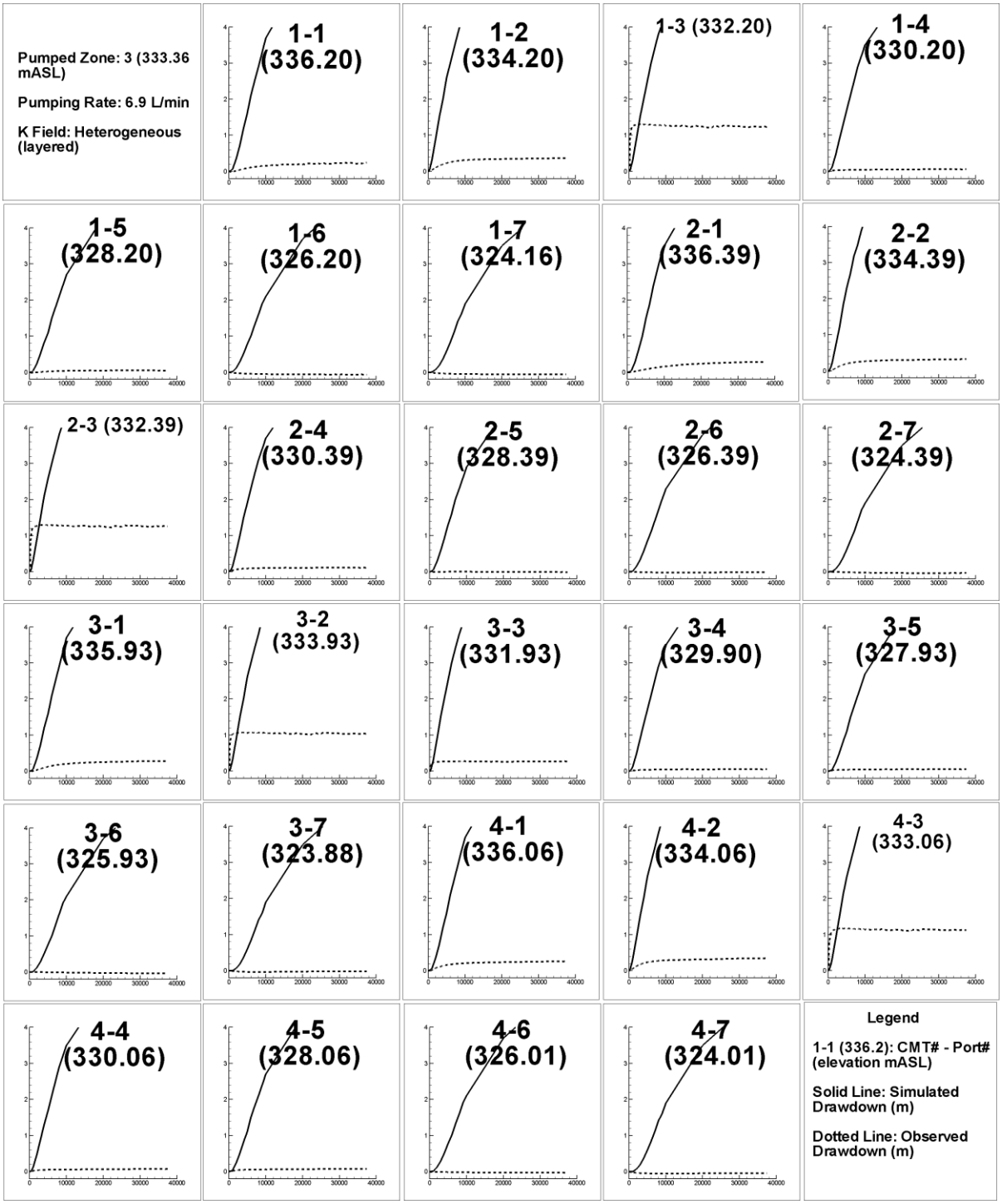

Figure A 16 Zone 3 *HGS* simulation results (heterogeneous layered K, homogeneous S_s from slug tests). X-Axis is time in seconds and Y-Axis is drawdown in metres.

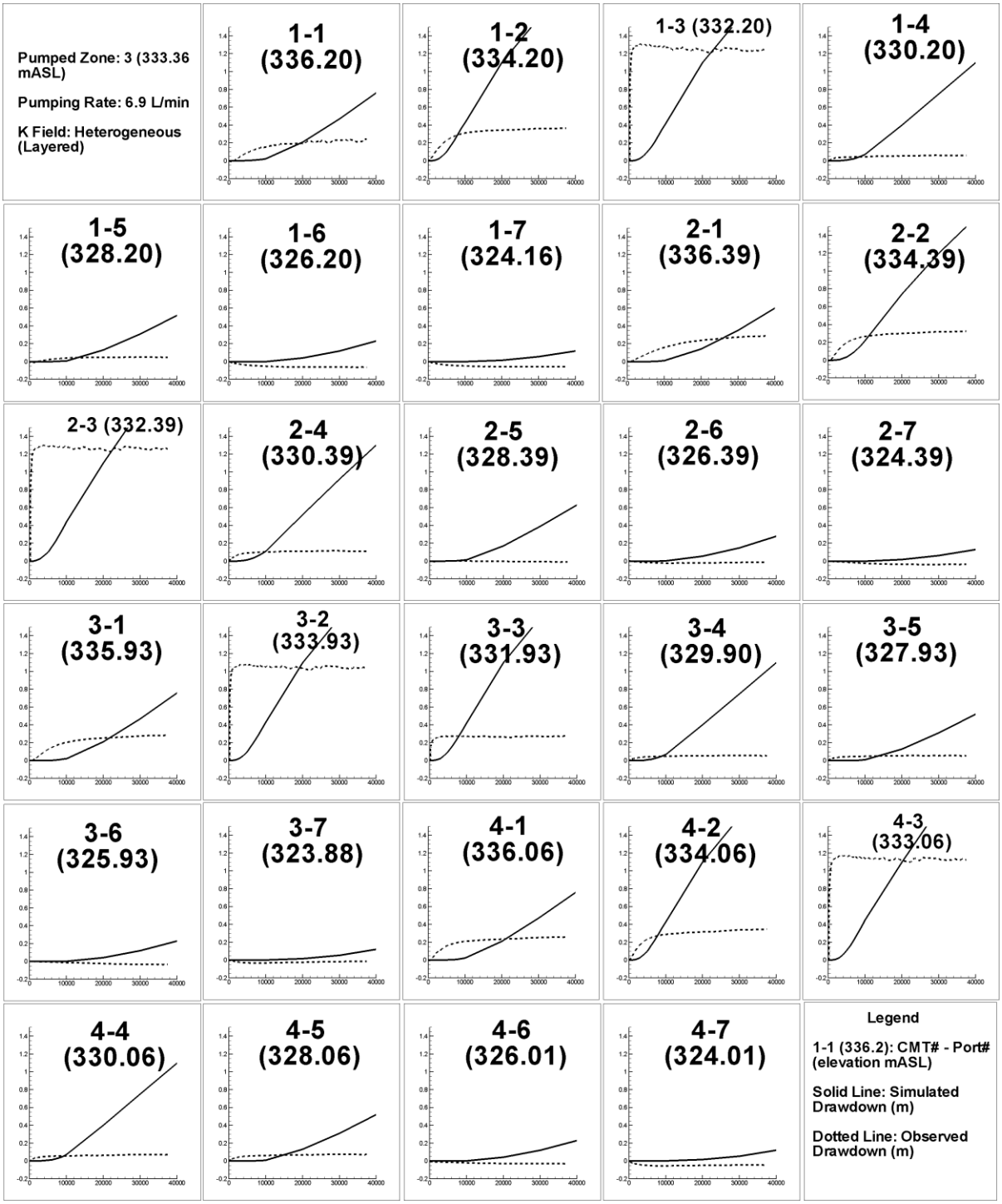

Figure A 17 Zone 3 *HGS* simulation results (heterogeneous layered K, homogeneous S_s from pumping tests). X-Axis is time in seconds and Y-Axis is drawdown in metres.

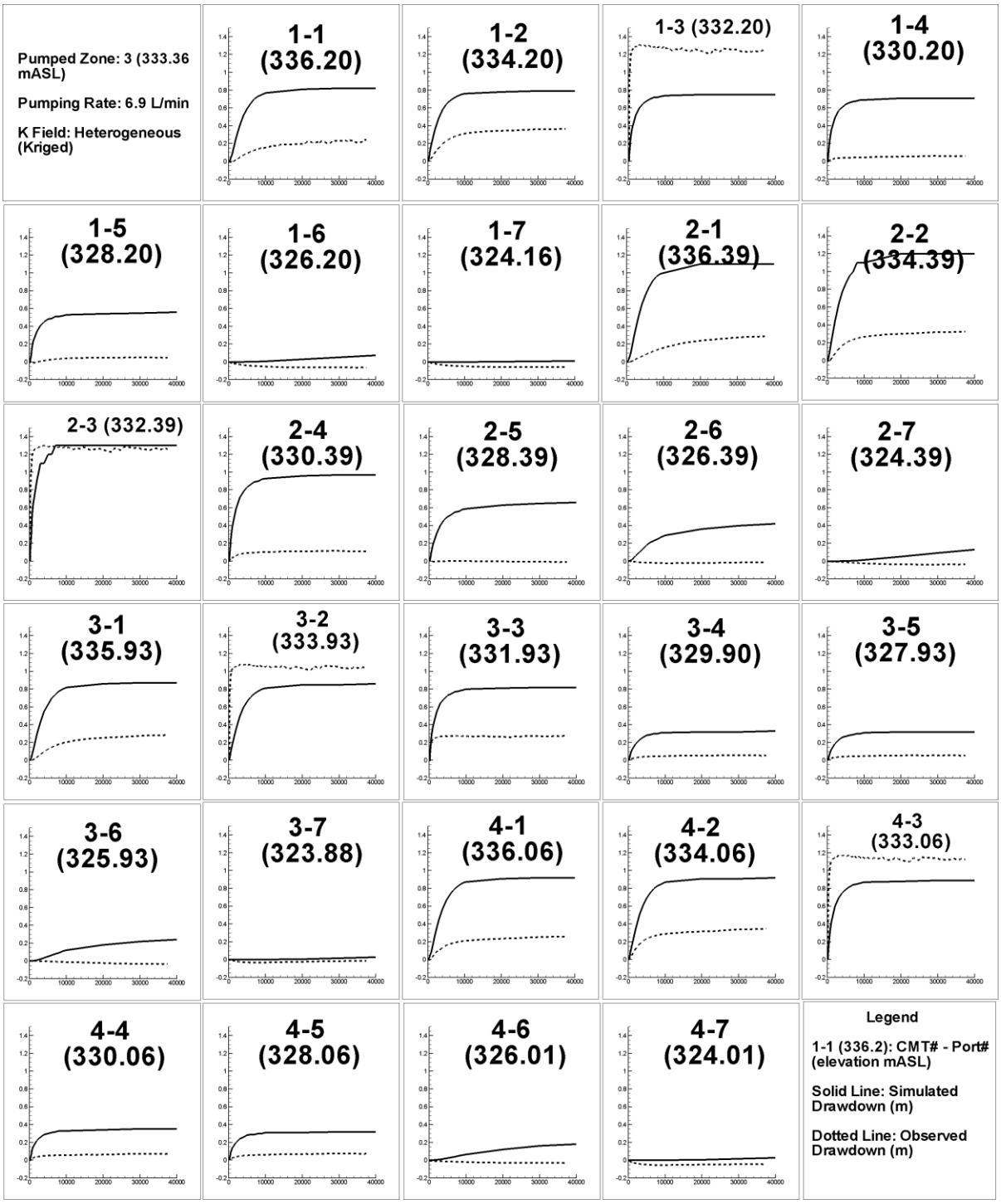

Figure A 18 Zone 3 *HGS* simulation results (heterogeneous kriged permeameter data case, slug test S_s values). X-Axis is time in seconds and Y-Axis is drawdown in metres.

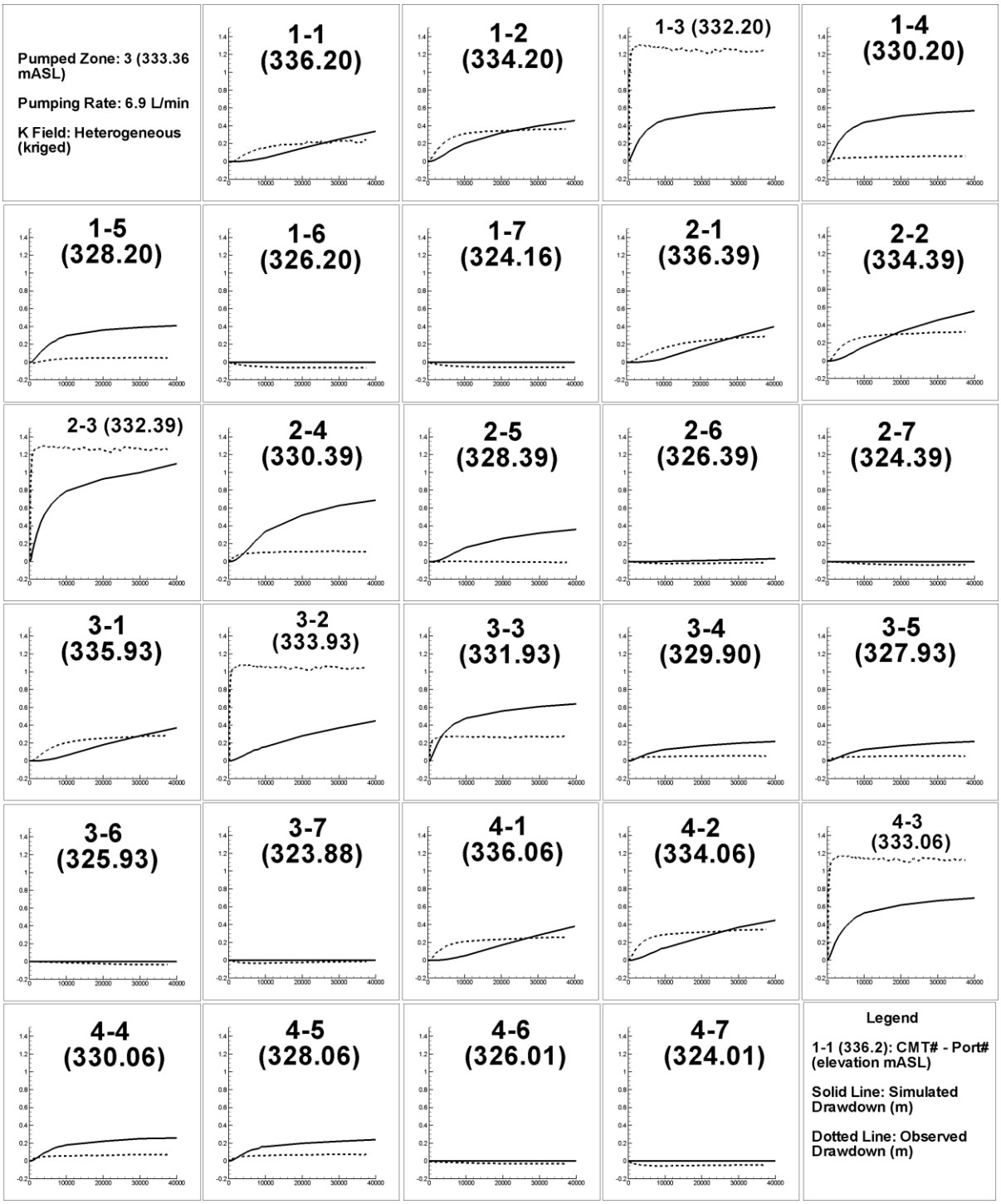

Figure A 19 Zone 3 *HGS* simulation results (heterogeneous kriged permeameter data case, tabulated S_s values). X-Axis is time in seconds and Y-Axis is drawdown in metres.

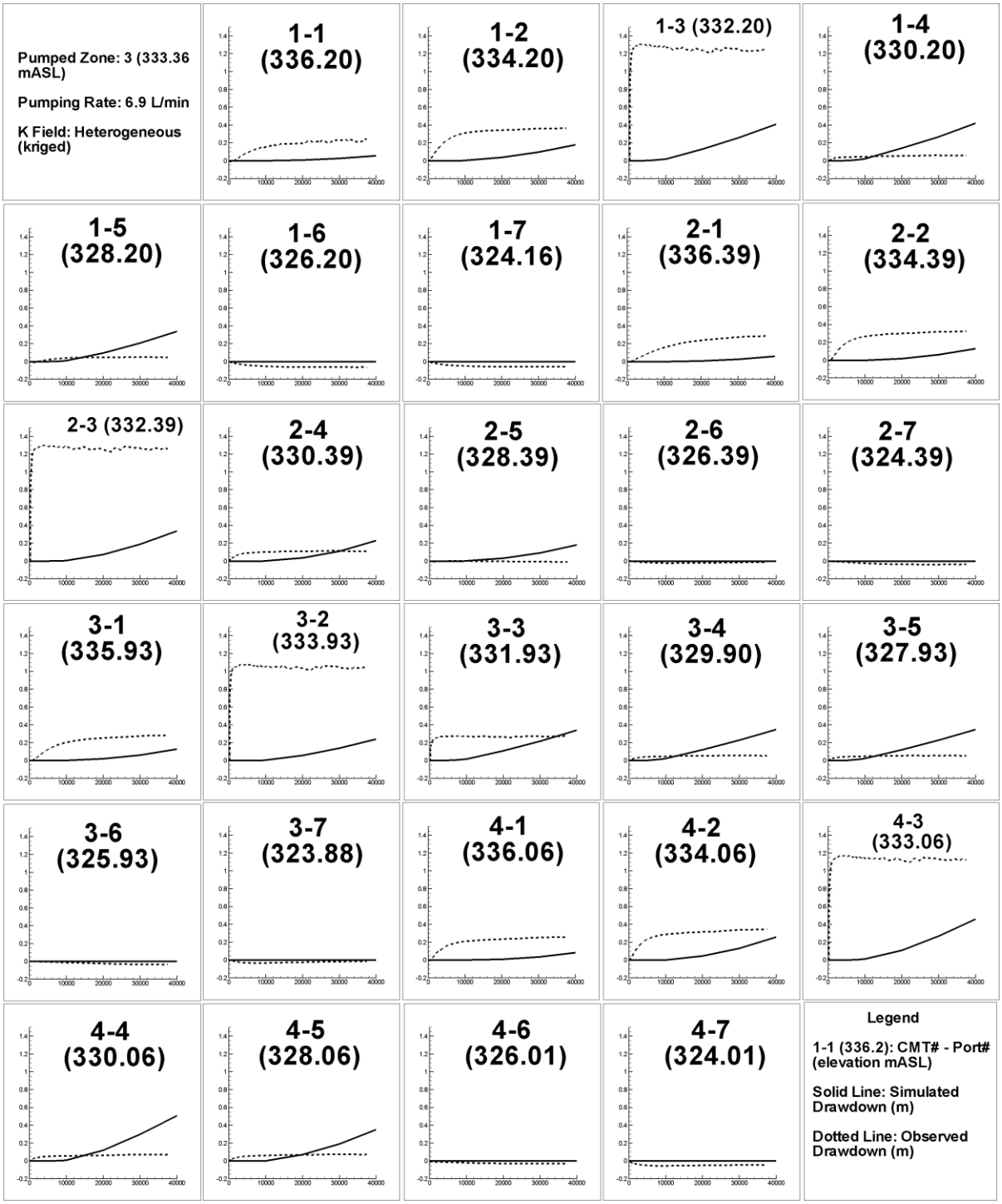

Figure A 20 Zone 3 *HGS* simulation results (heterogeneous kriged empirical data case). X-Axis is time in seconds and Y-Axis is drawdown in metres.

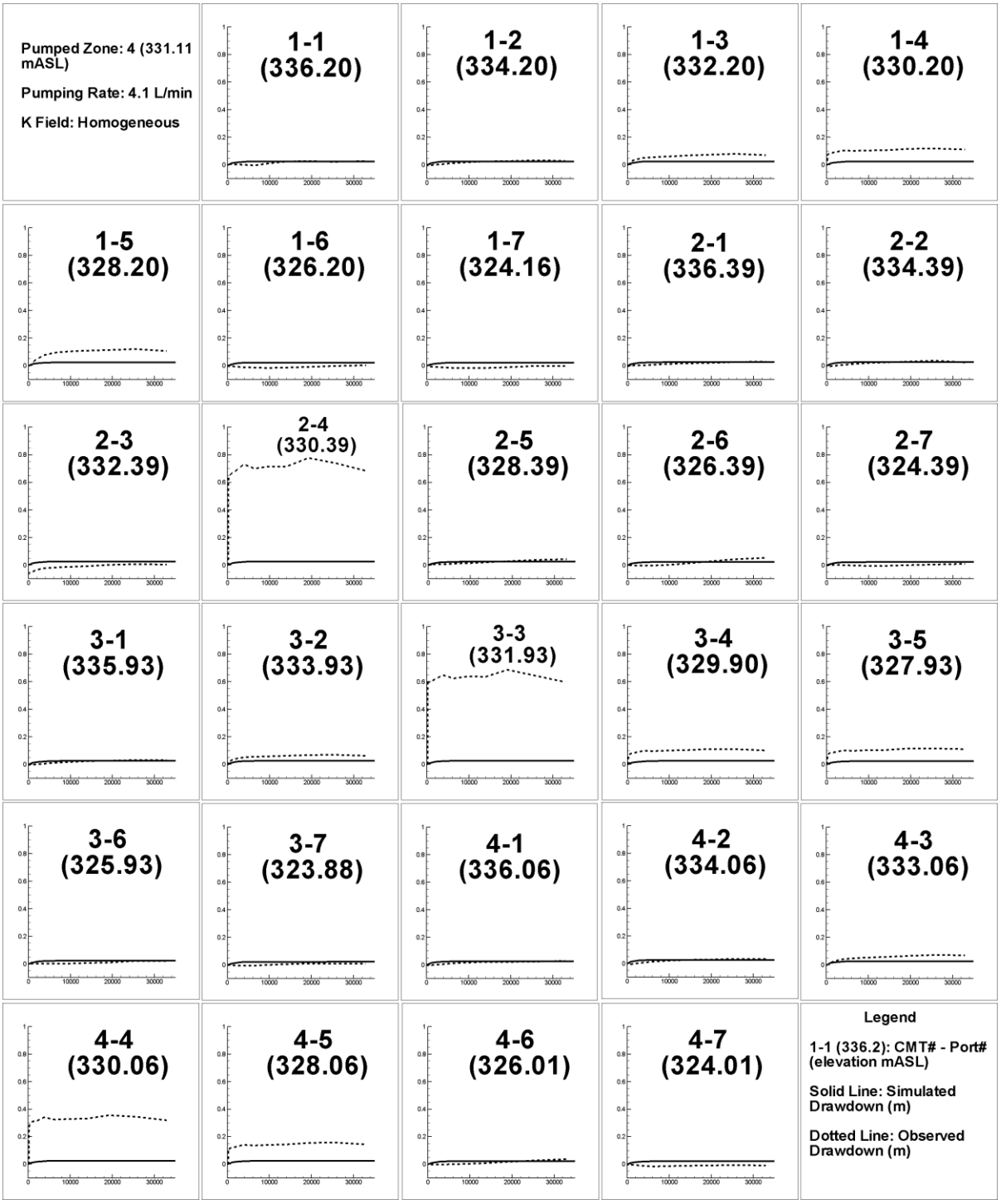

Figure A 21 Zone 4 *HGS* simulation results (homogeneous case). X-Axis is time in seconds and Y-Axis is drawdown in metres.

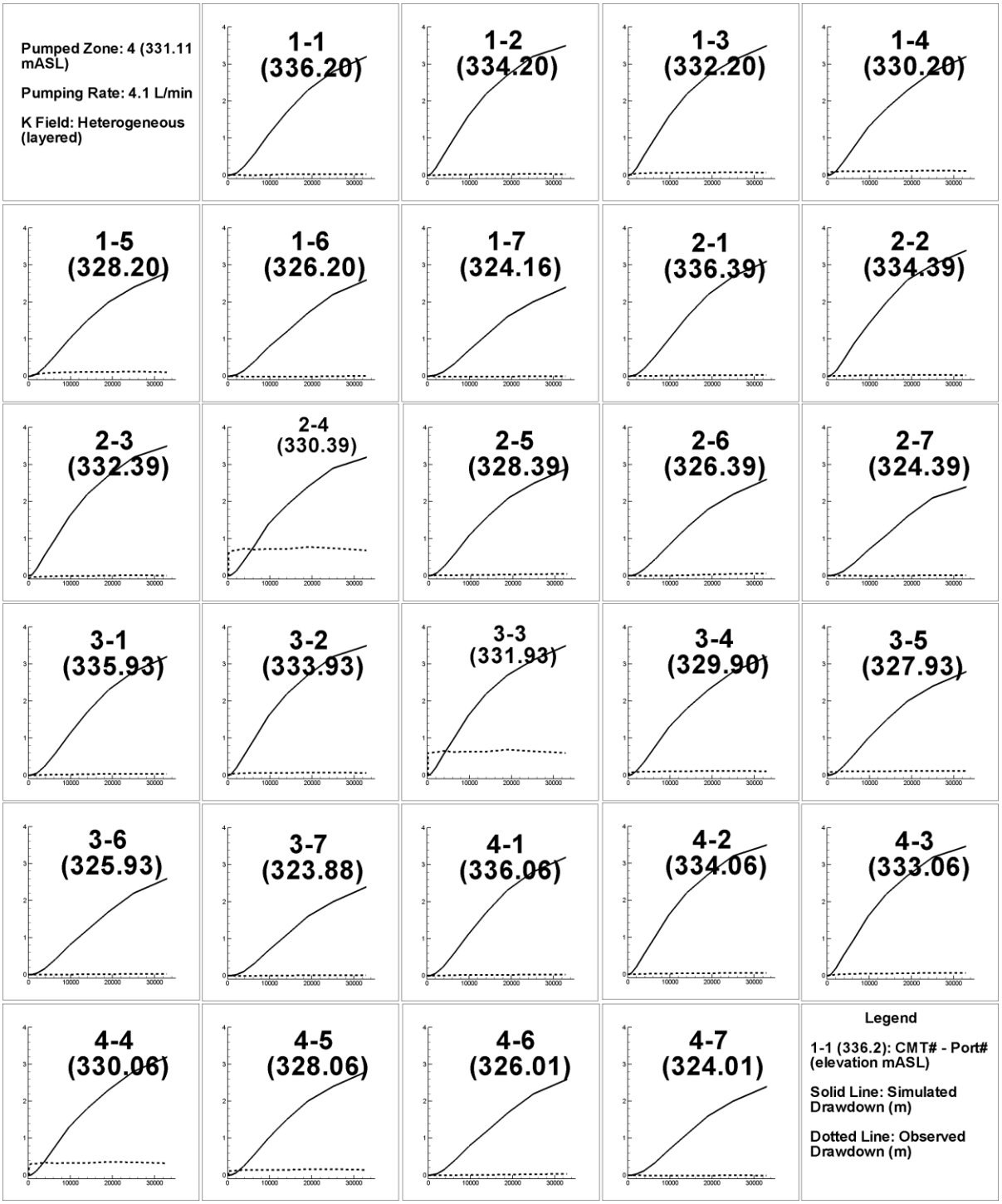

Figure A 22 Zone 4 *HGS* simulation results (heterogeneous layered case, slug test S_s values). X-Axis is time in seconds and Y-Axis is drawdown in metres.

Figure A 23 Zone 4 *HGS* simulation results (heterogeneous layered case, tabulated S_s values). X-Axis is time in seconds and Y-Axis is drawdown in metres.

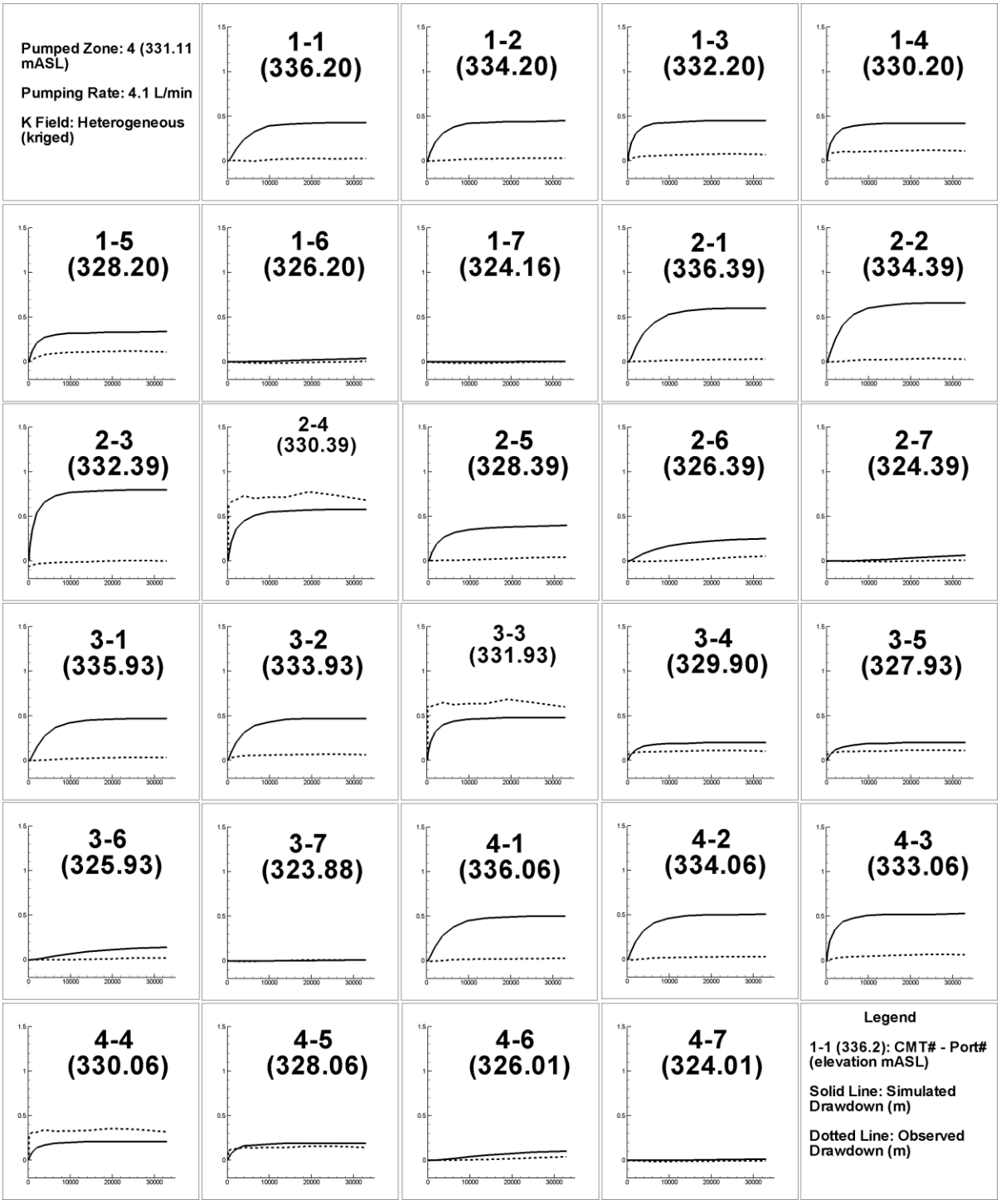

Figure A 24 Zone 4 *HGS* simulation results (heterogeneous kriged permeameter data case, slug test S_s values). X-Axis is time in seconds and Y-Axis is drawdown in metres.

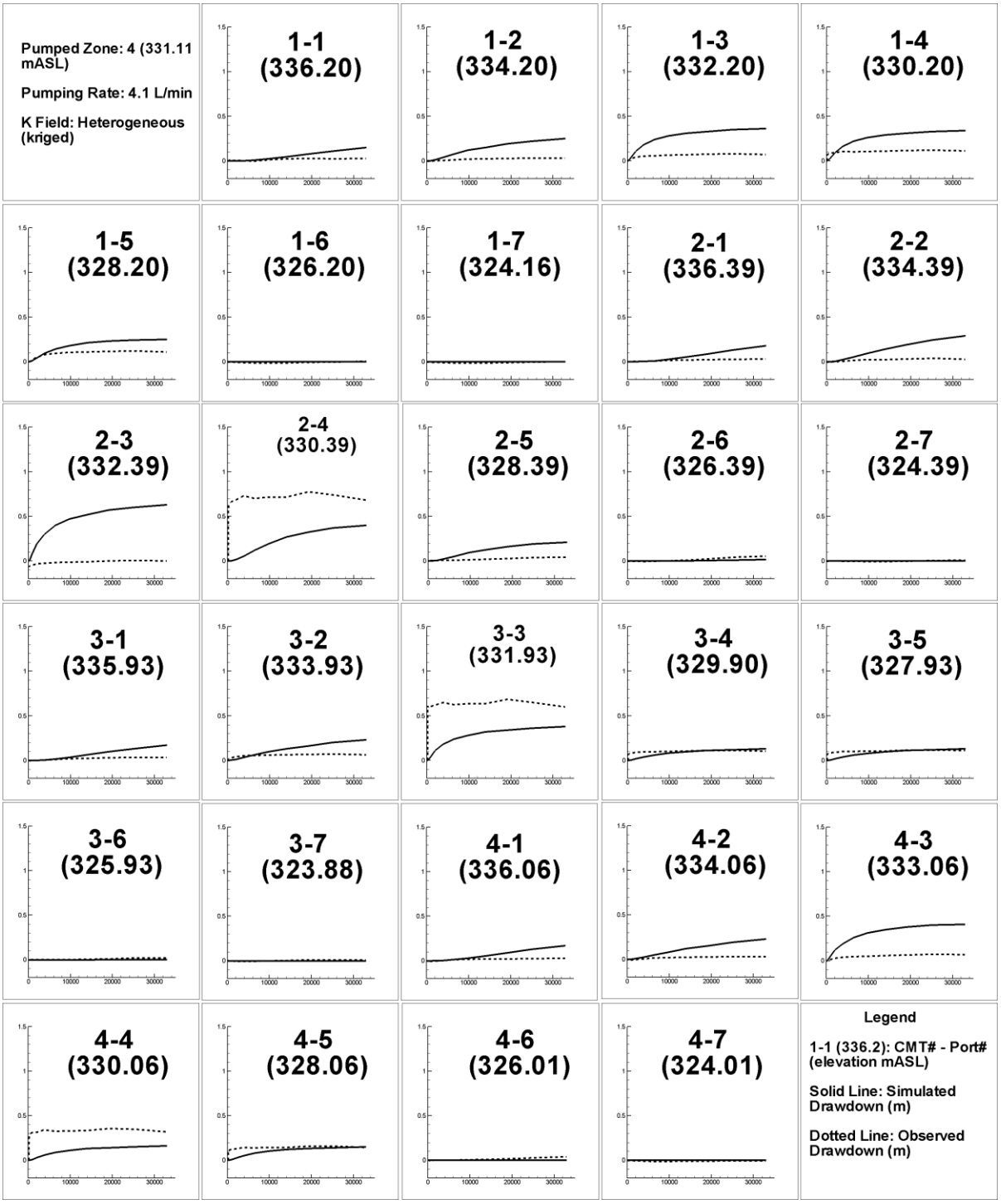

Figure A 25 Zone 4 *HGS* simulation results (heterogeneous kriged permeameter data case, tabulated S_s values). X-Axis is time in seconds and Y-Axis is drawdown in metres.

Figure A 26 Zone 4 *HGS* simulation results (heterogeneous kriged empirical equation data case). X-Axis is time in seconds and Y-Axis is drawdown in metres.

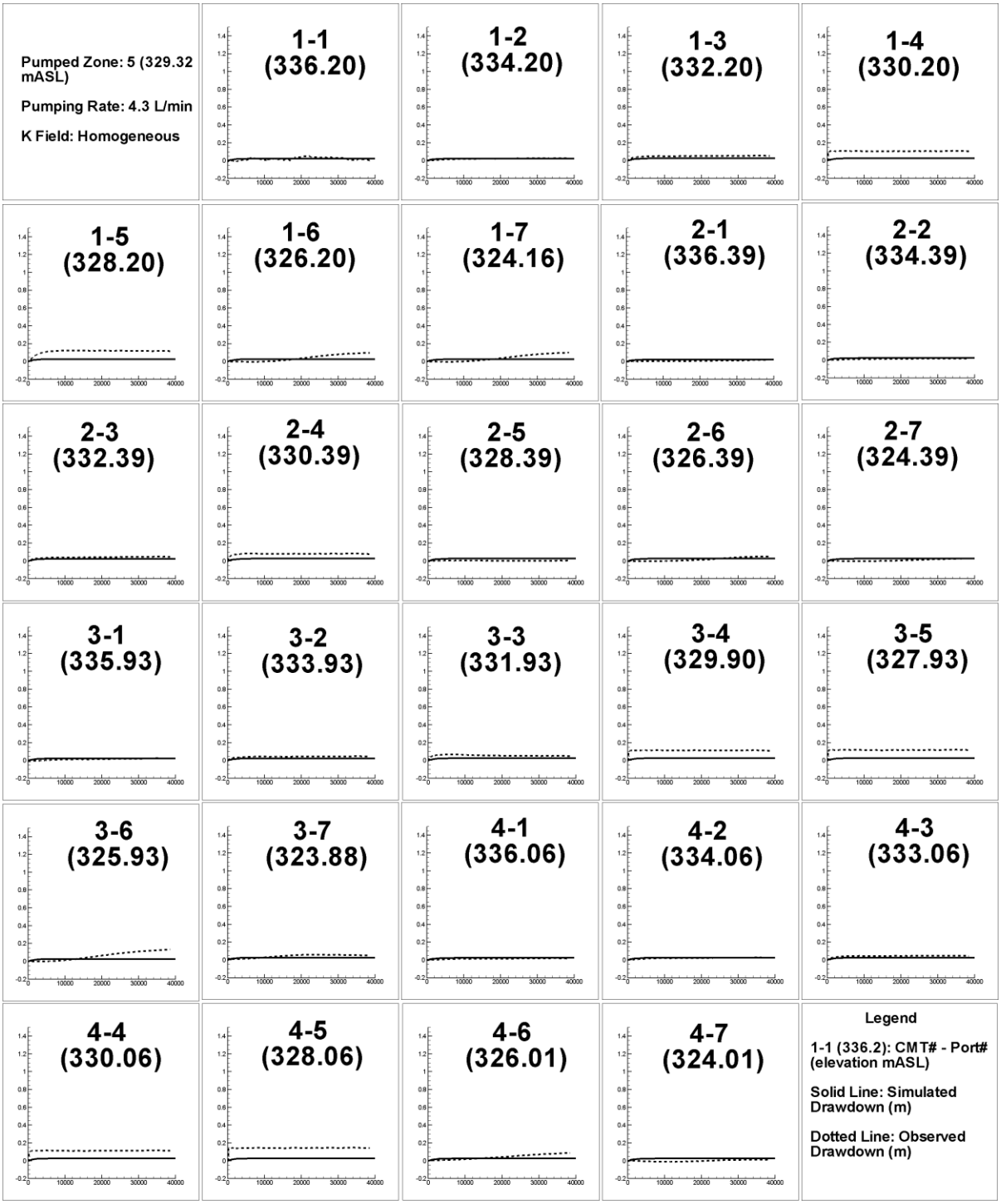

Figure A 27 Zone 5 *HGS* simulation results (homogeneous case). X-Axis is time in seconds and Y-Axis is drawdown in metres.

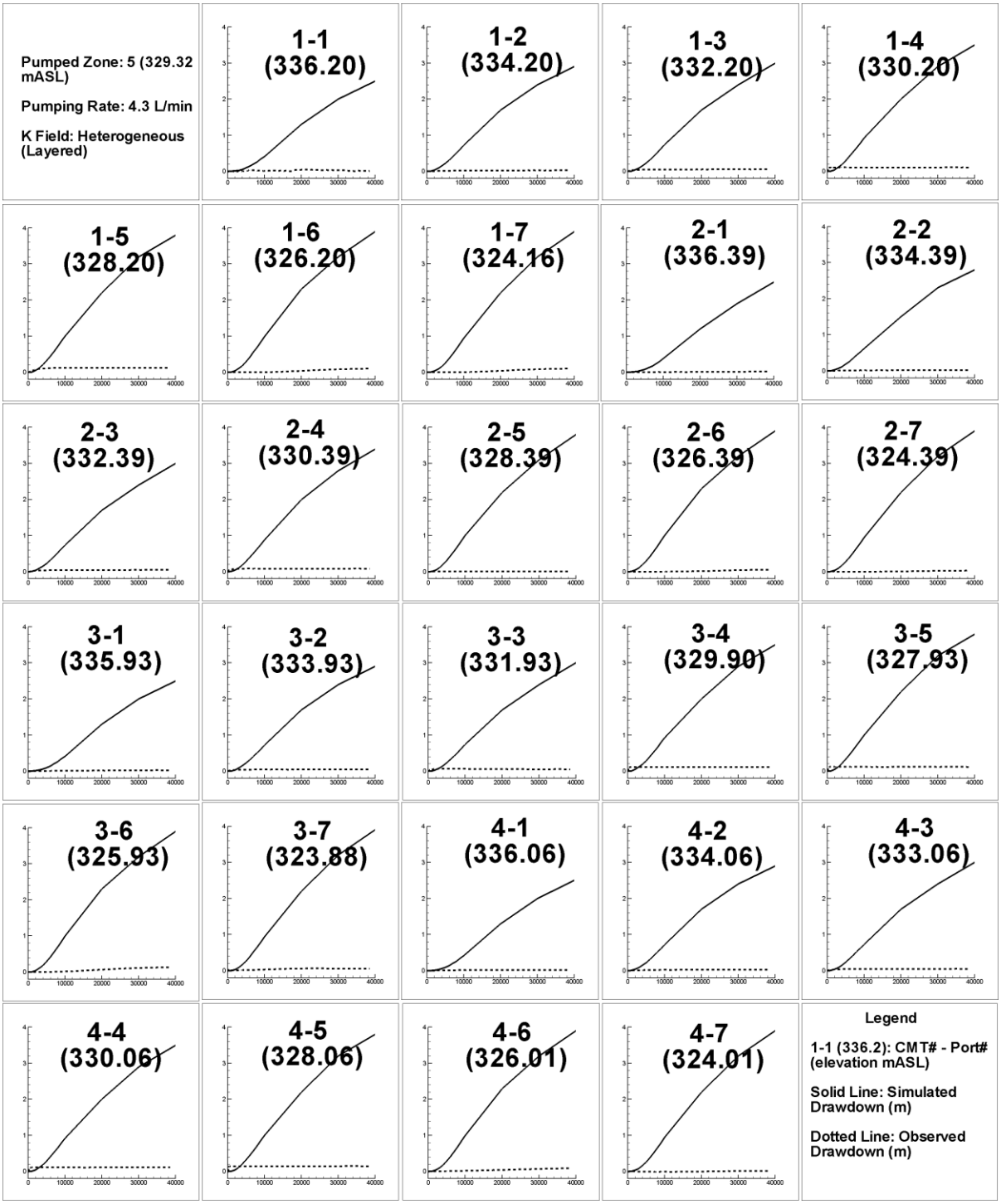

Figure A 28 Zone 5 *HGS* simulation results (heterogeneous layered case, slug test S_s values). X-Axis is time in seconds and Y-Axis is drawdown in metres.

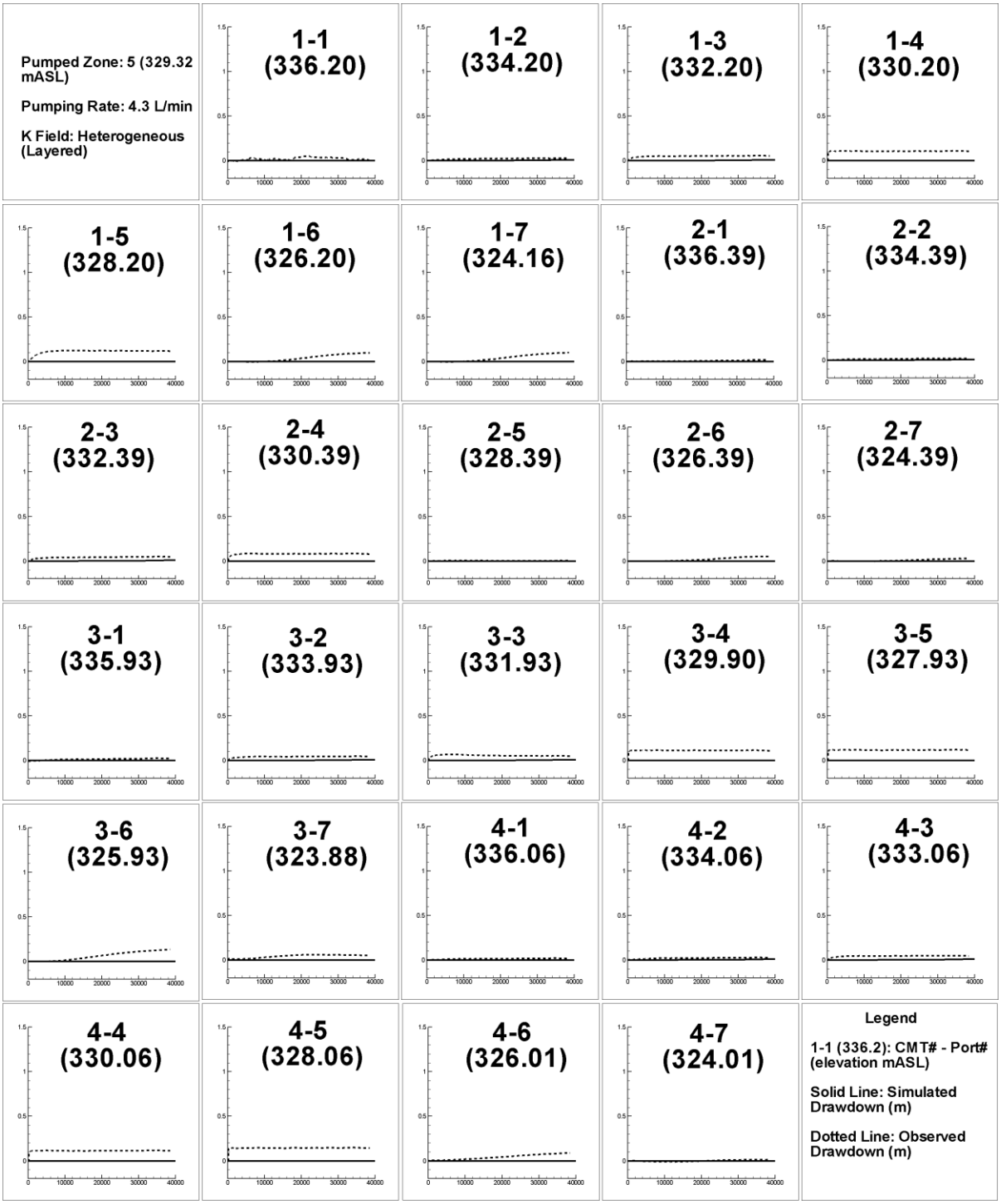

Figure A 29 Zone 5 *HGS* simulation results (heterogeneous layered case, tabulated S_s values). X-Axis is time in seconds and Y-Axis is drawdown in metres.

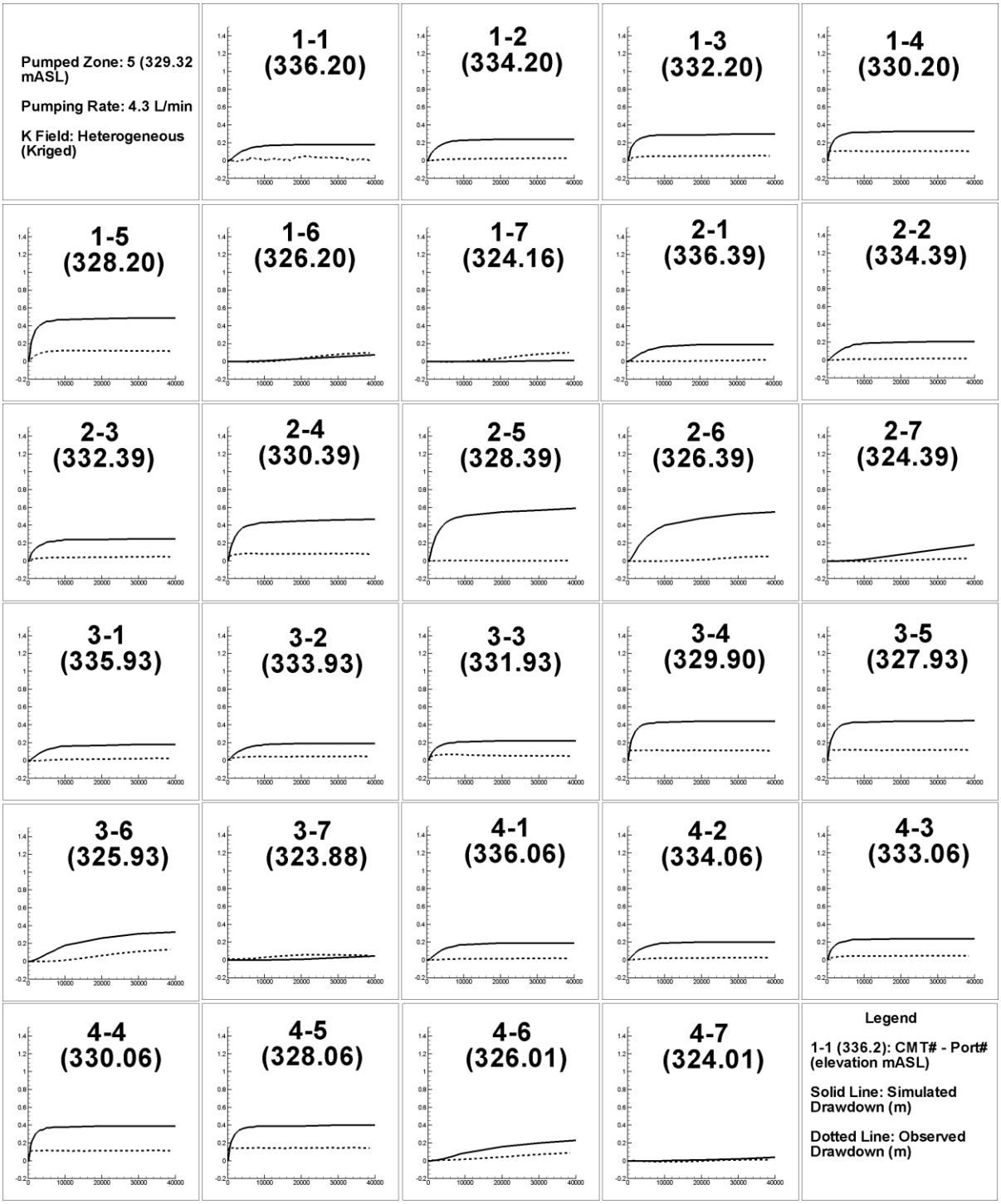

Figure A 30 Zone 5 *HGS* simulation results (heterogeneous kriged permeameter data case, slug test S_s values). X-Axis is time in seconds and Y-Axis is drawdown in metres.

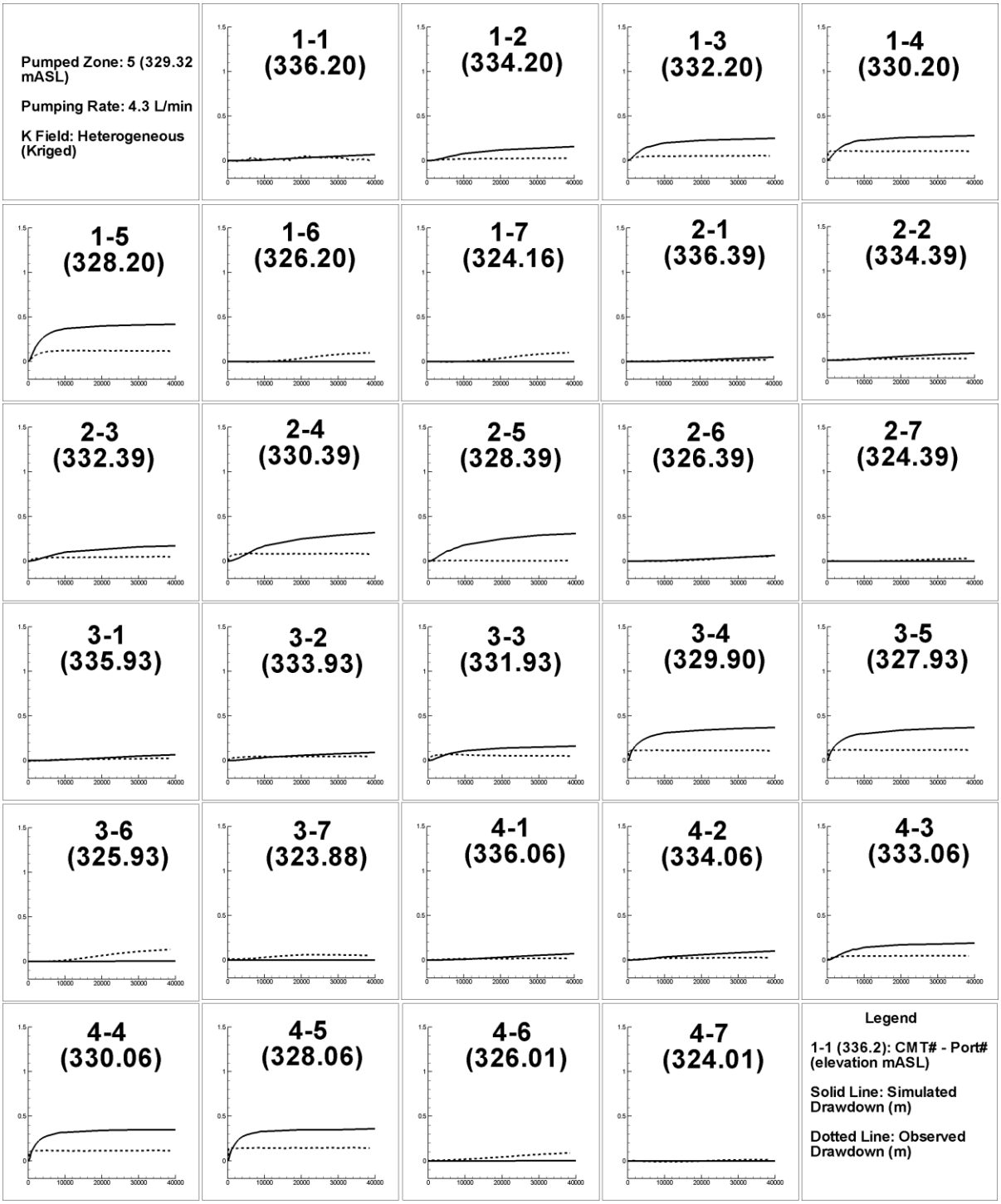

Figure A 31 Zone 5 *HGS* simulation results (heterogeneous kriged permeameter data case, tabulated S_s values). X-Axis is time in seconds and Y-Axis is drawdown in metres.

Figure A 32 Zone 5 *HGS* simulation results (heterogeneous kriged empirical equation data case). X-Axis is time in seconds and Y-Axis is drawdown in metres.

Appendix B

Additional Tables

Table B 1 USCS description of geology at CMT-1.

Top Elevation (mASL)	Bottom Elevation (mASL)	CMT-1
340.69	340.19	FILL
340.19	339.93	clayey SILT, little sand
339.93	339.88	SILT, some clay and sand
339.88	339.63	silty CLAY, trace sand
339.63	339.19	clayey SILT, sand content some to trace
339.19	338.84	CLAY and SILT, little sand
338.84	338.67	SILT, some clay and sand, trace gravel
338.67	338.12	silty CLAY, little to trace sand
338.12	337.64	sandy SILT, trace clay
337.64	337.59	SILT, trace clay
337.59	337.15	clayey SILT, trace sand
337.15	333.48	SILT, some sand, trace clay (sand and clay content variable throughout, sand absent below 6.63 m)
333.48	333.28	clayey SILT, trace sand
333.28	333.15	SILT, some clay, trace sand
333.15	331.22	silty SAND, trace clay
331.22	330.78	SILT, little clay, trace sand (sand and clay content variable throughout)
330.78	330.34	SAND, little silt, trace clay
330.34	330.14	silty SAND, some gravel, trace clay
330.14	330.02	gravelly SAND, some silt, trace clay
330.02	329.26	SILT, little gravel, sand and clay
329.26	328.50	SAND, little gravel, trace silt and clay
328.50	328.28	clayey SILT, trace sand
328.28	328.22	silty CLAY, trace sand
328.22	328.18	clayey and sandy SILT, trace gravel
328.18	327.14	CLAY and SILT, trace to little sand
327.14	326.88	clayey SILT, trace sand to sandy
326.88	326.15	silty CLAY, little to trace sand, trace gravel
326.15	325.90	clayey SILT, trace sand
325.90	325.88	SILT and SAND, little gravel and clay
325.88	325.00	CLAY and SILT, sand 'sandy' to some, trace gravel
325.00	323.93	silty CLAY, little sand, trace gravel
323.93	323.77	CLAY, some silt, little sand, trace gravel

Table B 2 USCS description of geology at CMT-2.

Top Elevation (mASL)	Bottom Elevation (mASL)	CMT-2
340.89	340.13	clayey and sandy SILT
340.13	339.83	sandy SILT, trace clay
339.83	339.48	clayey SILT, trace sand
339.48	338.91	silty CLAY, trace to little sand
338.91	338.82	clayey SILT, little sand, trace gravel
338.82	338.74	SILT, some clay and sand, trace gravel
338.74	338.60	CLAY and SILT, some sand
338.60	338.40	sandy SILT, trace clay
338.40	338.32	clayey SILT, little sand
338.32	337.95	SILT, some sand, little clay, trace gravel (clay, sand and gravel content variable)
337.95	336.66	clayey SILT, little sand (sand content decreasing with depth)
336.66	334.03	SILT, little sand, trace clay (sand and clay content variable throughout)
334.03	333.94	clayey SILT, trace sand
333.94	332.99	SILT, trace to some clay, trace sand and gravel
332.99	331.85	silty SAND, trace clay
331.85	331.75	clayey SILT, trace sand
331.75	331.40	SILT, trace sand, trace to some clay
331.40	330.98	clayey SILT, trace sand
330.98	330.74	SILT, some clay, trace sand
330.74	330.64	CLAY and SILT, trace sand
330.64	330.22	SILT, trace to little clay and sand
330.22	329.92	clayey SILT, trace sand
329.92	329.46	SILT, some clay, trace to little sand
329.46	328.70	CLAY and SILT, trace to little sand
328.70	328.03	silty CLAY, little to some sand
328.03	327.17	clayey SILT, trace sand
327.17	327.07	SILT, some clay and sand
327.07	326.80	silty CLAY, little sand, trace gravel
326.80	326.53	SILT, some clay
326.53	326.39	clayey and sandy SILT
326.39	326.10	clayey SILT and SAND
326.10	324.89	CLAY and SILT, sandy to some sand
324.89	324.85	clayey SILT and SAND, trace gravel
324.85	324.26	CLAY and SILT, little sand, trace gravel
324.26	324.13	SAND and SILT, little clay, trace gravel

Table B 3 USCS description of geology at CMT-3.

Top Elevation (mASL)	Bottom Elevation (mASL)	CMT-3
341.33	341.13	FILL
341.13	340.57	CLAY and SILT, trace sand
340.57	339.97	clayey and sandy SILT, trace gravel
339.97	339.81	SILT, trace clay and sand
339.81	339.45	CLAY and SILT, trace sand
339.45	339.09	silty CLAY, trace sand
339.09	338.27	silty SAND
338.27	338.13	clayey SILT, some sand, trace gravel
338.13	337.83	SILT, some sand, little clay (clay and sand content variable)
337.83	337.14	silty CLAY, trace sand (clay and silt content variable)
337.14	336.76	SILT, little clay, trace sand (clay absent below 4.33 m)
336.76	336.12	sandy SILT, trace clay
336.12	333.57	SILT, little sand, trace clay (clay and sand content variable, sand absent from 7.23-7.62)
333.57	333.29	clayey SILT, trace sand
333.29	333.18	SILT, some sand, little clay, trace gravel
333.18	332.18	silty SAND
332.18	331.29	SILT and SAND, trace clay
331.29	331.19	sandy SILT, little clay
331.19	330.79	SILT, some clay, trace sand and gravel
330.79	330.66	clayey SILT, trace sand
330.66	330.28	SILT, sand and clay increasing through interval, some gravel below 11.01 m
330.28	329.90	GRAVEL and SILT, little sand, trace clay
329.90	329.14	GRAVEL and SAND, some silt, trace clay
329.14	327.61	sandy GRAVEL, trace silt and clay
327.61	327.49	SAND, some silt and gravel, little clay
327.49	326.34	silty CLAY, little sand
326.34	326.09	clayey SILT, some sand
326.09	325.55	CLAY and SILT, some sand
325.55	325.33	SILT and SAND, some clay, trace gravel
325.33	324.57	silty CLAY, little sand
324.57	323.80	CLAY, some silt, trace sand and gravel
323.80	323.58	silty CLAY, trace sand and gravel
323.58	323.33	SAND and SILT, some clay, little gravel
323.33	323.04	sandy SILT and CLAY, some gravel

Table B 4 USCS description of geology at CMT-4.

Top Elevation (mASL)	Bottom Elevation (mASL)	CMT-4
340.41	339.65	FILL
339.65	337.36	clayey SILT, trace sand
337.36	337.28	sand
337.28	337.11	sandy SILT and CLAY
337.11	336.60	SILT, some sand, trace clay
336.60	335.84	sandy SILT, trace clay
335.84	335.19	SILT, some sand, some clay
335.19	334.31	sandy SILT, trace clay (some silty sand)
334.31	333.97	SILT, some clay, little sand (clay content variable)
333.97	333.77	clayey SILT, little sand
333.77	333.55	SILT, little clay, little sand (clay content variable)
333.55	332.96	clayey SILT, trace fine sand (sand content variable)
332.96	332.79	sandy SILT, trace clay
332.79	332.24	SAND, some silt, trace clay
332.24	331.98	silty SAND, trace clay
331.98	331.61	SAND and SILT, trace clay
331.61	331.36	clayey SILT
331.36	330.35	SILT, trace to little clay, trace sand
330.35	330.24	clayey SILT
330.24	328.22	SILT, trace to little clay, trace sand
328.22	328.06	silty, gravelly and clayey SAND
328.06	327.41	silty CLAY, little to some sand, trace gravel
327.41	327.29	CLAY and SILT, some sand, trace gravel
327.29	327.16	silty CLAY, little sand
327.16	326.89	clayey SILT, little sand
326.89	326.84	SILT, some sand, little clay
326.84	326.59	CLAY and SILT, some sand, trace gravel
326.59	326.34	silty CLAY, trace sand
326.34	325.93	SILT, little clay, trace sand
325.93	324.41	silty CLAY, trace to little sand
324.41	323.65	CLAY, some silt, trace sand

Table B 5 USCS description of geology at PW.

Top Elevation (mASL)	Bottom Elevation (mASL)	PW
339.29	338.86	CLAY and SILT, little sand
338.86	337.76	SILT, some clay and sand, trace gravel
337.76	337.60	sandy SILT, trace clay
337.60	337.33	CLAY and SILT, trace sand and gravel
337.33	337.29	clayey SILT, trace sand
337.29	334.35	SILT, little to some clay, trace to some sand
334.35	334.08	clayey SILT
334.08	333.32	SILT, some clay, trace sand
333.32	333.19	clayey SILT, trace sand
333.19	333.05	SILT, some clay, little sand, trace gravel
333.05	332.43	silty SAND, trace clay
332.43	332.03	sandy SILT, trace clay
332.03	331.65	CLAY and SILT, trace sand
331.65	331.39	clayey SILT, trace sand
331.39	331.17	SILT, some clay, trace sand
331.17	330.80	clayey SILT, trace to little sand
330.80	329.68	SILT, little to some clay, trace to little sand
329.68	329.38	SAND and SILT, trace clay
329.38	328.48	silty SAND, trace clay
328.48	328.36	SAND, some silt, trace clay and gravel
328.36	328.03	GRAVEL, little sand, trace silt and clay
328.03	327.86	CLAY and SILT, trace sand and gravel
327.86	325.92	silty CLAY, little sand, trace gravel and cobbles
325.92	325.66	clayey and sandy SILT, trace gravel and cobbles
325.66	325.57	CLAY and SILT, trace gravel
325.57	324.93	sandy SILT and CLAY, trace gravel
324.93	324.81	clayey and sandy SILT, trace gravel
324.81	323.96	silty CLAY, little sand, trace gravel
323.96	323.28	SAND and SILT, some gravel and clay, trace cobbles

Table B 6 Hazen coefficient for a range of sediments.

Sediment Description	C value
Very fine sand, poorly sorted	40-80
Fine sand with appreciable fines	40-80
Medium sand, well sorted	80-120
Coarse sand, poorly sorted	80-120
Coarse sand, well sorted, clean	120-150

Table B 7 CMT-1 hydraulic conductivity estimates from grain size empirical equations.

Elevation (mASL)	Hazen K (m/s)	Puckett et al. K (m/s)	Elevation (mASL)	Hazen K (m/s)	Puckett et al. K (m/s)
338.10	2.6E-07	2.0E-05	334.06	6.8E-09	4.5E-06
337.62	4.0E-09	2.1E-07	333.87	5.0E-08	1.3E-05
337.54	3.6E-08	9.9E-06	333.78	1.3E-08	5.0E-06
337.11	7.0E-07	4.4E-05	333.48	4.6E-08	1.8E-05
336.99	7.3E-07	2.0E-05	333.28	3.6E-06	3.6E-05
336.73	9.0E-07	2.7E-05	332.16	1.3E-05	4.0E-05
336.36	1.9E-06	2.6E-05	331.77	8.7E-06	2.9E-05
335.98	7.3E-07	2.7E-05	331.51	1.3E-08	5.0E-06
335.68	2.6E-07	2.7E-05	331.19	1.6E-08	2.7E-05
335.49	1.1E-08	5.0E-06	331.11	1.6E-08	6.0E-06
335.29	3.6E-08	7.4E-06	330.81	4.7E-05	2.0E-05
334.92	6.4E-08	7.4E-06	330.73	7.2E-05	4.1E-05
334.71	1.0E-07	1.5E-05	330.43	2.4E-06	4.0E-05
334.55	7.1E-08	1.3E-05	330.25	3.8E-05	4.4E-05
334.36	8.5E-08	1.5E-05	330.14	2.5E-08	7.4E-06

Elevation (mASL)	Hazen K (m/s)	Puckett et al. K (m/s)
330.02	8.6E-04	4.4E-05
329.26	1.6E-10	3.5E-07
328.46	6.8E-11	1.2E-09
328.28	4.1E-10	2.8E-07
328.22	9.0E-11	1.3E-08
327.88	1.3E-10	7.3E-09
327.74	3.0E-10	6.4E-08
327.34	4.1E-10	8.7E-08
327.14	2.0E-09	1.0E-06
326.97	7.8E-11	3.4E-10
326.67	3.2E-11	1.2E-09
326.25	2.6E-09	8.4E-07
326.15	1.5E-07	1.3E-05
325.90	3.6E-10	2.6E-07
325.88	1.8E-10	2.1E-07
325.82	6.8E-11	2.2E-08
325.65	1.9E-10	4.3E-08
325.39	6.8E-11	1.0E-09
324.90	1.3E-11	1.5E-09
324.69	1.2E-11	1.7E-10

Table B 8 CMT-2 hydraulic conductivity estimates from grain size empirical equations.

Elevation (mASL)	Hazen K (m/s)	Puckett et al. K (m/s)	Elevation (mASL)	Hazen K (m/s)	Puckett et al. K (m/s)
340.54	1.0E-09	8.4E-07	334.47	2.3E-08	6.0E-06
340.07	1.0E-07	1.5E-05	334.34	7.8E-07	3.6E-05
338.91	2.5E-09	4.6E-07	334.25	4.0E-07	4.0E-05
338.82	1.1E-08	3.3E-06	334.01	7.3E-09	3.0E-06
338.74	2.5E-09	3.1E-07	333.89	1.2E-08	3.7E-06
338.55	2.9E-06	2.9E-05	333.79	4.9E-08	1.3E-05
338.35	6.4E-10	4.6E-07	333.55	2.6E-08	6.0E-06
338.25	1.4E-07	1.6E-05	333.33	4.2E-08	9.9E-06
338.15	2.5E-08	8.1E-06	333.21	1.7E-08	5.0E-06
338.05	5.5E-07	2.9E-05	333.13	9.2E-08	2.7E-05
337.95	1.0E-07	1.8E-05	333.03	6.3E-07	4.4E-05
337.73	1.0E-09	2.0E-06	332.92	1.6E-05	4.4E-05
337.68	6.3E-09	1.5E-06	332.47	1.0E-05	4.4E-05
337.61	1.0E-09	2.6E-07	331.81	1.4E-09	5.7E-07
337.01	1.0E-09	2.6E-07	331.69	7.1E-08	1.5E-05
336.62	1.3E-06	4.1E-06	331.50	1.6E-08	6.0E-06
336.54	9.0E-07	2.9E-05	331.40	5.3E-09	1.8E-06
336.44	1.8E-06	4.4E-05	331.21	2.6E-09	5.7E-07
336.07	1.3E-06	3.2E-05	330.95	4.0E-07	9.9E-06
335.51	5.3E-07	3.6E-05	330.74	5.3E-10	1.2E-07
335.22	2.3E-08	8.1E-06	330.64	4.6E-08	9.0E-06
334.93	2.6E-07	3.6E-05	330.43	4.0E-07	3.2E-05
334.74	1.1E-07	2.2E-05	330.12	2.6E-09	4.5E-06

Elevation (mASL)	Hazen K (m/s)	Puckett et al. K (m/s)
329.92	1.6E-08	6.0E-06
329.69	1.6E-08	6.0E-06
329.55	2.2E-08	7.4E-06
329.36	1.9E-10	7.3E-09
328.86	2.7E-10	4.3E-08
328.70	3.2E-11	2.1E-10
328.40	1.0E-10	1.3E-08
328.01	2.6E-09	1.8E-06
327.14	2.0E-09	3.3E-06
327.04	1.0E-11	8.9E-09
326.73	2.0E-09	3.7E-06
326.53	5.0E-10	1.9E-07
326.39	2.6E-09	1.5E-06
326.10	2.1E-10	2.9E-08
325.78	6.0E-09	2.1E-07
325.51	2.2E-09	4.6E-07
324.89	1.4E-09	8.4E-07
324.74	4.8E-11	2.2E-09
324.21	1.6E-08	6.0E-06

Table B 9 CMT-3 hydraulic conductivity estimates from grain size empirical equations.

Elevation (mASL)	Hazen K (m/s)	Puckett et al. K (m/s)	Elevation (mASL)	Hazen K (m/s)	Puckett et al. K (m/s)
340.27	2.9E-09	6.9E-07	333.11	1.4E-06	2.5E-05
339.88	4.4E-07	2.4E-05	332.51	2.0E-05	4.4E-05
339.16	1.0E-09	4.3E-08	332.18	1.0E-05	4.4E-05
338.23	4.8E-09	8.4E-07	331.38	1.5E-05	4.4E-05
338.13	8.3E-08	1.3E-05	331.29	3.4E-07	2.7E-05
337.94	1.7E-07	2.4E-05	331.19	1.8E-07	2.0E-05
337.83	6.4E-10	8.9E-09	330.95	5.1E-08	1.2E-05
337.63	2.0E-09	1.7E-07	330.78	1.6E-08	6.0E-06
337.47	2.7E-10	2.6E-08	330.60	3.2E-07	2.9E-05
337.07	2.3E-08	7.4E-06	330.42	1.8E-07	1.1E-05
336.96	1.3E-06	4.4E-05	330.32	4.0E-07	1.6E-05
336.71	2.5E-06	3.6E-05	330.11	2.4E-07	2.4E-05
336.12	2.1E-06	3.6E-05	329.90	5.8E-05	4.4E-05
335.18	1.2E-07	1.6E-05	329.08	1.8E-04	4.4E-05
334.98	4.4E-08	9.9E-06	328.70	1.6E-04	4.4E-05
334.59	2.3E-07	1.5E-05	327.58	5.4E-08	9.0E-06
334.43	2.7E-07	2.0E-05	327.37	4.7E-08	1.8E-08
334.23	2.6E-05	2.2E-05	326.70	5.8E-11	1.0E-09
334.03	2.3E-08	7.4E-06	326.34	3.1E-10	1.4E-07
333.82	3.6E-08	1.2E-05	325.93	1.6E-10	2.4E-08
333.66	2.1E-08	7.4E-06	325.55	7.8E-09	3.7E-06
333.57	4.8E-07	2.7E-05	325.18	4.0E-11	1.2E-09
333.37	6.8E-09	2.3E-06	324.07	5.3E-11	3.2E-11
333.29	1.1E-07	1.8E-05	323.74	4.0E-11	1.8E-10

Elevation (mASL)	Hazen K (m/s)	Puckett et al. K (m/s)
323.54	1.3E-08	5.0E-06
323.47	6.5E-09	2.3E-06
323.30	1.3E-09	3.1E-07

Table B 10 CMT-4 hydraulic conductivity estimates from grain size empirical equations.

Elevation (mASL)	Hazen K (m/s)	Puckett et al. K (m/s)	Elevation (mASL)	Hazen K (m/s)	Puckett et al. K (m/s)
339.12	3.2E-09	5.1E-07	334.27	1.0E-07	1.6E-05
337.16	2.6E-09	8.4E-07	334.17	6.0E-09	7.4E-06
337.06	3.6E-08	9.0E-06	334.07	1.0E-07	7.4E-06
336.96	5.3E-07	3.2E-05	333.97	4.0E-09	2.7E-06
336.86	2.0E-06	3.6E-05	333.87	4.0E-09	1.4E-06
336.76	3.5E-06	4.4E-05	333.77	4.0E-07	2.4E-05
336.60	1.2E-06	2.9E-05	333.67	4.1E-08	1.3E-05
336.40	3.3E-06	2.9E-05	333.58	4.9E-08	2.0E-05
336.30	3.5E-06	3.6E-05	332.97	4.0E-09	1.5E-06
336.20	2.2E-06	3.6E-05	332.86	1.9E-06	4.4E-05
336.10	1.9E-06	4.0E-05	332.54	2.4E-05	3.6E-05
336.00	7.2E-06	4.4E-05	332.24	2.0E-05	3.2E-05
335.90	1.3E-06	2.7E-05	331.98	1.3E-05	2.7E-05
335.80	1.0E-07	1.6E-05	331.61	1.4E-08	1.5E-06
335.69	7.1E-08	1.1E-05	331.36	4.9E-08	7.4E-06
335.61	4.0E-09	5.0E-06	331.22	4.4E-08	1.1E-05
335.49	7.1E-08	1.1E-05	331.10	1.8E-08	7.4E-06
335.40	1.7E-07	1.6E-05	330.95	1.0E-08	5.0E-06
335.27	6.3E-07	4.4E-05	330.84	6.6E-07	2.9E-05
335.19	1.3E-07	9.0E-06	330.74	1.2E-07	2.2E-05
335.14	7.9E-07	1.6E-05	330.64	4.4E-08	1.3E-05

Elevation (mASL)	Hazen K (m/s)	Puckett et al. K (m/s)
330.44	8.8E-08	1.1E-05
330.35	1.4E-09	8.4E-07
330.24	2.0E-07	1.6E-05
330.17	9.0E-09	5.0E-06
329.96	2.6E-07	1.6E-05
329.71	1.8E-07	1.6E-05
328.18	2.0E-09	1.7E-06
328.06	1.0E-10	6.0E-09
327.65	5.8E-11	6.0E-09
327.41	1.3E-10	7.1E-08
327.29	5.3E-11	3.3E-09
327.14	6.4E-10	3.5E-07
326.86	2.9E-08	7.4E-06
326.84	3.2E-11	1.2E-07
326.56	3.2E-11	6.9E-10
326.31	1.6E-08	6.0E-06
325.78	1.4E-11	7.0E-11
325.17	2.9E-11	3.1E-10
324.89	4.4E-11	3.1E-10
324.01	1.4E-11	4.3E-11

Table B 11 PW hydraulic conductivity estimates from grain size empirical equations.

Elevation (mASL)	Hazen K (m/s)	Puckett et al. K (m/s)	Elevation (mASL)	Hazen K (m/s)	Puckett et al. K (m/s)
337.72	2.1E-06	3.1E-05	327.69	6.3E-11	4.1E-09
337.53	1.3E-09	4.3E-08	327.06	4.0E-11	2.2E-09
337.33	4.8E-09	2.5E-06	326.30	3.2E-11	4.1E-09
337.23	1.2E-07	2.5E-06	325.92	2.3E-09	6.9E-07
335.69	3.1E-08	6.7E-06	325.66	1.2E-09	8.4E-07
335.35	1.3E-08	5.0E-06	325.54	3.6E-10	2.8E-07
334.94	9.2E-08	1.2E-05	325.32	1.9E-10	8.7E-08
334.68	3.8E-07	1.8E-05	324.93	1.4E-09	1.0E-06
334.28	2.9E-09	8.4E-07	324.59	1.4E-11	3.1E-10
334.08	1.3E-08	5.5E-06	324.01	1.4E-11	2.1E-10
333.79	1.6E-08	6.0E-06	323.82	9.0E-09	5.0E-06
333.32	9.6E-09	2.9E-06			
333.06	1.4E-08	5.0E-06			
332.76	9.1E-06	4.0E-05			
332.29	3.6E-06	3.7E-05			
331.74	2.0E-09	3.7E-05			
331.62	4.0E-09	7.6E-07			
331.33	6.3E-09	3.7E-06			
331.14	2.6E-09	1.4E-06			
330.86	1.4E-09	1.2E-06			
330.76	2.1E-08	7.4E-06			
330.53	1.2E-07	1.5E-05			
330.36	6.4E-08	1.1E-05			
330.07	3.6E-08	7.4E-06			
329.80	3.6E-08	9.0E-06			
329.50	1.1E-06	2.0E-05			
328.58	1.2E-05	2.7E-05			
328.45	2.1E-05	3.2E-05			
328.28	2.5E-03	4.4E-05			
327.96	2.3E-10	1.8E-08			

Table B 12 CMT-1 falling head permeameter measurements.

CMT-1			
Elevation (mASL)	**K (m/s)**	**Elevation (mASL)**	**K (m/s)**
338.08	2.3E-06	334.39	8.8E-08
338.00	5.4E-06	334.29	1.3E-07
337.64	1.7E-06	334.19	1.6E-07
337.52	5.2E-09	334.09	1.6E-07
337.44	5.4E-09	333.99	1.9E-07
337.34	2.8E-09	333.89	8.8E-08
337.24	2.0E-09	333.83	1.5E-07
337.14	8.6E-08	333.73	4.9E-07
337.04	8.9E-07	333.63	2.8E-08
336.94	2.1E-06	333.53	4.5E-08
336.88	2.6E-06	333.43	3.9E-08
336.78	3.2E-06	333.33	8.5E-08
336.68	2.3E-06	333.23	1.3E-07
336.58	5.0E-06	333.13	2.0E-08
336.48	4.2E-06	332.31	1.0E-05
336.38	6.1E-06	332.21	1.0E-05
336.28	4.5E-06	332.11	1.1E-05
336.18	5.5E-06	332.01	1.2E-05
336.12	5.3E-06	331.91	8.7E-06
336.02	2.9E-06	331.81	1.3E-05
335.92	2.7E-06	331.71	1.7E-05
335.82	3.8E-06	331.70	1.9E-05
335.72	4.6E-06	331.55	9.5E-06
335.62	3.2E-07	331.45	5.8E-06
335.52	4.6E-07	331.35	1.0E-05
335.42	1.7E-07	331.25	7.7E-06
335.36	2.3E-07	331.15	3.4E-07
335.26	2.4E-07	331.05	6.3E-08
335.16	2.3E-07	330.85	7.0E-08
335.06	3.9E-07	330.78	4.7E-05
334.96	4.3E-07	330.68	2.2E-04
334.76	8.0E-08	330.58	2.7E-04
334.66	1.1E-07	330.48	1.8E-04
334.59	3.2E-07	330.38	4.4E-05
334.49	2.6E-07	330.28	6.9E-07

Elevation (mASL)	K (m/s)	Elevation (mASL)	K (m/s)
330.18	2.8E-05	326.94	6.4E-08
330.08	2.2E-07	326.54	2.8E-09
329.69	3.1E-08	326.27	8.7E-10
329.19	2.8E-04	325.84	3.8E-09
328.40	1.6E-09	325.54	5.2E-08
328.20	1.1E-07	325.53	2.0E-07
327.90	1.4E-08	325.45	7.5E-09
327.71	1.4E-08	325.33	5.2E-08
327.29	1.4E-09	324.32	1.4E-09
327.09	6.3E-09	323.93	1.2E-09

Table B 13 CMT-2 falling head permeameter measurements.

CMT-2			
Elevation (mASL)	K (m/s)	Elevation (mASL)	K (m/s)
340.59	2.6E-07	336.22	1.5E-06
340.13	1.1E-07	336.12	1.8E-06
340.03	4.2E-07	336.02	3.0E-06
339.93	3.2E-08	335.92	2.4E-06
338.60	6.3E-06	335.82	2.0E-06
338.50	9.7E-06	335.72	1.8E-06
338.30	3.0E-07	335.56	4.1E-07
338.20	1.3E-07	335.46	6.3E-07
338.10	4.4E-07	335.36	5.5E-07
338.00	1.1E-07	335.26	2.1E-07
337.84	3.8E-08	335.16	6.3E-08
337.74	2.1E-08	335.06	5.6E-08
337.64	4.2E-08	335.16	2.0E-07
336.98	1.1E-08	334.86	4.3E-07
336.88	4.7E-09	334.79	5.9E-08
336.68	1.1E-07	334.69	1.6E-07
336.58	2.3E-07	334.59	2.1E-07
336.48	1.8E-06	334.49	8.1E-08
336.38	3.0E-06	334.39	5.3E-07
336.32	5.8E-07	334.29	8.4E-07

Elevation (mASL)	K (m/s)	Elevation (mASL)	K (m/s)
334.19	2.8E-07	330.28	1.9E-07
334.03	8.0E-09	330.22	7.7E-08
333.93	4.7E-08	330.09	1.1E-07
333.83	2.6E-08	330.02	6.7E-08
333.73	9.7E-08	329.90	6.5E-08
333.63	1.6E-07	329.82	2.1E-07
333.44	5.1E-07	329.72	8.1E-08
333.37	1.8E-07	329.55	2.2E-07
333.27	1.8E-08	329.06	8.9E-09
333.17	3.3E-08	328.60	2.9E-08
333.07	1.4E-07	328.15	3.0E-09
332.97	2.1E-07	328.03	7.1E-08
332.87	2.3E-05	327.17	1.4E-06
332.77	1.2E-05	327.07	2.1E-09
332.67	1.1E-05	326.77	1.8E-07
332.57	9.4E-06	326.67	1.3E-07
332.51	1.8E-05	326.57	2.4E-09
332.41	1.9E-05	326.41	3.3E-08
332.31	1.5E-05	326.31	8.8E-08
332.21	1.4E-05	326.21	9.2E-09
332.11	9.9E-06	326.11	1.8E-08
332.01	2.3E-05	326.01	1.9E-08
331.91	1.7E-05	325.91	6.1E-08
331.75	1.3E-08	325.81	2.5E-08
331.65	9.4E-08	325.71	3.1E-08
331.55	6.3E-08	325.65	8.6E-08
331.35	8.9E-09	325.55	2.0E-08
330.98	6.7E-08	325.45	2.8E-08
330.88	5.4E-07	325.35	1.1E-08
330.68	2.9E-08	325.25	4.2E-08
330.58	4.9E-08	324.88	4.0E-08
330.48	3.8E-07	324.72	5.7E-10
330.38	2.6E-07		

Table B 14 CMT-3 falling head permeameter measurements.

CMT-3			
Elevation (mASL)	**K (m/s)**	**Elevation (mASL)**	**K (m/s)**
340.57	6.3E-08	333.97	1.6E-07
340.17	1.2E-07	333.87	1.0E-07
339.87	1.2E-06	333.77	2.8E-07
339.08	4.0E-07	333.61	8.1E-08
338.28	7.2E-08	333.51	1.6E-08
338.18	5.4E-07	333.41	1.3E-08
338.08	3.2E-07	333.31	3.4E-08
337.98	2.6E-07	333.21	1.6E-07
337.88	2.7E-09	333.11	5.6E-05
337.68	4.6E-09	333.01	1.9E-05
337.32	2.2E-09	332.95	2.1E-05
337.12	3.1E-08	332.85	2.7E-05
337.02	7.1E-07	332.75	3.3E-05
336.92	1.5E-06	332.65	2.8E-05
336.82	1.2E-06	332.55	3.0E-05
336.76	3.4E-06	332.45	3.2E-05
336.66	4.9E-06	332.35	2.6E-05
336.56	7.0E-06	332.25	3.2E-05
336.46	4.0E-06	332.19	1.2E-05
336.36	1.8E-06	331.42	1.2E-05
336.26	3.9E-06	331.32	7.4E-06
336.16	3.4E-06	331.22	3.5E-07
335.23	8.7E-07	331.12	6.9E-08
335.13	2.3E-07	331.02	8.5E-08
335.03	1.9E-07	330.92	5.2E-08
334.93	7.2E-07	330.82	4.1E-08
334.83	4.6E-06	330.72	1.8E-07
334.73	4.3E-06	330.66	7.4E-08
334.63	2.5E-07	330.56	4.1E-07
334.53	3.7E-07	330.46	1.6E-07
334.47	5.4E-07	330.36	3.6E-08
334.37	7.5E-07	330.26	7.5E-08
334.27	6.2E-07	330.16	5.5E-08
334.17	3.7E-07	329.90	4.8E-05
334.07	1.3E-07	329.14	1.2E-05

Elevation (mASL)	K (m/s)	Elevation (mASL)	K (m/s)
329.04	5.5E-06	326.65	8.0E-09
328.94	4.0E-05	326.18	1.4E-08
328.84	2.9E-05	325.83	1.1E-08
328.74	3.1E-05	324.77	1.1E-09
328.64	1.7E-05	324.33	2.6E-09
328.54	2.0E-05	323.64	7.2E-08
327.61	4.1E-07	323.57	6.2E-08
327.08	3.7E-08	323.50	3.7E-08

Table B 15 CMT-4 falling head permeameter measurements.

CMT-4			
Elevation (mASL)	K (m/s)	Elevation (mASL)	K (m/s)
340.31	1.9E-07	336.10	4.0E-06
340.11	1.1E-07	336.00	3.1E-06
340.01	1.9E-07	335.90	1.6E-06
339.55	2.1E-07	335.84	9.9E-08
339.45	1.8E-07	335.74	2.7E-06
339.35	5.4E-07	335.64	1.6E-07
339.25	2.3E-08	335.54	3.1E-07
337.72	1.0E-07	335.44	3.0E-07
337.62	1.5E-07	335.34	3.9E-07
337.52	4.7E-07	335.24	2.2E-06
337.42	7.3E-07	335.14	1.0E-06
337.36	1.3E-06	334.31	2.7E-07
337.26	7.5E-09	334.21	3.8E-07
337.16	5.4E-09	334.11	5.8E-07
337.06	6.5E-08	334.01	1.0E-07
336.96	6.9E-07	333.91	3.6E-08
336.86	1.9E-06	333.81	1.0E-07
336.76	2.7E-06	333.71	4.0E-08
336.60	1.1E-06	333.61	8.2E-08
336.50	3.3E-06	333.55	1.1E-07
336.40	2.3E-06	332.79	2.7E-05
336.30	2.9E-06	332.69	2.7E-05
336.20	3.1E-06	332.59	2.7E-05

Elevation (mASL)	K (m/s)	Elevation (mASL)	K (m/s)
332.49	2.0E-05	330.20	2.5E-07
332.39	2.2E-05	330.10	7.1E-08
332.29	2.0E-05	330.00	2.0E-07
332.19	2.2E-05	329.90	9.2E-07
332.09	2.3E-05	329.74	1.5E-06
332.03	9.1E-06	328.22	3.5E-07
331.93	1.1E-05	327.82	1.6E-09
331.83	9.4E-06	327.46	1.2E-07
331.73	8.7E-06	327.32	4.5E-09
331.63	6.7E-09	327.16	7.2E-08
331.53	5.0E-06	327.11	1.1E-08
331.43	1.7E-07	327.01	1.8E-08
331.27	5.3E-07	326.91	2.6E-08
331.17	2.4E-07	326.89	2.2E-07
331.07	3.7E-07	326.81	9.7E-09
330.97	7.5E-08	326.59	2.2E-09
330.87	6.9E-07	326.34	8.6E-08
330.77	1.2E-07	325.83	2.0E-09
330.67	8.9E-08	325.63	6.4E-09
330.50	2.8E-07	324.86	1.1E-08
330.40	3.0E-07	324.08	4.5E-09
330.30	5.1E-07		

Table B 16 PW falling head permeameter measurements.

PW			
Elevation (mASL)	K (m/s)	Elevation (mASL)	K (m/s)
338.20	2.3E-06	336.14	9.0E-07
337.76	5.4E-06	336.04	1.8E-06
337.66	2.9E-06	335.94	1.9E-06
337.56	2.2E-09	335.84	2.2E-06
337.36	4.7E-08	335.74	3.0E-06
337.26	2.0E-06	335.64	2.0E-06
337.16	1.2E-06	335.54	1.1E-06
337.06	1.7E-06	335.48	1.7E-07
336.24	6.9E-07	335.38	2.6E-07

Elevation (mASL)	K (m/s)	Elevation (mASL)	K (m/s)
335.28	2.8E-07	331.47	3.6E-08
335.18	8.5E-08	331.37	2.4E-07
335.08	2.9E-07	331.27	1.2E-07
334.98	2.6E-07	331.17	3.4E-08
334.88	4.9E-07	331.07	1.5E-08
334.71	3.2E-07	330.97	3.3E-08
334.61	5.1E-07	330.90	1.9E-08
334.51	4.5E-07	330.80	7.7E-08
334.41	1.7E-07	330.70	1.0E-07
334.31	3.7E-08	330.60	1.0E-07
334.21	1.7E-07	330.50	1.5E-07
334.11	1.5E-07	330.40	4.3E-08
334.01	4.2E-07	330.30	1.9E-07
333.95	1.3E-07	330.20	1.8E-07
333.85	1.1E-07	330.14	1.3E-07
333.75	2.3E-07	330.04	9.6E-08
333.65	1.8E-07	329.94	8.9E-08
333.55	4.1E-07	329.84	1.1E-07
333.45	1.2E-07	329.74	7.5E-08
333.35	2.4E-07	329.64	6.1E-08
333.25	3.2E-08	329.54	2.5E-07
333.19	1.9E-08	329.44	4.0E-07
333.09	2.9E-08	328.62	1.9E-05
332.99	1.9E-07	328.52	4.2E-05
332.89	1.9E-05	328.42	1.7E-05
332.79	1.9E-05	328.32	1.9E-07
332.69	2.5E-05	328.22	1.8E-06
332.59	1.2E-05	328.01	1.4E-07
332.43	1.0E-05	327.91	8.6E-08
332.33	1.0E-05	327.76	2.9E-09
332.23	9.8E-06	327.09	2.1E-09
332.13	1.2E-05	326.23	2.1E-09
331.86	4.1E-09	326.03	1.9E-08
331.67	1.1E-07	325.93	1.0E-07
331.57	3.5E-07	325.83	3.7E-08

Elevation (mASL)	K (m/s)	Elevation (mASL)	K (m/s)
325.73	6.4E-08	323.95	8.8E-08
325.69	1.5E-07	323.85	3.4E-07
325.57	8.9E-09	323.75	3.0E-07
324.87	4.8E-08	323.65	1.2E-06
324.66	1.5E-08	323.55	2.5E-07
324.05	4.1E-09	323.45	7.6E-08